POLITECNICO
MILANO 1863

SCHOOL OF CIVIL, ENVIRONMENTAL AND LAND MANAGEMENT ENGINEERING
MASTER OF SCIENCE IN ENVIRONMENTAL AND LAND PLANNING ENGINEERING

# INFORMING WATER RESERVOIR OPERATIONS WITH CLIMATE TELECONNECTIONS

Master Thesis by:
**Gentile Alessandro**
Matr. 858519

Advisor:
**Prof. Matteo Giuliani**

Co-Advisor:
**Marta Zaniolo**

Academic Year 2017 – 2018

# Acknowledgements

I have a lot of people (and even objects, like Pocket Coffees) to thank for this thesis. Mentioning all of them, would be annoying to write and to read, and I'd forget someone for sure. So, I'll just say: "Thank you" when I see you.
Anyway, an exception must be made. I must thank here Matteo Giuliani and Marta Zaniolo, for helping me with this last step to graduation.
And my turtle, I must thank my turtle.

# Abstract

Increasingly uncertain hydrologic regimes combined with more frequent and intense extreme events are challenging water systems management worldwide, emphasizing the need of accurate medium- to long-term predictions to timely prompt anticipatory operations. Despite modern forecasts being skilful over short lead time, predictability generally tends to decrease on longer lead times. Global climate teleconnection, such as El Niño Southern Oscillation (ENSO) and the North Atlantic Oscillation (NAO), may contribute in extending forecast lead times. However, ENSO teleconnection is well defined in some locations, such as Australia or Chile, while there is no consensus on how it can be detected and used in other regions, like Europe or Africa. The same is true for NAO teleconnection. In this work, we employ the Niño Index Phase Analysis, to capture the state of two large scale climate signals, i.e. ENSO and NAO, and we use these teleconnections to forecast hydroclimatic variables on a seasonal time scale. For each phase of the considered climate signals, our approach identifies relevant anomalies in Sea Surface Temperature that influence the local hydrologic conditions, which are first aggregated via Principal Component Analysis and then used as inputs in a multivariate forecast model of seasonal precipitation. The resulting seasonal meteorological forecasts , are then transformed into daily streamflow predictions, by means of a time scaling procedure (k Nearest-Neighbour) combined with an hydrological model (HBV). Lastly, the streamflow forecasts are used as additional inputs for informing the water system operations. The value of the addicted information is then evaluated as the gain in the system performance obtained with the more informed operations. The potential of this framework is demonstrated through an application to the Lake Como system, a regulated lake in northern Italy which is mainly operated for flood control and irrigation supply. The results for each step are overall good, with a final performance improvement of 48% when the lake is simulated under the comparing the Informed Operating Policy with respect to the baseline solution.

# Riassunto

La crescente incertezza dei regimi idrologici, combinata con la maggiore frequenza di eventi estremi sta accrescendo la difficoltá nella gestione dei sistemi idrici nel mondo, evidenziando la necessitá di previsioni accurate di medio lungo periodo per ottimizzare le operazioni. Nonostante siano performanti nel breve periodo, gli attuali modelli previsionali tendono a perdere accuratezza su orizzonti previsionali piú lunghi. Teleconnessioni climatiche globali, quali El Niño Southern Oscillation (ENSO) e la North Atlantic Oscillation (NAO) possono contribuire all'estensione dei periodi di previsione. Tuttavia, gli effetti di ENSO sono definiti solo in poche aree, come Australia e USA, mentre quelli in altre, quali l'Europa, sono meno conosciuti. Lo stesso si puó dire per gli effetti associati al NAO. In questo lavoro, usiamo la Niño Index Phase Analysis, per comprendere lo stato di ENSO e NAO, e sfruttiamo tali teleconnesioni per prevedere variabili idro-climatiche su un periodo stagionale. Per ogni fase di ciascun segnale, l'approccio identifica anomalie di temperature al livello del mare rilevanti che influenzino le condizioni della variabile idrologica locale. Esse vengono prima aggregate attraverso l'analisi delle componenti principali e poi usate come input per un modello di previsione multivariato per fornire previsioni stagionali di precipitazione. Quest'ultime sono poi trasformate in portate giornaliere, con prima una procedura di scomposizione temporale (k Nearest-Neighbour) combinate con un modello idrologico (HBV). Da ultimo, le previsioni di portata sono usate come informazione aggiuntiva nella gestione del sistema. Il valore di tale informazione viene calcolato in termini di miglioramento nelle performance del sistema quando questo viene gestito utilizzando le previsioni di portata. Il potenziale della procedura é dimostrato applicandola sul sistema del Lago di Como, un lago regolato nel nord Italia, operato prevalentemente per controllare le piene e per l'irrigazione. I risultati sono stati soddisfacenti con un miglioramento complessivo della gestione tradizionale del sistema pari al 48% quando si utilizza una gestione piú informata.

# Contents

# List of Figures

# List of Tables

# 1 Introduction

## 1.1 The context

The world contains a total volume of 1400 million $km^3$ of water. Of this volume, only the 0.003%, equivalent to about 45000 $km^3$, is fresh water, meaning water that theoretically can be used for drinking, hygiene, agriculture and industry. But not all of this water is accessible nor equally distributed around the world. Floods, for example, make it difficult to capture and utilize water before it runs off. So, the total amount humanity can really rely on is about 9000 to 14000 $m^3$. Besides, the problem of water quality must be also considered. Because of this, 343 conflicts going on for its use and possession (see Figure 1.1 ) (*Gleick*, 1998, 1994; *PacificInstitute*, 2018) .

This situation is bound to get even worse. This because of the grow of demand, due to world population increase, meaning growing agriculture and energy production, but also for the raising of the awareness about environmental and ecological needs (*Whateley et al.* (2014); *Culley et al.* (2016)). Climate change is increasing uncertainty of hydrological regimes all over the world (*Giuliani et al.*, 2016; *Giuliani and Castelletti*, 2016), with expected dryer conditions in some of the most populated areas. Figure 1.2 shows the expected change in water stress in year 2050 compared to today in 4 different scenarios. All of them show a worsening of the situation in most of the world's countries, with just few exceptions like for example in Canada and some zones between China and Russia. This could lead to a further exacerbation of the existing conflicts

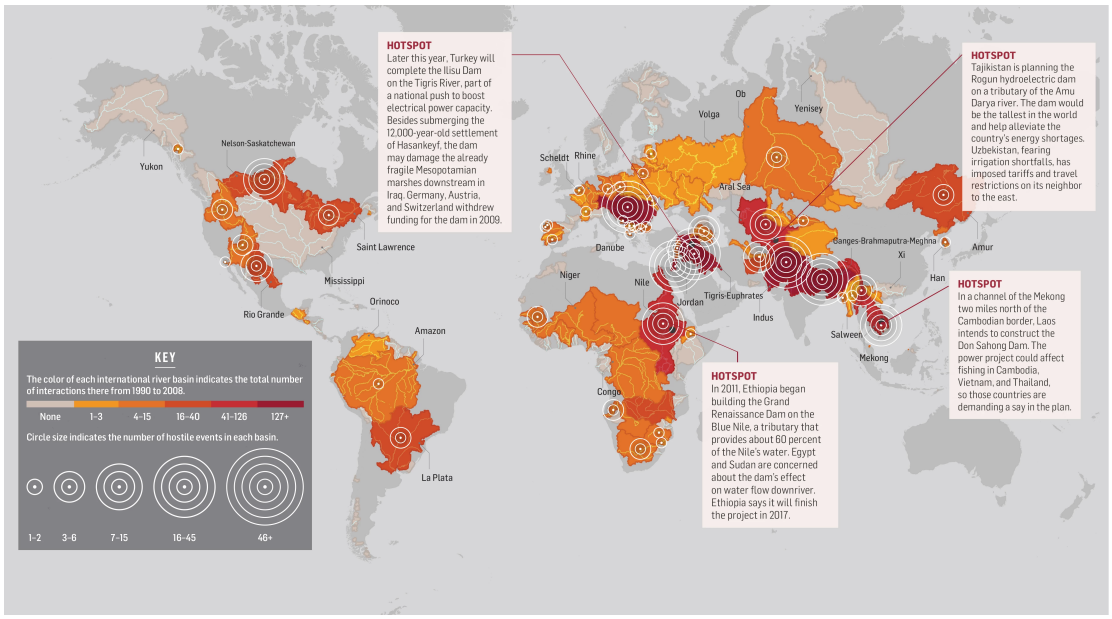


**Figure 1.1:** *Water related hostile events from 1990 to 2008. Image from "https://www.popsci.com".*

and to the birth of new ones.

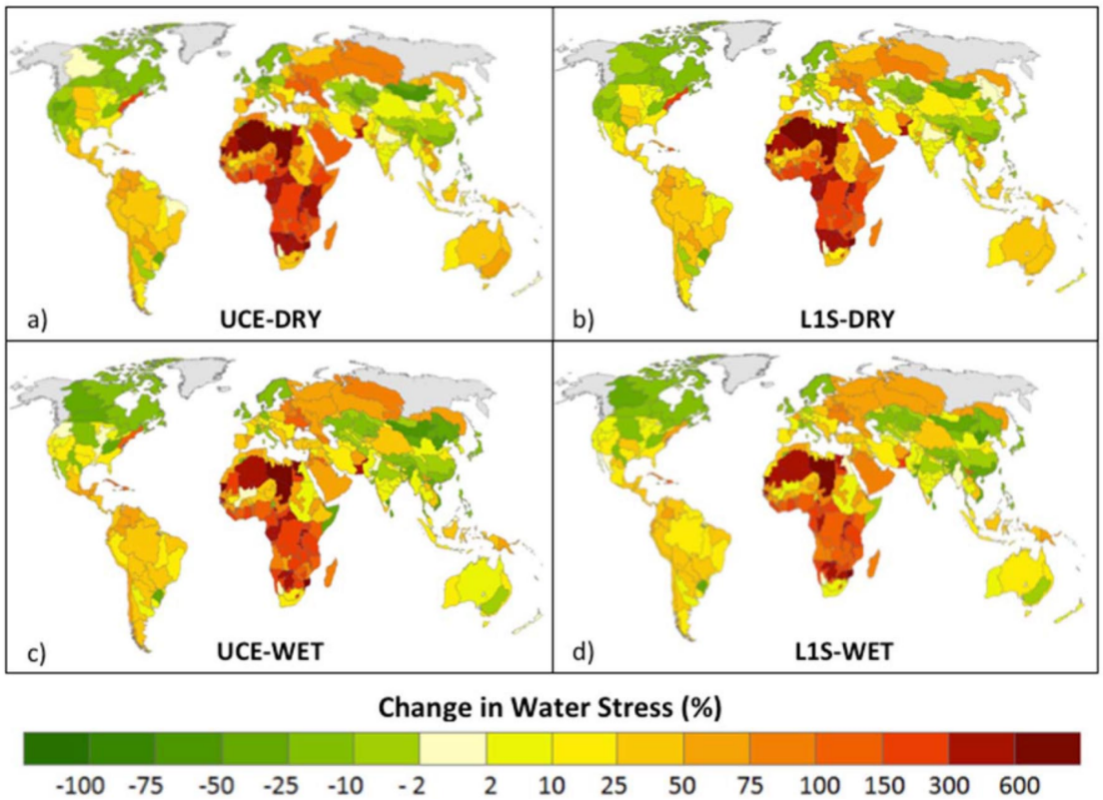


**Figure 1.2:** *Worldwide water stress scenarios in 2050. "http://populationgrowth.org/".*

Looking at this future, a better management of the available water resources

is needed.
Apart from locally suitable solutions, which cannot be applied globally, a generally low-cost option for supporting better water management strategies is the development of models able to make skilful predictions of future water availability, especially in terms of precipitation and streamflow forecast. This information could greatly help water management in making better decision in general, but be particularly effective in case of extreme events (*Block*, 2016).
Recently, many studies have investigated this field, and, in particular, climate variability and its causes, because it is thought to be a fundamental premise for the forecast of future hydro-climatological. One very promising aspect, is the correlation between large scale oceanic-atmospheric phenomena, and local hydrological processes (*Sharma*, 2000; *Goddard et al.*, 2001; *Block and Rajagopalan*, 2007; *Block and Goddard*, 2011).
Such teleconnections are recurring and persistent large scale pattern of pression and circulation anomalies that interests large areas. They are known to have effects on global circulation and even on local hydro-meteorological variables. Large scale processes like teleconnections generally have slower dynamics compared to local ones and long term effects, so they can be used to make predictions with a certain time lead (*Lloyd-Hughes and Saunders*, 2002). In particular, many works focused on the correlations between El Niño Southern Oscillation (ENSO), a teleconnection taking place in the southern Pacific ocean, and local climate anomalies in different parts of the world (*Ropelewski and Halpert*, 1987; *Chiew and McMahon*, 2002; *Ward et al.*, 2010). This is done both for areas more expected to receive an effect because closer to the Pacific Ocean, including the Andean region of South America (*Daniels and Veblen*, 2000) or the western USA (*Kahya and Dracup*, 1993; *Harrison and Larkin*, 1998) and more recently, also in distant areas such as Europe (*Brönnimann et al.*, 2007; *Fraedrich and Müller*, 1992). However, in some locations, the effects are still not clear. In particular, the Alpine region considered in this thesis is one of the areas lacking complete and coherent results. The studies for the area do not always agree on the results and do not provide a complete view of the effects teleconnections have on the area.

## 1.2 Objective of the thesis

The objective of this thesis is to construct reliable long term (i.e. seasonal) hydrologic forecast for an Alpine river basin, based on the state of global teleconnections. In addition, the value of these forecast in informing the system

operations is assessed. The methodology is demonstrated on the case of Lake Como, a regulated lake in Northern Italy, operated mainly to avoid floods and feed the agricultural districts downstream.
In particular, this thesis employs machine learning techniques to capture the state of multiple large-scale climate signals (i.e. ENSO, and North Atlantic Oscillation) to forecast hydroclimatic variables on a seasonal time scale. For each phase of the considered climate signals, our approach identifies relevant anomalies in Sea Surface Temperature (SST) that influence the local meteorological conditions.
This is done by applying the Niño Index Phase Analysis (NIPA) to find the Principal Components (PC) for a multi-variate forecast model of precipitations on the Lake Como basin. Seasonal precipitation is then transformed into streamflow values by means of a basin rainfall runoff model of Lake Como catchment, after the disaggregation of seasonal values into daily ones.
Finally, we demonstrate the potential of such long term forecasts in informing the lake operations. We re-design the operation of Lake Como by including the forecasts among the inputs of the control policy and we contrast the resulting performance with the one of a policy relying on traditional information only. The policy performance improvement represents the value of the forecasts in informing the water system operations.

## 1.3 Thesis outline

The thesis is structured as follows.

Chapter 2 introduces the concept of climate variability, focusing on teleconnections. It reviews the literature regarding the effects of teleconnections on the considered zone and illustrates the study already utilizing this type of information for reservoirs operations.

Chapter 3 provides the description of the methods employed in this thesis. It starts with the description of the data collection and analysis. Then proceeds to explain the Niño Index Phase Analysis procedure, used to find the Principal Components. It then describes the Multi-Variate (MV) seasonal rainfall forecast model adopted. After that, the method for the downscaling to daily precipitations is presented. In the next step, it explains the hydrological model used to transforms the daily rainfall into daily inflow to the Lake. Finally, the Evolutionary Multi-Objective Direct Policy Search used for designing the optimal control policy for the operation of Lake Como is introduced, along with the

metric for the evaluation of the resulting performance.

Chapter 4 describes the Lake Como study case, including its geomorphological features, stakeholders and conflicts, the data and models utilized and the experimental settings.

Chapter 5 contains the results of the thesis. The first part of this chapter discusses the relationship between the considered teleconnections and the local hydrological variable. The second reports the results of the Multi Variate prediction with the different models. The third shows the results of the time downscaling of the precipitation and its transformation into streamflow. Finally, the last part reports the result of the optimization model and the quantification of the value of the forecast information.

Chapter 6 sums up the conclusions and suggests some starting points for further research about the topic.

# 2

# State of art

This chapter gives a general overview on global climate variability, with a focus on long term variability due to global teleconnections.
In particular, we first give a definition for climate variability in section 2.1.
Then, in section 2.2 we review a specific climate phenomena, namely the teleconnections, focusing in particular on ENSO and NAO.
Section 2.3 reviews a number of works concerning the effects of ENSO and NAO on the Alpine region, where the Lake Como case study is located.
Finally, section 2.4 gives an overview of how teleconnections have already been employed in different ways to manage hydrological systems in the known literature.

## 2.1 Climate variability introduction

Climate naturally varies in time and space and it is well known that atmospheric circulation boosts substantial variability. This variability comes in different time ranges (*NOAA*, 2018a):

- Few days: e.g. normal storms and frontal passages;
- Few weeks: e.g. mid-winter warm-up or a mid summer wet period;
- Few months: e.g. particularly cold winters or hot summers;
- Few years: e.g. cold winters happen for several years on a row;
- Several centuries: e.g. long-term climate changes.

In addition to time variability, atmospheric circulation may also come in different spacial scales, from local to continental. Climate variability is defined by the World Meteorological Association as "variation in the mean state and other statistics of the climate on all temporal and spatial scales, beyond individual weather events" (*WMO*, 2018). So, basically, climate variability is the difference between the actual climate and its average expected value. It may affect any hydrological variable, from rainfall and temperature to air pressure and many others and is generally due to natural oscillations. Most of this variability, is demonstrated to be caused by teleconnections (*Ropelewski and Halpert*, 1987; *Harger*, 1995; *Holmgren et al.*, 2006).

## 2.2 Teleconnections

A teleconnection is, as defined by NOAA (*NOAA*, 2018b), a recurring and persistent large scale pattern of pression and circulation anomalies that interests large areas. They are the most notable example of low frequency, long time scale climate variability. They are typically characterized by a duration ranging from several weeks to several months, but their effects can in some case last for years (*NOAA*, 2018b). Consequently, they play an important role for both the inter-annual and inter-decadal variability of the atmospheric circulation. A large number of teleconnections have a world-wide scale magnitude of effects and may affect entire ocean basins and continents.
Teleconnections are natural occurring aspects of the chaotic atmospheric system, i.e. the interaction of the atmospheric circulation with both land and oceans. They are the aftermath of large-scale changes in the atmospheric wave and jet stream patterns, and influence many hydrological variables in large areas.
Between all the variables connected to the process, Sea Surface Temperatures (SSTs) appear to play a particularly prominent role. A great amount of energy is absorbed or dispersed when a region's SST changes, and even slow or contained variations may have great effects on some climate patterns and consequently on the climate variability.
As shown in Figure 2.1 there are many teleconnections around the world, from the Pacific Ocean to the Arctic Glacial Sea. In this thesis, we focus on the two most important teleconnections active in Europe, namely El Niño Souther Oscillation (ENSO) and North Atlantic Oscillation (*Vincent et al.*, 2005; *Beniston*, 2005a; *Steirou et al.*, 2017; *Barcikowska et al.*, 2017; *Samale et al.*, 2017)

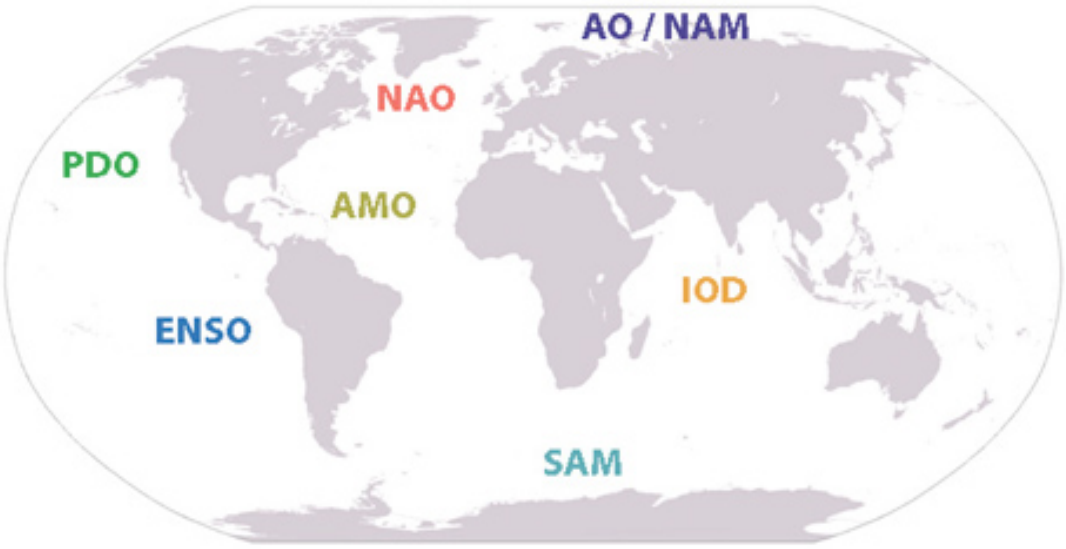


**Figure 2.1:** *Map showing the different locations of some of the world known teleconnections. "https://www2.ucar.edu/news/backgrounders/weather-maker-patterns-map".*

### 2.2.1 ENSO

El Niño Southern Oscillation (ENSO) is a periodic climatological phenomena that occurs in the Pacific ocean. It takes its name from the fact that it generally happens during the Christmas eve, associated by the populations of the area most interested by it with the arrive of baby Jesus (El Niño in spanish). "El Niño" refers to the oceanic component, while Southern Oscillation represents the atmospheric one. It is characterized by a shifting of Sea Surface Temperatures and air pressure of the overlying atmosphere. The two components are mutually coupled and strictly bounded one to the other (*Trenberth*, 1997).
El Niño represents only one of the two phases of the phenomena, with La Niña being the other and having opposite effects.
On neutral years, the Walker current flows from east to west, carrying humidity and hot water. This way, the eastern part is normally left cool and dry. Then, after arriving on the occidental zone of the Pacific, both the wind and the current return westwards, passing respectively in the upper atmosphere and deeper ocean (Figure 2.4)(*Picaut et al.*, 1996). The warm SSTs in the occidental Pacific cause the formation of heat and moisture in the air, leading to the formation of Cumulonimbus clouds and consequently rain. So, during this neutral phase opposite conditions can be found in the occidental and oriental parts of the meridional Pacific, with an high pression in the east and a low one in the west, warm western waters and cool ones in the east and persistent presence of rain in the Pacific-Indonesia zone opposed to the dryness of the coasts of South

America. This neutral year condition is altered during the El Niño and La Niña phases (*Rasmusson and Wallace*, 1983).

During El Niño phase, the conditions change dramatically from the normal ones. The trade winds brought by the Walker current weaken or may even reverse, making it possible for the warm water to travel from the West region towards the central and eastern one as shown in Figure 2.2. The upwelling of cool ocean waters weakens during this phase, contributing to the warming and the associated deepening of the thermocline in the central to eastern Pacific. The persistent precipitation zone shifts its position towards the now hotter central and eastern region. As a result, droughts number and intensity increase in the Indonesian and east Australian zone while the normally arid coasts of Chile and Peru are interested by precipitations (*Sarachik and Cane*, 2010). At the same time, the usual air pressure pattern reverses, being characterized by high air pressure at the sea surface in the western Pacific and low air pressure in eastern Pacific. In addition, the thermocline characterizing the waters near South American coasts weakens in this period, leaving the waters poor of nutrients, with large detrimental effects on the region's fisheries and economies. The main worldwide effects of El Niño can be seen in Figure 2.5.

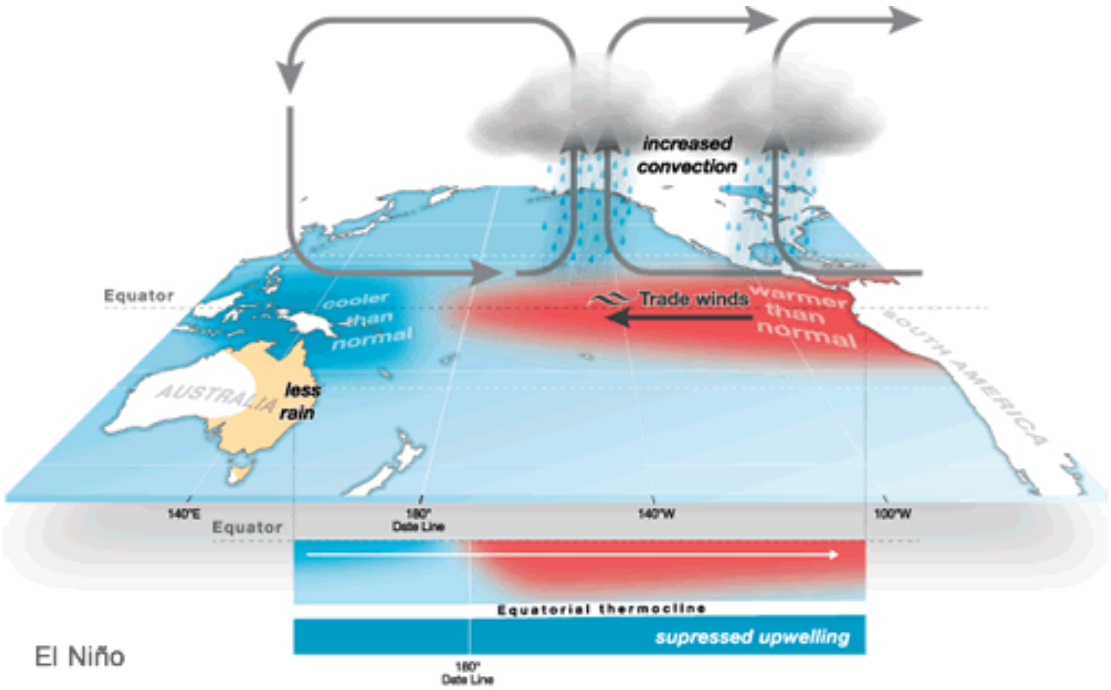


**Figure 2.2:** *Graphic representation of the effects of El Niño.*

During La Niña phase, instead, the situation reverses. In particular, the

Walker circulation is stronger than in neutral years, causing a raise in water level of about 80-100 cm in the west coasts of the Pacific compared to the east ones. The convection over the Pacific intensifies and the trade winds blow stronger. This causes the warm water to remain confined in the occidental region, with higher than usual SSTs in the northern region of Australia as shown in Figure 2.3. On the contrary, waters in the western part of the pacific, become even cooler than usual, causing also a more marked thermocline (*Larkin and Harrison*, 2002; *Jin and An*, 1999). The up welling strengthens and the deeper waters are drawn to the surface enriching it of nutrients and enhancing the growth of marine organisms, with positive effects on fisheries and economies in the region (*Waluda et al.*, 2006). The main worldwide effects can be seen in Figure 2.6.

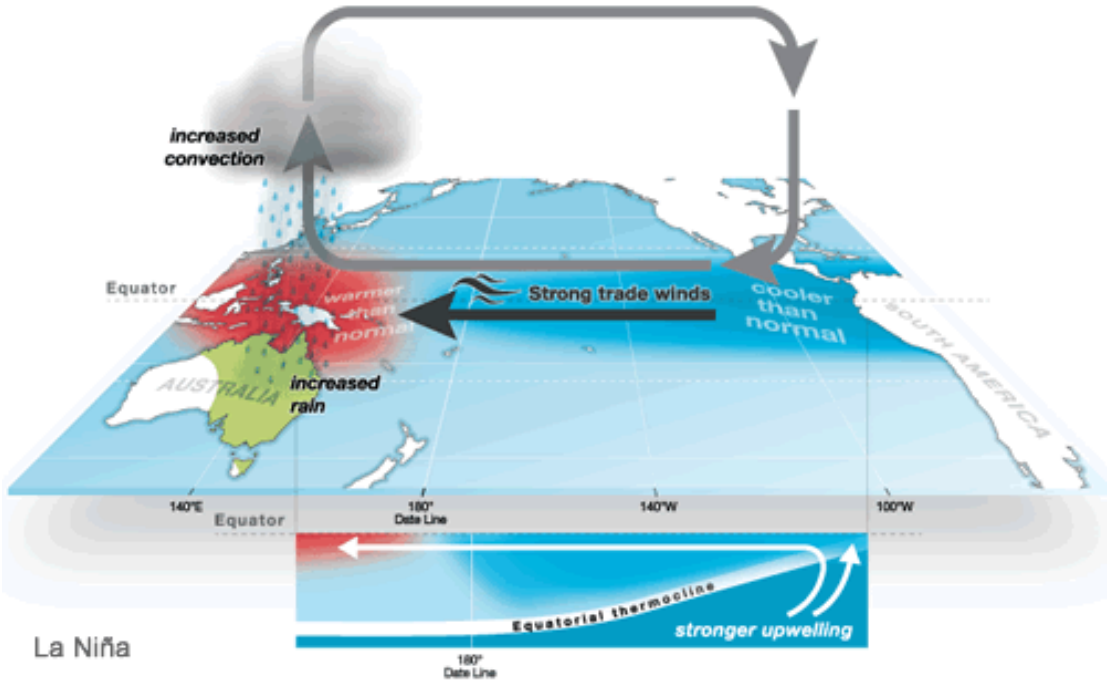


**Figure 2.3:** *Graphic representation of the effects of La Niña.*

ENSO is an irregular phenomenon, meaning that the timing of its occurrence cannot be predicted. It occurs on average every two to seven years, with El Niño more frequent than La Niña, and it typically lasts from nine to twelve months (or sometimes even longer during La Niña events). It shows its first signs of development during the Borealis spring and reaches its maximum strength during autumn and winter.
ENSO is known to have worldwide effects (Figure 2.5, 2.6) and has been studied for works concerning large parts of the world like for example in the United

States (*Ropelewski and Halpert*, 1986; *Harrison and Larkin*, 1998) , in Australia, South America, Africa (*Ropelewski and Halpert*, 1987) , in Australia and New Zealand, South and Central America (*Chiew and McMahon*, 2002) , in Vietnam (*Beltrame and Carbonin*, 2013), in China (*Zhang et al.*, 1999) , in Europe (*Hafez*, 2017) and worldwide (*Terray et al.*, 2016; *Veldkamp et al.*, 2015; *Ward et al.*, 2014). ENSO effects are not limited to hydrological variables but also impacts directly other important processes, like for example the way it affects the fish populations on the coasts of South America (*Sandweiss et al.* (2004),*Fiedler* (2002)).

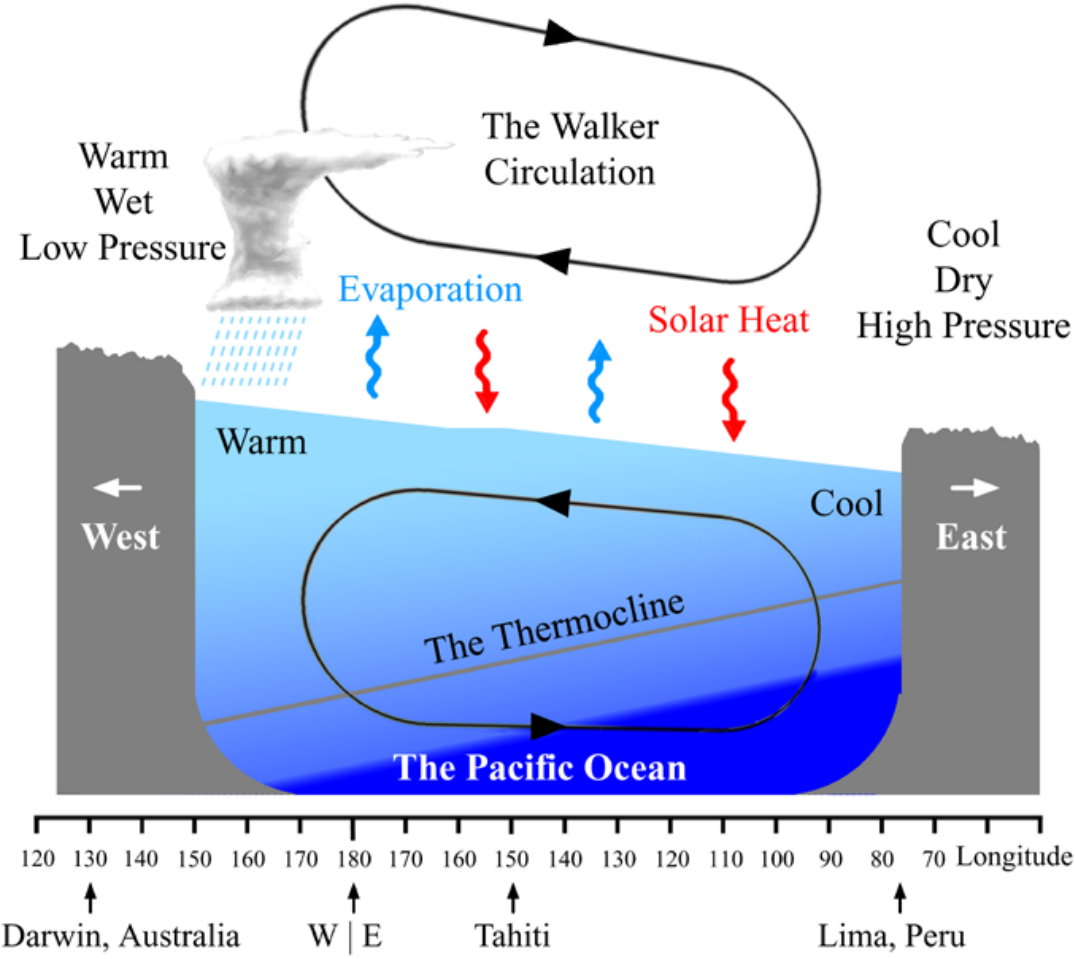


**Figure 2.4:** *ENSO neutral year and Walker circulation.*

#### ENSO indexes

Many indexes are available to analyse and assess ENSO. The most used is the Southern Oscillation Index (SOI), computed as the difference in sea level pressure between Tahiti (French Polynesia) and Darwin (Australia) (*Chen*, 1982). Other indexes are the Sea Surface Temperature (SST) index, which relies on

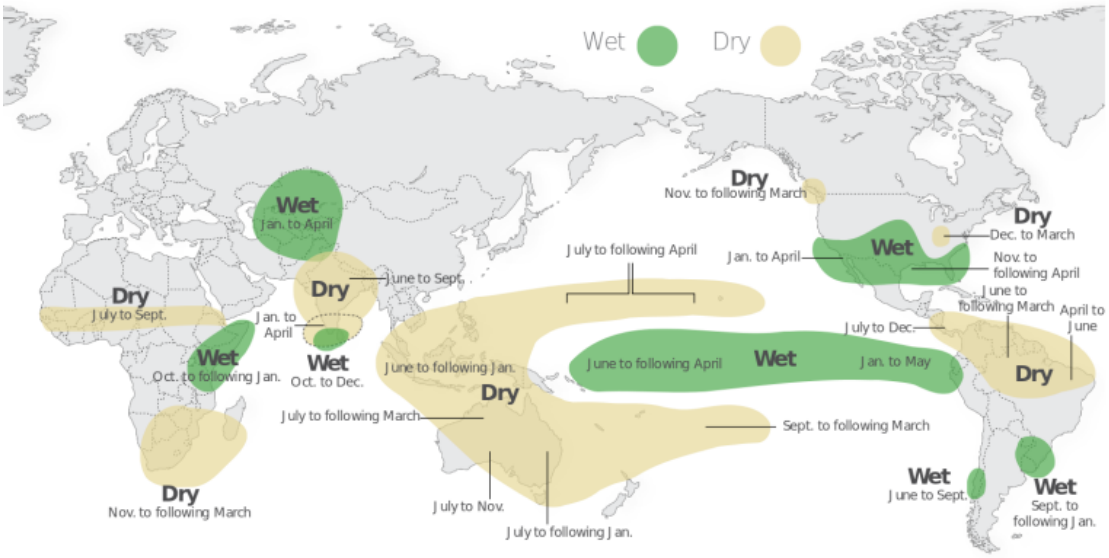


**Figure 2.5:** *Map of the worldwide best known effects of El Niño on precipitations.*

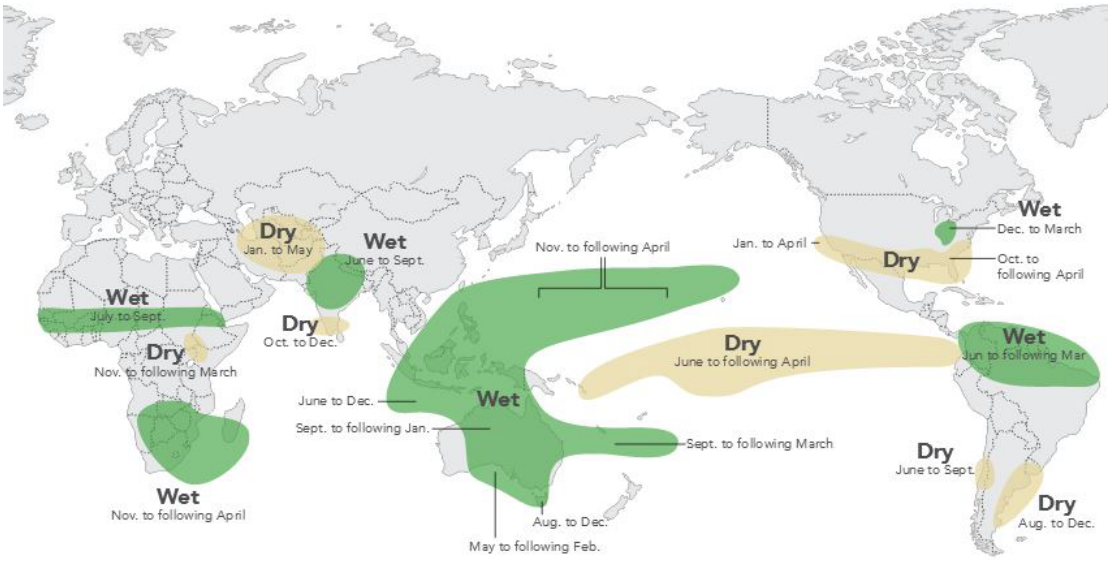


**Figure 2.6:** *Map of the worldwide best known effects of La Niña on precipitations.*

the difference of sea temperature in some specific area of the Pacific Oceans and the Multivariate ENSO Index (MEI). There is no consensus in the scientific community over which of them best represents ENSO years, or the strength or duration of events (*Hanley et al.*, 2003).
For this thesis however, due to the overall good performances, the Multivariate ENSO Index (MEI) was used. Its calculation is based on 6 variables:

1. Sea level pressure;

2. Zonal component of the surface wind;
3. Meridional component of the surface wind;
4. Sea surface temperature;
5. Surface air temperature;
6. Total cloudiness fraction of the sky.

Observations for these data have been collected and published by the Comprehensive Ocean-Atmosphere Data Set for a long period and have then been used by *Wolter and Timlin*, *Wolter* (1993) and *Wolter and Timlin* (1998) to formulate the index. It is calculated twelve times per year, for each sliding bi-monthly season, characterized as January-February, February-March, March-April, and so on. In the index, positive values correspond to the El Niño phase, while negative ones to La Niña. This indicator was chosen because it is one of the most accurate in all the fields due to the use of six different variables and because of the long timeseries of available data.

### 2.2.2 NAO

The North Atlantic Oscillation (NAO) is the most prominent and recurrent pattern of atmospheric variability in the middle and high latitudes of the Northern hemisphere (*Hurrell et al.*, 2003). It is an atmospheric circulation pattern localized in the North Atlantic ocean, characterized by a cyclic oscillation of the difference of pressure at sea level between Iceland and the Azores islands. Trough the oscillation motion east to west of the Iceland depression and the anti-cyclone of the Azores, NAO determines the strength and direction of the occidental zonal flow and the direction of the perturbations all over the northern Atlantic (*Hurrell*, 1995; *Hurrell and Van Loon*, 1997; *Hurrell*, 2005). Unlike ENSO, NAO is a teleconnection with only a strictly atmospheric component and doesn't have a corresponding oceanic water flow.
In neutral conditions, the occidental winds, called westerlies, flow trough the Atlantic, bringing wet air over the European continent. When the winds blow strongly, the summers of the affected areas are cool and the winters mild and wet. Instead, when winds are weaker, the temperatures become more extreme, higher in the summer and lower in winter, and the precipitations diminish. These winds are caused by a semi-permanent system of low pressure over Iceland (namely, Iceland Depression) and high pressure over the Azores (namely, Anti-Cyclone of the Azores). The relative strength and position of the two, regulates the intensity and direction of the Westerlies.

This pattern is mostly observable during the Boreal cold season and does not only control winds speed and direction, but also air temperatures, heat and moisture transports and precipitation. The Atlantic ocean is also affected, in terms of temperature and salinity characteristics of the water, vertical mixing, circulation patterns and, at higher latitudes, ice formation.

Based on the state of NAO, two possible conditions can be found: NAO positive (NAO+) and NAO negative (NAO-) with opposite effects (Figure 2.7).

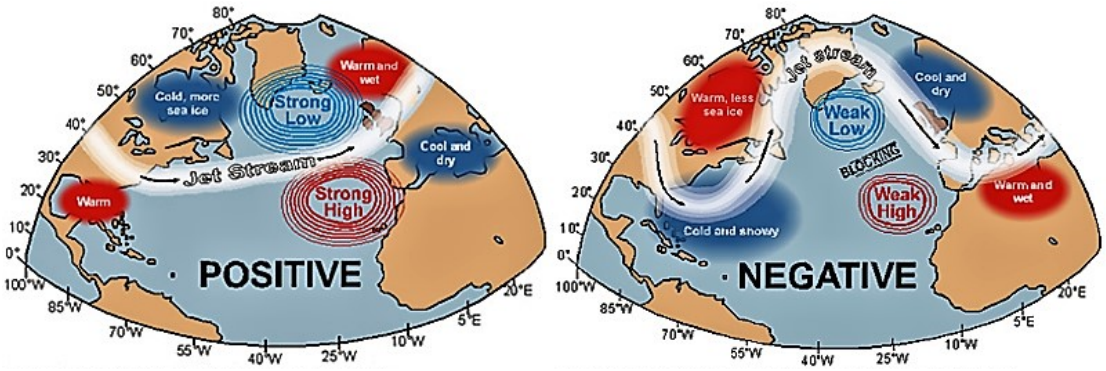


**Figure 2.7:** *Map of the different effects of NAO+ and NAO- phases.*

In particular, when the Icelandic low and Azores' high pressure fields are enhanced, the system enters the NAO+ phase. The significant pressure differences between the two centres strengthens the Westerliesand produces effects (see Figure 2.8):

- The temperatures over eastern North America and across Northern Europe are higher than in neutral years (*Folland et al.*, 2009);
- The temperatures over Greenland and sometimes Southern Europe and Middle East tend to get lower (*Vicente-Serrano and Trigo*, 2011; *Trigo et al.*, 2004);
- There is a precipitation increase over Northern Europe and Scandinavia during winter(*Uvo and Berndtsson*, 2002; *Uvo*, 2003; *Bierkens and Van Beek*, 2009);
- There is a precipitation decrease over Southern and Central Europe (*Rodó et al.*, 1997; *Castro-Díez et al.*, 2002).

Conversely, when the Icelandic low and Azores' high pressure fields are weakened, the system enters the NAO- phase. A decrease in the gradient of

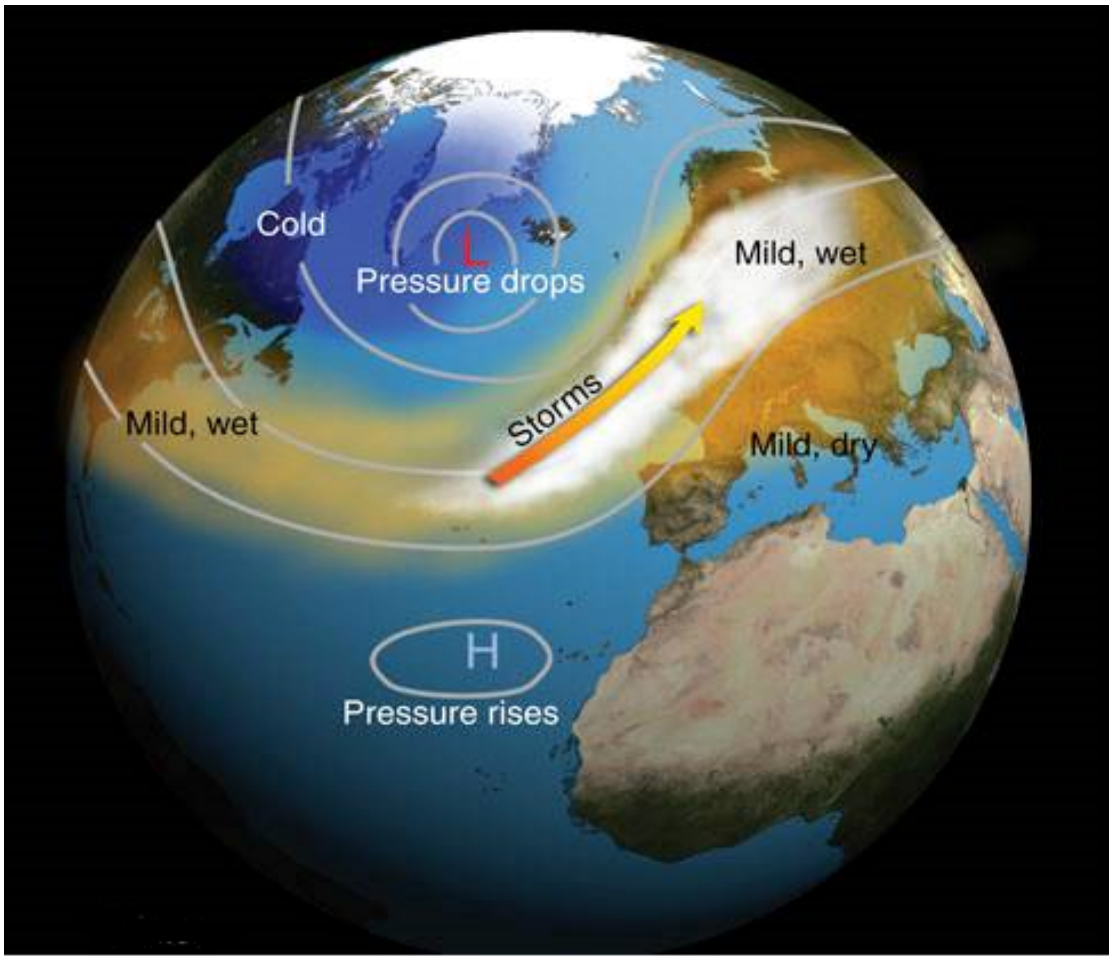


**Figure 2.8:** *Map of the effects of NAO+ phase.*

pressure between the two centres can be observed, weakening or even stopping the Westerlies. The effects are opposite to those in the NAO+ phase (see Figure 2.9):

- A decrease of temperature can be observed in North America and Northern Europe(*Bojariu and Paliu*, 2001);
- An increase of temperature in Greenland, Southern Europe and middle east (*Kahya*, 2011; *Cullen et al.*, 2002);
- More precipitations on meridional and central Europe(*Vicente-Serrano and Trigo*, 2011);
- Less precipitations over Northern Europe and Scandinavia (*Uvo and Berndtsson*, 2002; *Rogers*, 1997; *Nesje et al.*, 2000).

By altering climatological variables, NAO is also responsible for other documented related effects, e.g. on European ecosystems (*Gordo et al.*, 2011; *Stenseth*

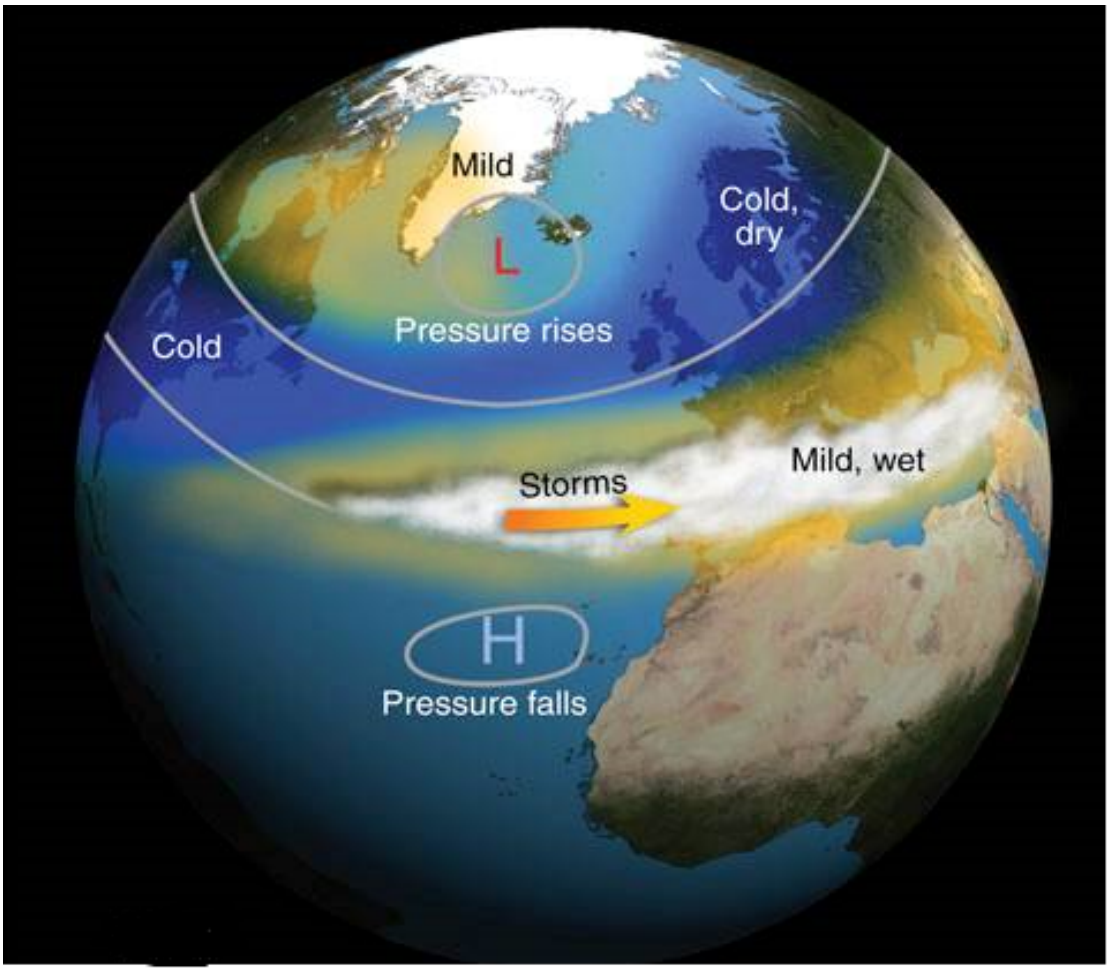


**Figure 2.9:** *Map of the effects of NAO- phase.*

*et al.*, 2003), fisheries in the Mediterranean sea (*Maynou*, 2011), crop production (*Orlandini et al.*, 2011) and even pollution on the Mediterranean basin (*Dayan*, 2011).

#### NAO index

The index utilized to measure the state of NAO is computed as the difference the difference between the normalized mean winter (from December to March) Sea Level Pressure anomalies at Lisbon, Portugal and Stykkisholmur, Iceland (*Hurrell and Van Loon*, 1997). The stations were changed from those used before, (Ponta Delgada, Azores and Akureyri, Iceland) (*Walker*, 1932) to get 30 additional years of data, starting from 1864.

## 2.3 ENSO and NAO impacts on Alps

The effects of ENSO and NAO have been widely studied, like for example in America and Australia (*Holmgren et al.*, 2006), in the USA (*Harrison and Larkin*, 1998), in Indonesia, Philippines and El Salvador (*Harger*, 1995), in Mexico (*Pavia et al.*, 2006), in the Fenno-Scandic region (*Uvo*, 2003), worldwide (*Diaz and Markgraf* (2000) *Stenseth et al.* (2003); *Wanner et al.* (2001), in Europe (*Rodwell et al.*, 1999)). However, not many works cover the Alpine region. Studies concerning ENSO effects, in particular, are few and often with conflicting results.
A number of studies have investigated the correlation between NAO phases and the snow in the Alpine region. All the studies agree that NAO has a certain influence on its quantity and melting but there is no agreement on how much does it really affect the process, with some stating that it is an overall large one (*Beniston* (1997); *Scherrer et al.* (2004); *Steirou et al.* (2017)) and others arguing that its role is marginal (*Durand et al.* (2009); *López-Moreno et al.* (2007, 2011)). In particular, the negative phase of NAO, (associated with higher temperatures and precipitations in Southern Europe), seem to transform most of the precipitations in rain (particularly during winter) and accelerate the melting, while the positive NAO phase is characterised by more precipitations under the form of snow and a slower melting due to lower temperatures.
The studies considering ENSO generally define its role as marginal (*Steirou et al.*, 2017; *Durand et al.*, 2009). Other studies investigate correlations between NAO and ENSO phases with different climatic signals, precipitation and temperature in particular (*Wanner et al.*, 2001). Regarding this, the results have been different and sometimes contrasting, with some affirming that the effects are overall negligible for both teleconnections (*Casty et al.*, 2005; *Bartolini et al.*, 2009; *Shaman*, 2014), with ENSO in particular not having any role (*Efthymiadis et al.*, 2007), while other studies observed significant correlations on the area (*Bojariu and Paliu*, 2001; *Beniston*, 2005a,b; *Folland et al.*, 2009; *Brandimarte et al.*, 2011).
Other works studied different aspects of the relations between ENSO, NAO and hydro-climatological variables in the Alpine region. Some authors studied the correlation with the streamflow and the floods of the rivers in the region, finding good correlation (*Bierkens and Van Beek*, 2009; *Callegari et al.*, 2015; *Nobre et al.*, 2017). Others investigated their connections in the zone with climate change and how it is expected to impact in the region's climate (*Beniston*, 2005b; *Rohrer et al.*, 2017). One study also investigated the correlation between ENSO, NAO and the glaciers fluctuations, finding that the temperature shifts caused by the different phases of ENSO and particularly of NAO play an important

role in determining the size of glaciers (*Vincent et al.*, 2005). Other studies focused on the correlation between ENSO, NAO and the frequency of winter storms (*Kamil et al.*, 2017) or renewable (hydroelectric, solar and wind) energy production in the Alpine area (*François*, 2016), summer heat waves (*Hafez*, 2017) or crop anomalies (*Ceglar et al.*, 2017).
To sum up, despite a lack of agreement on the intensity, it is reasonable to conclude that there exist a relation between many hydro-climatological variables in the area and the two considered teleconnections.

## 2.4 Use of ENSO and NAO for reservoir operations

Information coming from ENSO and NAO has already been used in many cases to improve the forecasts for hydrological variables, while only few studies use this information for making better operational decisions. As far as the forecasts are concerned, the most common procedure is to use the state of the signal (i.e., El Nino or la Nina, NAO+ or NAO-) as an input in a hydrological model (*Sharma*, 2000; *Beltrame et al.*, 2014). Successful examples include the use of ENSO in North America, such as in Colorado (*Pulwarty and Melis*, 2001), Texas (*Chen et al.*, 2005) Florida (*Abtew and Trimble*, 2010), Canada (*Sellars et al.*, 2008). Additional applications were developed in Australia (*Simpson et al.*, 1993; *Everingham et al.*, 2012), China (*Wei et al.*, 2014), Iran (*Banihabib et al.*, 2017), India (*Robertson et al.*, 2013; *Maity and Nagesh Kumar*, 2009), Sri Lanka (*Chandrasekara et al.*, 2017; *Chandimala and Zubair*, 2007), Ecuador (*Gelati et al.*, 2014), Brasil (*Bouvy et al.*, 2003), Uganda and Nigeria (*Phillips and McIntyre*, 2000). An interesting case is that of Ghana, where the state of ENSO is used not only for climatological variables prediction, but also for optimal management of the reservoir and of the agricultural system, meaning that what to plant is decided also on the expected state of ENSO that year (*MacCarthy et al.*, 2017). Similarly, (*Turner and Galelli*, 2016) used a regime state variable for informing water release decisions and to quantify the potential gains in operating performance that could be obtained by allowing for regime-shifting behaviour in reservoir inflow, namely when the distribution of the streamflow shifts in concert with an unobserved (climate) state, such as ENSO. At the global scale, ENSO was demonstrated to impact more than 30% of hydropower dams, even though the variability in power production tends to be less than that of the forcing inflows (*Ng et al.*, 2017).
Finally, some cases are present also in Europe, where the main signal considered is NAO along with ENSO. That's for example the case of Spain , where ENSO and NAO are used to make forecast for the precipitations (*López-Moreno*

*et al.*, 2007, 2011; *López and Francés*, 2013). But, regarding Italy or the considered region, apart from the work by *Samale et al.* (2017), there are no works considering information coming from ENSO or NAO to enhance the management of hydrological systems.

# 3

# Methods

This chapter provides the methodological context for this thesis, by detailing the methods and tools employed. Figure 3.1 shows the main components of the proposed framework. Each of the sections is devoted to the description of one of the flowchart blocks.
In particular, section 3.1 searches the most relevant climate teleconnections for the selected river basin by means of Niño Index Phase Analysis (NIPA), developed by (*Zimmerman et al.*, 2016).
Section 3.2 combines the results of NIPA detection into a Multi-Variate model, to get seasonal rainfall forecast. The model structure is selected by comparing the performances of three different structures (linear model, Artificial Neaural Networks and Extreme Learning Machine).
Then in section 3.3, hydrological forecasts are obtained from the seasonal rainfall forecast. The step requires the forecast to be first downscaled in time (from seasonal rain to daily) and then transformed into streamflow.
Finally, section 3.4 illustrates the Evolutionary Multi-Objectives Direct Policy Search (EMODPS) algorithm, used for the design of Lake Como control policy.

## 3.1 Detection of climate teleconnections

Teleconnection signals are recurring and persistent large scale patterns of pression and circulation anomalies that interests large areas. As seen in chapter 2, they influence hydrology also at the local scale, so they can represent a valuable information for water management.

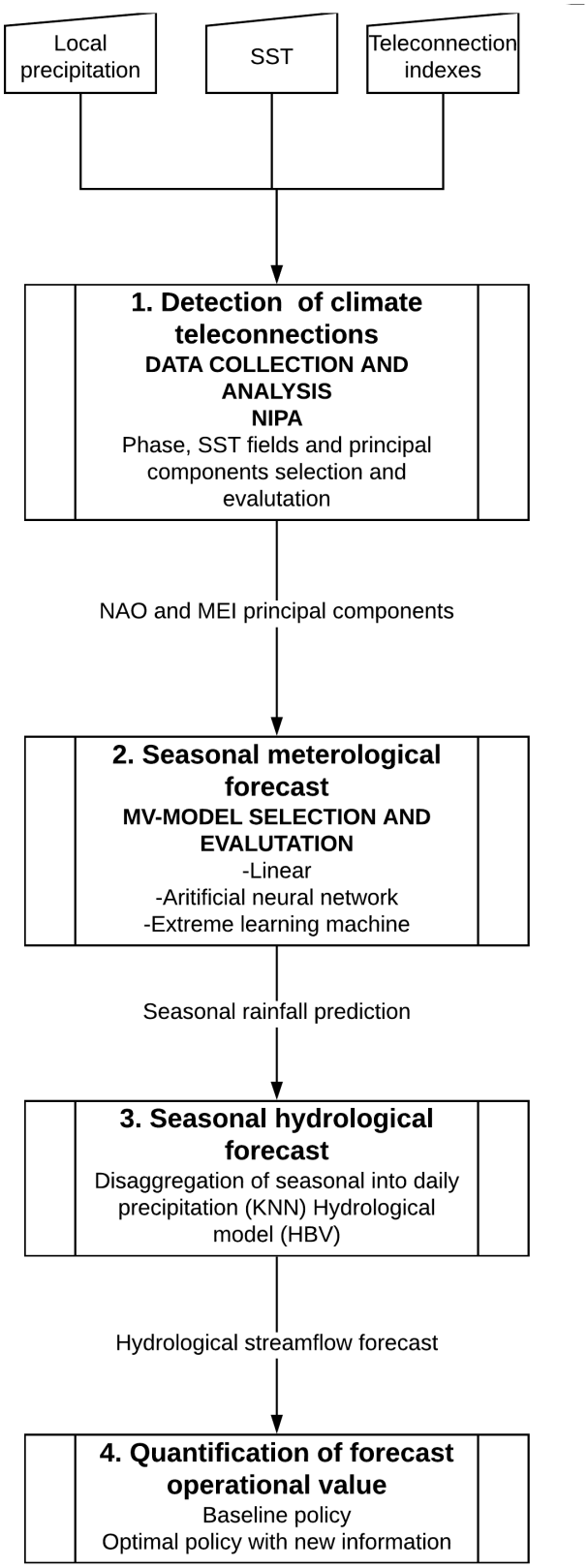


**Figure 3.1:** *Thesis flowchart.*

The following section analyses the influence of ENSO and NAO for the selected study case, using the Niño Index Phase Analysis (NIPA).
Most of the traditional approaches use just an index of the current phase of the teleconnection as a single input for a single model to improve the forecast. The peculiarity of NIPA is instead of using it as a physical influence of the average state of the atmosphere-ocean system (*Zimmerman et al.*, 2016). This allows using information that wouldn't be considered otherwise, possibly resulting in a skill improvement for the seasonal forecast.

### 3.1.1 Data collection and analysis

The first step is to decide which variable to predict and to find the most informing teleconnections to use for the forecast models. Following the work from (*Samale et al.*, 2017), already based on the same system, we decide to use precipitations as the variable to predict and ENSO and NAO as climate signals.

### 3.1.2 NIPA

The Nino Index Phase Analysis, NIPA for short, is a statistical framework for seasonal forecast, originally based on the state of ENSO. Its main steps can be seen in Figure 3.2. The main idea behind the method, is to bin the considered periods into different phases, based on the state of the selected climate signal, using an index. After that, phase-specific Sea Surface Temperature (SST) correlated cells are identified to be used as predictors in a Principal Component Regression (PCR) model.

The first step is to bin the considered time periods into different phases according to one climate signal index. This is done because the occurrence of large-scale climate events is associated with hydro-climatic anomalies that are expected to alter the mean state of the atmospheric oceanic system and those changes can be caught by some indexes (*Block and Rajagopalan*, 2007; *Block*, 2016). Based on the considered index, like for example the MEI index for ENSO, it is possible to classify a time period. An example of it can be seen in Table 3.1, where January, February and March (JFM) months of the years from 1896 to 2014 are classified in different Nino phases based on the value of the MEI index.

In order to make NIPA a predictive model, the climate index is observed in the season prior to the one that has to be predicted, and the period is classified on its value. For example, to have a January, February and March prediction (JFM), the average value of the index from October, November and December

**Table 3.1:** *Binning of January, February and March period for years from 1896 to 2014 in ENSO phases, using MEI index (NOAA elaboration).*

| El Nino | Neutral | La Nina |
|---|---|---|
| 1897 | 1896 | 1904 |
| 1900 | 1898-1899 | 1909 |
| 1903 | 1901-1902 | 1910 |
| 1906 | 1905 | 1911 |
| 1915 | 1907-1908 | 1917 |
| 1919 | 1912-1914 | 1918 |
| 1926 | 1916 | 1925 |
| 1931 | 1920-1924 | 1934 |
| 1941 | 1927-1930 | 1939 |
| 1942 | 1932-1933 | 1943 |
| 1958 | 1935-1938 | 1950 |
| 1966 | 1940 | 1951 |
| 1973 | 1944-1949 | 1955 |
| 1978 | 1952-1954 | 1956 |
| 1980 | 1957 | 1962 |
| 1983 | 1959-1961 | 1971 |
| 1987 | 1963-1965 | 1974 |
| 1988 | 1967-1970 | 1976 |
| 1992 | 1972 | 1989 |
| 1995 | 1975 | 1999 |
| 1998 | 1977 | 2000 |
| 2003 | 1979 | 2008 |
| 2007 | 1981-1982 | 2011 |
| 2010 | 1984-1986 | 2012 |
| | 1990-1991 | |
| | 1993-1994 | |
| | 1996-1997 | |
| | 2001-2002 | |
| | 2004-2006 | |
| | 2009 | |
| | 2013-2014 | |

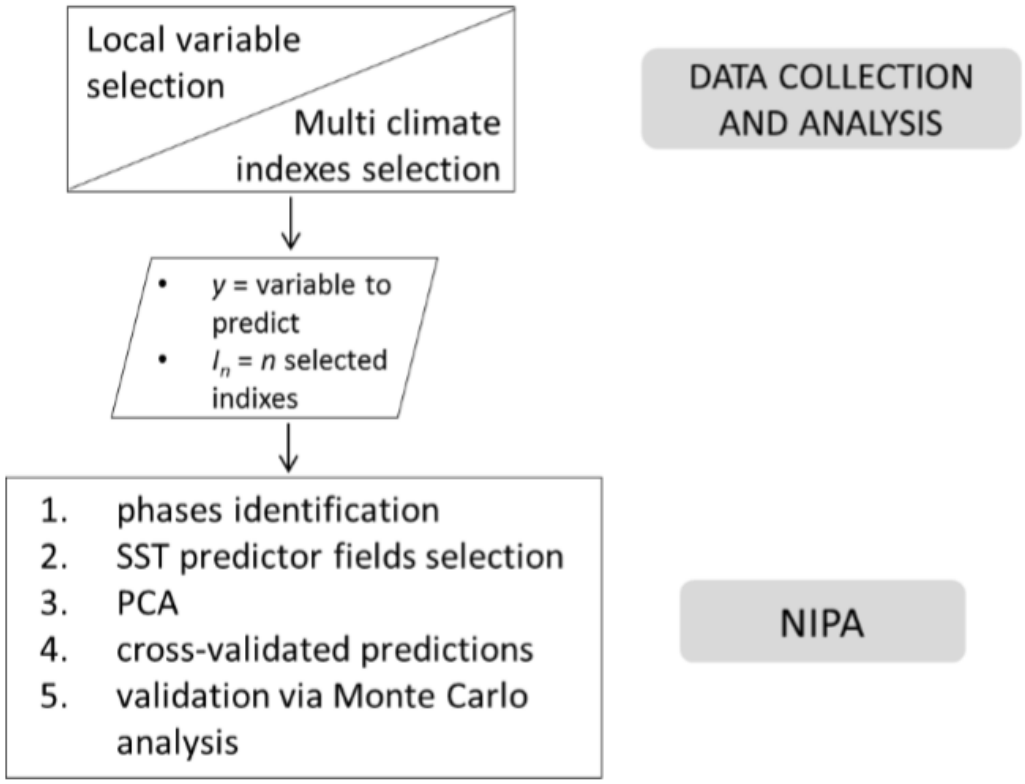


**Figure 3.2:** *NIPA procedure scheme.*

(OND) is used. The period is characterized using a percentile threshold defined on the basis of how many different phases are to be identified, i.e. the $50^{th}$ percentile can be used as threshold to bin the years into the two different phases (positive and negative). As a result of the process, all the considered time periods are binned into the two different phases.

After classifying the considered time periods in different phases, each phase is evaluated individually, thus constructing as many predictive models as the number of the phases.
The first step of the modelling procedure consists in identifying the most significant SST predictor regions. For this purpose, correlation maps between the seasonal mean of the local hydroclimatic variable and pre-season gridded SST anomalies are used, and regions correlated at the 95% significance level for each phase are identified.
After identifying the SST predictor regions, a Principal Component Analysis (PCA, see *Joliffe* (2002)) is conducted on the entire predictor field and the first $m$ resulting Principal Components (PCs) are retained as predictors in the fore-

cast model. In this work, we considered only the first Principal Component for each phase ($PC_1$), because it explains most of the variance in the selected SST gridpoints. The forecast model is defined as follows:

$$\hat{y} = \beta * PC_1 + \alpha \tag{3.1}$$

where $\hat{y}$ is the estimated local hydroclimatic variable (i.e., season precipitation), $\beta$ the regression coefficient, and $\alpha$ the intercept. A leave-one-out cross-validation procedure is then applied to the model obtained from eq. 3.1 to avoid model overfitting and improving the statistical significance of the results. The predicted values and the observations are contrasted by using as evaluation metric the Pearson correlation coefficient, calculated as in formula 3.2:

$$r = \frac{\sum_{i=1}((x_i - E[x_i])(y_i - E[y_i])}{\sqrt{\sum_{i=1}((x_i - E[x_i])^2)\sum_{i=1}(y_i - E[y_i])^2}} \tag{3.2}$$

Lastly, a Monte Carlo test is performed to verify that the obtained results are statistically significant at a high level of confidence.

## 3.2 Multi variate seasonal meteorological forecast

The second step of the framework in Figure 3.1 combines the results of NIPA detection into a multivariate model.
The results of the NIPA detection procedure described in the previous section allow identifying for the selected climate signals the SST fields that produce the best results in terms of prediction accuracy (i.e., high values of the Pearson correlation coefficient at high level of confidence). These outputs are then combined into a multivariate prediction model to exploit all the information provided by the two different climate signals.
For the first step, the values of the climate indexes associated to the selected signals are used for binning the years in "meta-phases", combinations of the original phases distinguished for each index. To better understand the procedure, we consider two teleconnections. One is $\tau^i$ , whose phases can be 1 or 2, and $\tau^j$, whose phases are a and b. The procedure classifies each period based on its $\tau^i$ and $\tau^j$ signals phase. So, one period can either be $\tau^i_1$ and $\tau^j_a$, $\tau^i_1$ and $\tau^j_b$, $\tau^i_2$ and $\tau^j_a$ or $\tau^i_2$ and $\tau^j_b$. The way it is done for this thesis can be seen in Table 3.2. At the end of this step, each considered time period is associated with a meta-phase.

After the definition of the metaphases, models are built for next season's precipitation forecast. Three alternative models are explored: linear, Artificial Neural Networks (ANNs) and Extreme Learning Machines (ELMs).
To obtain the parameters while limiting the possibility of over-fitting and over-parametrization, a leave-one-out cross-validation is used for all models. The leave-one-out is a particular kind of cross-validation where only one value at a time is excluded from the calibration set and is used for validation (*Kohavi et al.*, 1995; *Refaeilzadeh et al.*, 2009). By doing so, the dataset is split in a number of folds equal to the number $n$ of the input data. For $n$ times, the model is trained on all the data minus one sample, which is used for the model validation. The value of the performance is then calculated as the average of all the different validation step performed.

The first considered model is the linear one. Four equations as eq. 3.3, are calibrated for each meta-phase, and used to calculate the value of the total seasonal precipitation.

$$Y = a \times PC_{mei} + b \times PC_{nao} + c \tag{3.3}$$

Where: Y is the predicted rainfall, a and b are the coefficients that multiply MEI and NAO PCs, varying depending on the metaphase, and c is a metaphase specific constant.

The second class of model is the Artificial Neural Networks (ANNs), first introduced in 1943 by *McCulloch and Pitts* (1943), are simplified mathematical models of how the human neurons work (*Abraham*, 2005; *Ranković et al.*, 2010). They work by processing an input through a series of non-linear, sigmoidal, functions (equal to the number of neurons), with a shape depending on their parametrization. Then, through a function which gives a weight to each neuron, the output of each of them is added to get the final result (Figure 3.3). The universal approximation theorem, firstly demonstrated by *Cybenko* (1989) says that "A feed forward network with a single hidden layer containing a finite number of neurons (i.e. a multi-layer perceptron) can approximate any kind of continuous functions on compact subsects of $R^n$, under mild assumptions on the activation function". So ANNs appear particularly apt at reproducing the inner complex non-linear connections between the variables of this problem.

The formulation of the ANN is the following (eq. 3.4):

$$Y = ANN(PC_{mei}, PC_{nao}, Mph) \tag{3.4}$$

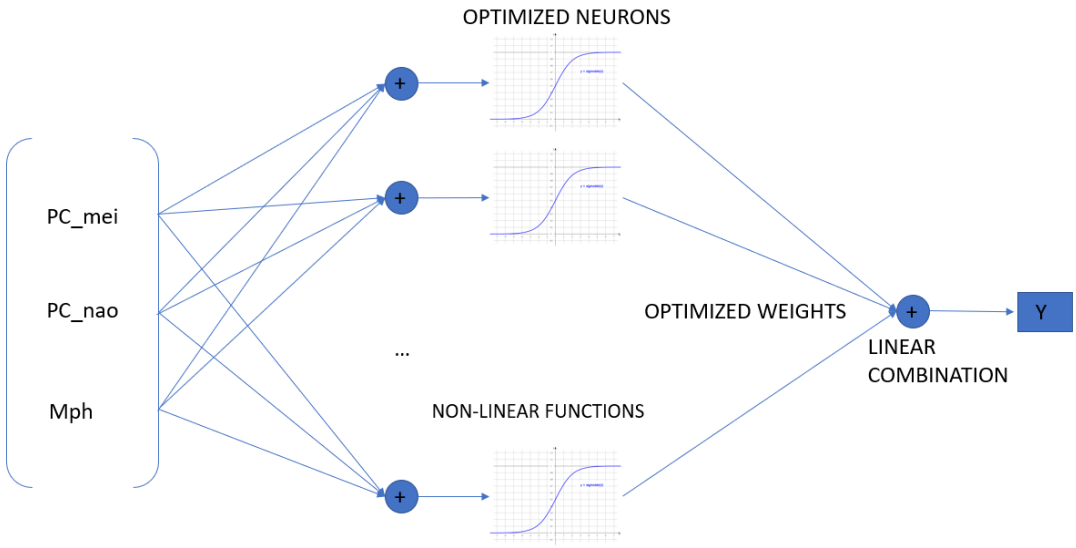


**Figure 3.3:** *ANNs' scheme.*

**Table 3.2:** *Mph vector building*

| MEI phase | NAO phase | Mph |
|---|---|---|
| 1 | 1 | 1 |
| 1 | 2 | 2 |
| 2 | 1 | 3 |
| 2 | 2 | 4 |

where Mph indicates the metaphase of the considered season, as reported in Table 3.2.

The last model class is Extreme learning machines (ELMs), an evolution of ANN models. ELM models only need to calibrate the weights vector of the output layer, while the neurons are randomly parametrized (Figure 3.4). This means that only the weights for the random neurons are adjusted to fit the model , resulting in a lower computational effort with an equal number of neurons(*Huang et al.*, 2004). ELMs are demonstrated to be faster and to have generally better performances in reproducing data and better generalization performance than ANNs (*Huang et al.*, 2006).

The ELMs are formulated as follows:

$$Y = ELM(PC_{mei}, PC_{nao}, Mph) \tag{3.5}$$

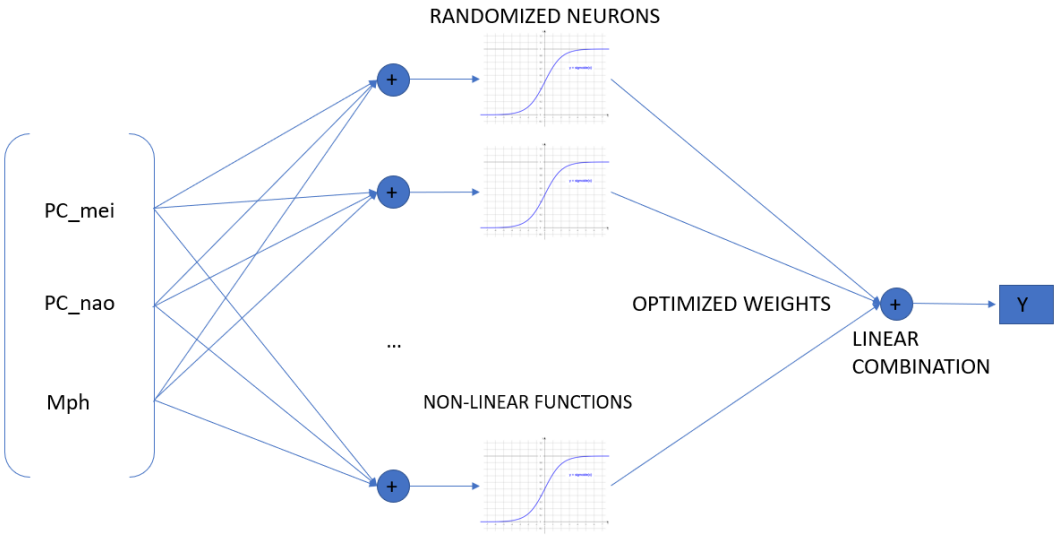


**Figure 3.4:** *ELMs' scheme.*

## 3.3 Seasonal hydrological forecast

The third step of the framework illustrated in Figure 3.1 transforms the meteorological forecast produced by the MV models described in the previous section to hydrological forecasts. This step first requires the disaggregation of the predicted seasonal precipitation to a temporal resolution, suitable for running a hydrological model. In particular, the disaggregation is performed via k-Nearest Neighbour (KNN) (*Nowak et al.*, 2010) and the hydrological processes are reproduced by means of a Hydrologiska Byrans Vattenbalansavdelning (HBV) model.

### 3.3.1 Daily disaggregation - k-Nearest Neighbour (KNN)

The k- Nearest Neighbour is a downscaling technique used to derive information at fine spatial and/or temporal scale, starting from aggregated data. In this thesis we employ KNN to disaggregate seasonal precipitation into daily amounts.
The algorithm works by comparing predicted and historical precipitations. The daily observed rainfall data are summed into seasonal rain data $R_{season} = \sum R_{day}$. After that, daily values are divided by the seasonal total for each year $w^{i,j} = R^{i,j}_{day}/R_{season}$, obtaining a weight matrix, where each column represents the

same season for each year, and each row is a day of the considered season. Each cell contains the percentage of rain, compared to the total seasonal one, that has fallen on that day.

The predicted seasonal rainfall series are then compared to the observed ones, and the k most similar among the observed ones are chosen for each predicted value.
The daily sequence is derived by randomly extracting one proportion vector from the k candidates, with a probability of extraction that depends on the candidate ranking as follows:

$$P(j) = \frac{1}{j} / \sum 1/j \tag{3.6}$$

The rank is given according to the Euclidean distance between seasonal predicted and observed precipitations, i.e.

$$dist = |R_{pred} - R_{real}| \tag{3.7}$$

Finally, the proportion matrix corresponding to the selected real year is multiplied for the value of the predicted seasonal total rain and thus the daily rain is obtained.
KNN method was chosen as it captures the observed statistics, is consistent with the correlation structures, and ensures summability and continuity across the daily time scale (*Rajagopalan et al.*, 1997).
The final output of this step is a forecast of daily precipitation.

### 3.3.2 HBV model

The daily forecasted rainfall is employed to feed a hydrological model of Lake Como basin, and finally obtain a prediction of daily inflow to Lake Como. The hydrological model used in this thesis is a hybrid physically-based and empirical model called Hydrologiska Byrans Vattenbalansavdelning (HBV)(*Bergstrom*, 1976). HBV (*Bergström*, 1992; *Lindström et al.*, 1997) is a model developed for operational flood forecasting in Sweden. Its working scheme can be seen in Figure 3.6. The model has four storage units, one for the snow and the other three for different ground layers. Each of them is treated as a reservoir with its own state (Figure 3.5), parameters (Figure 3.7), inputs and outputs.

Depending on the temperature, the precipitation can become a flow directly or be stored as snow, which later melts and becomes flowing water. The snowmelt and the rain then enter the soil moisture unit, where part of it is lost due to evapo-transpiration, calculated with the Hamon method (*Hamon*, 1960). The

| State | Description |
|---|---|
| *sowat* | soil water storage |
| *sdep* | snow store |
| *ldep* | depth of liquid in the snow store |
| *stw1* | soil storage - shallow layer |
| *stw2* | soil storage - deep layer |

**Figure 3.5:** *HBV states.*

remaining water transfers into the shallow layer storage unit. There, the water can take 3 paths:

1. Near Surface Flow: water that flows on the surface and is directly transformed into discharge

2. Interflow: intended as thorughflow, water lateral movement in the unsaturated zone (Vadose zone), that returns on the surface and becomes discharge.

3. Percolation: water that flows in the deeper layers of the ground.Percolated water reaches the deep layer storage, where it can either be stored or transformed into baseflow.

The sum of near-surface flow, interflow and baseflow gives the total discharge.

So, the final output of the HBV model is the discharge at the basin outlet, namely the inflow entering in the Lake Como.

## 3.4 Quantification of forecast operational value

After getting the streamflow predictions, the next step is to quantify their operational value in informing the system management.
To do that, the new information is used as input to the control policy adopted in the operations of the lake.
The comparison of the performance of policies informed with the forecast, and solutions which do not use such information, allows the quantification of the forecast operational value, by means of an appropriate indicator, namely the Hypervolume indicator.

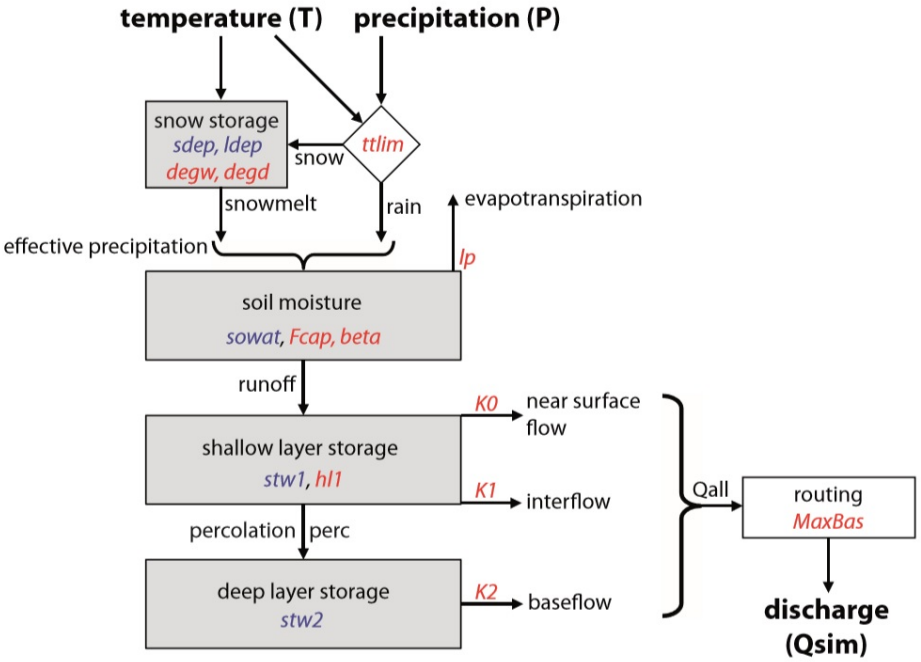


**Figure 3.6:** *HBV working scheme.*

| Parameter | Units | Description | Range |
|---|---|---|---|
| $K_2$ | [day] | withdrawal rate from deep layer | (10; 20,000) |
| $K_1$ | [day] | withdrawal rate for shallow layer overflow | (1; 100) |
| $K_0$ | [day] | withdrawal rate from shallow layer (interflow) | (0.5; 20) |
| $MaxBas$ | [hour] | length of hydrograph routing transformation | (24; 120) |
| $degd$ | [mm/(day °C)] | degree day factor (snowmelt rate) | (0; 20) |
| $degw$ | [°C] | base temperature above which melt occurs | (-3; 3) |
| $ttlim$ | [°C] | temperature threshold below which freezing occurs | (-3; 3) |
| $perc$ | [mm/day] | percolation rate into deep layer | (0; 100) |
| $\beta$ | [-] | distribution of soil stores | (0; 7) |
| $lp$ | [-] | limiting soil moisture at which PET takes place | (0.3; 1) |
| $F_{cap}$ | [mm] | maximum soil moisture storage | (10; 2,000) |
| $hl1$ | [mm] | maximum shallow layer storage | (0; 100) |

**Figure 3.7:** *HBV parameters.*

### 3.4.1 EMODPS

To design optimal operating policies for water reservoirs, Dynamic Programming (DP) is generally employed, in particular its stochastic extension (SDP) (*Bellman*, 1958; *Yeh*, 1985). SDP formulates the operating policy design problem as a sequential decision-making process, where a decision taken now produces an immediate reward, affects the next system state and, through that, all the subsequent rewards. The policies are searched employing value functions defined over a discrete (or discretized) state-decision space, obtained by looking at future events and computing a backed-up value.
SDP can help finding optimal solutions, but its application is limited by the presence of three curses. The first is the curse of dimensionality (*Bellman*, 1957), which states that the cost of SDP grows exponentially with the state vector dimensionality, meaning that only a limited number of states can be considered by it. The second is the curse of modelling: any information included into the SDP framework must be explicitly modelled to predict the one step-ahead model transition and ultimately the value function (*Tsitsiklis and Van Roy*, 1996). This means that no exogenous information can be added to the model, unless turned into a state variable of a dynamic model or a stochastic and time independent disturbance. The last curse is the curse of multiple objectives (*Powell*, 2007): multiple contrasting objectives requires to generate a set of non-dominated alternatives, i.e., a Pareto front.
These three curses limit the possibility of using SDP on complex systems, but, in recent years new methods have emerged.

In this thesis, to design the optimal control policies for the Lake Como operations, we use an Evolutionary Multi-Objective Direct Policy Search (EMODPS) methos (*Giuliani et al.*, 2015). EMODPS replaces the traditional SDP approach based on the computation of the value function, with a simulation based optimization that directly operates in the policy space (*Giuliani et al.*, 2017). EMODPS explores the parameter space $\Theta$ seeking the best parameterization for the operating policy $p_\theta$, defined within a given family of functions. The parameters are chosen in order to optimize the expected longterm cost defined by the objectives of the problem, formulated as in equation 3.8:

$$P_\theta^* = arg \min_{P_\theta} J(P_\theta, x_0, \epsilon_1^h) \tag{3.8}$$

Finding $p_\theta^*$ corresponds to finding the best parameters $\theta^*$ for the class of policy $p_\theta$, measured by the objectives J. Figure 3.8 shows a scheme of the algo-

rithm.

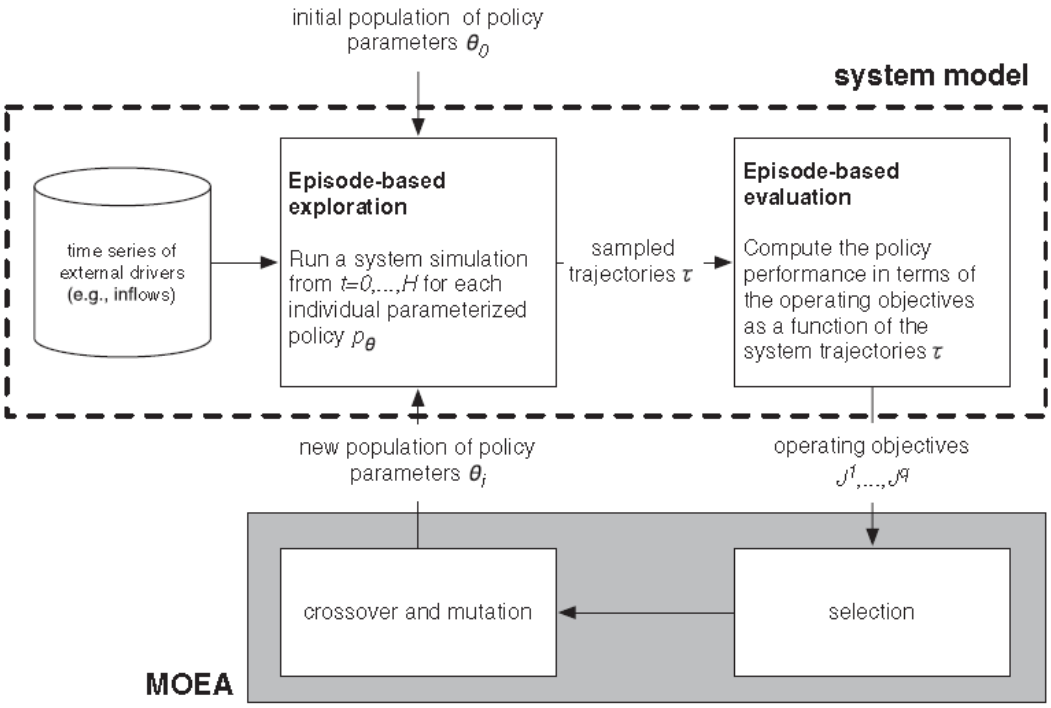


**Figure 3.8:** *Schematization of EMODPS approach. The dashed line represents the model of the system and the gray box the MOEA algorithm (Giuliani et al., 2015).*

EMODPS boasts a simulation-based nature, meaning that the variables do not need to be discretized and the value of the function computed. This way, it is possible to overcome the curse of dimensionality and the biases introduced by the discretization of continuous variables (*Baxter and Bartlett*, 2001). It is also possible to introduce exogenous information or models, avoiding this way the curse of modelling (*Giuliani et al.*, 2015; *Denaro et al.*, 2017). Finally, the combination of DPS with the MOEA framework, allows producing an approximation of the Pareto front for up to 10 objectives, thus avoiding in most cases the curse of multiple objectives (*Giuliani et al.*, 2014a).

EMODPS finds the optimal set of parameters for a given function to maximize the performance given one or more objectives. So, what it does, is finding the best solution inside a given class of functions. If the system is already being operated, the class of function can be extrapolated from that already in use, but there is no guarantee that the manager is already using the most efficient one. If there are no data, or the system is under construction, the policy structure must be guessed a priori on the base of empirical evaluations. When guessing the structure, is important for it to be flexible and highly adaptable to any sys-

tem, in order not to end up with a not efficient one. So, a very flexible class of functions, with many parameters to be calibrated is advised. In this case we use a Radial Basis Function (RBF) (*Zoppoli et al.*, 2002). A three layers RBF has been demonstrated to be able to approximate any continuous function defined on a closed and bounded set (*Park and Sandberg*, 1991; *Chen and Chen*, 1995).The superiority of RBF for the role over other approximators, such as ANN, has been demonstrated (*Giuliani et al.*, 2014b). It has also been demonstrated that they work particularly well when exogenous information is used directly to condition the operations

For the optimization step, we use the Multi-Objective Evolutionary Algorithms (MOEA) framework, which work by mimicking biological systems, allowing them to better adapt to multi-objective problems characterized by multimodality, nonlinearity, stochasticity, and discreteness (*Maier et al.*, 2014). MOEAs are proven to better handle performance uncertainties than gradient-based methods (*Busa-Fekete et al.*, 2014). We use a the self-adaptive Borg Multi-Objective Evolutionary Algorithm (MOEA) to perform the optimization (*Hadka and Reed*, 2013). Borg procedure is highly robust in solving multi-objective optimal control problems, where it met or exceeded the performance of other state-of-the-art MOEAs (*Salazar et al.*, 2016).

### 3.4.2 Value of exogenous information

EMOPDS allows to condition the designed operating policy with exogenous information. The operational value of exogenous informations can be evaluated as the difference between the performance achieved relying on a policy based only on traditional information Baseline Operating Policy (BOP), the one found with the additional ones Informed Operating Policy (IOP) and the one calculated assuming to have perfect forecast, the Perfect Operating Policy (POP).

There are many metrics that could be used (*Zitzler et al.*, 2003; *Maier et al.*, 2014), but for this thesis, we choose to evaluate the performance improvement gained trough the use of exogenous informations by using the hypervolume (HV). It captures the convergence and distance of the IOP and BOP Pareto front $F$ and the optimal one $F^\star$ over the whole trade-offs in the objective space (*Zitzler et al.*, 2003). HV varies from 0 to 1, and measures the volume of the objective space dominated ($D$) by the considered set of solutions (Figure 3.9). It allows set-to-set evaluations, where values of HV close to 1 indicate Pareto fronts close

to the reference (POP). We calculate HV by finding the hypervolume ration between $F$ and $F^{\star}$, where $F^{\star}$ is the reference Pareto front. The formula to calculate HV is:

$$HV(F, F^{\star}) = \frac{\int \alpha_{F(x)} dx}{\int \alpha_{F^{\star}(x)} dx} \tag{3.9}$$

where $\alpha_{F(x)}$ is:

$$\begin{cases} 1 \, if \, \exists \, x^{'} \in F \, such \, that \, x^{'} \leq x \\ 0 \, else \end{cases} \tag{3.10}$$

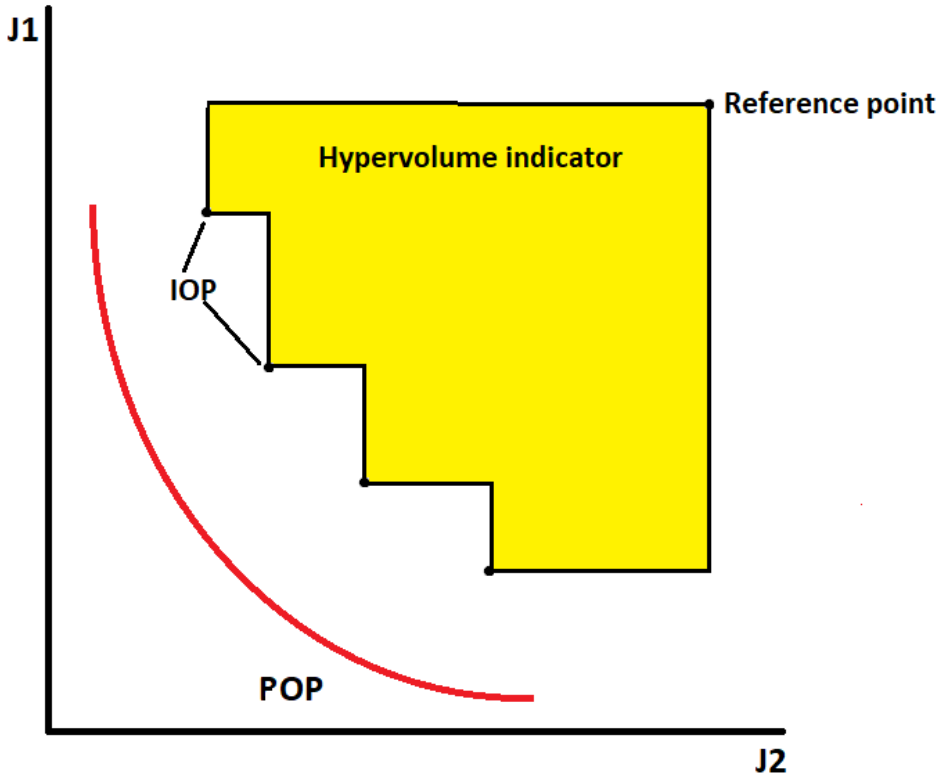


**Figure 3.9:** *Example of hypervolume.*

# 4

# Case study

## 4.1 Lake Como

Lake Como, also known as Lario, is a regulated sub-alpine lake of glacial origin located in Lombardy, Italy, in the provinces of Como and Lecco.
With a surface of 145 km² and 185 km of shores, it is the third biggest in Italy, after Lake Garda and Lake Maggiore, and the longest in perimeter. The average depth of Lake Como is 161 m, while the maximum is 418 m, making it the fifth-deepest in Europe.
The lake's shape resembles a reverse Y (Figure 4.1): with the northern branch located near the city of Colico, and 2 southern branches, in correspondence of the cities of Como (west) and Lecco (east).

The lake is fed by a 4552 km² basin almost completely located in Italy (90%), with the remaining part (10%) located in Switzerland. The Lake's main tributary is the Adda river, originating on the Alps north-east of Lake Como, at an height of 2150 m. Pre-lacual Adda flows westwards in Valtellina valley, collecting water from many other courses, and enters the Lake Como in its northern branch. The river has an average discharge of 88 $m^3/s$ ranging from 18 $m^3/s$ to 918 $m^3/s$ (*Giacomelli et al.*, 2008).
Besides Adda river, 37 other smaller water courses flow into Lake Como, most with limited and discontinuous discharge.
The sub-lacual Adda is the only emissary of the lake, flowing from its south-eastern branch southwards towards the Padana plain. The south-western branch

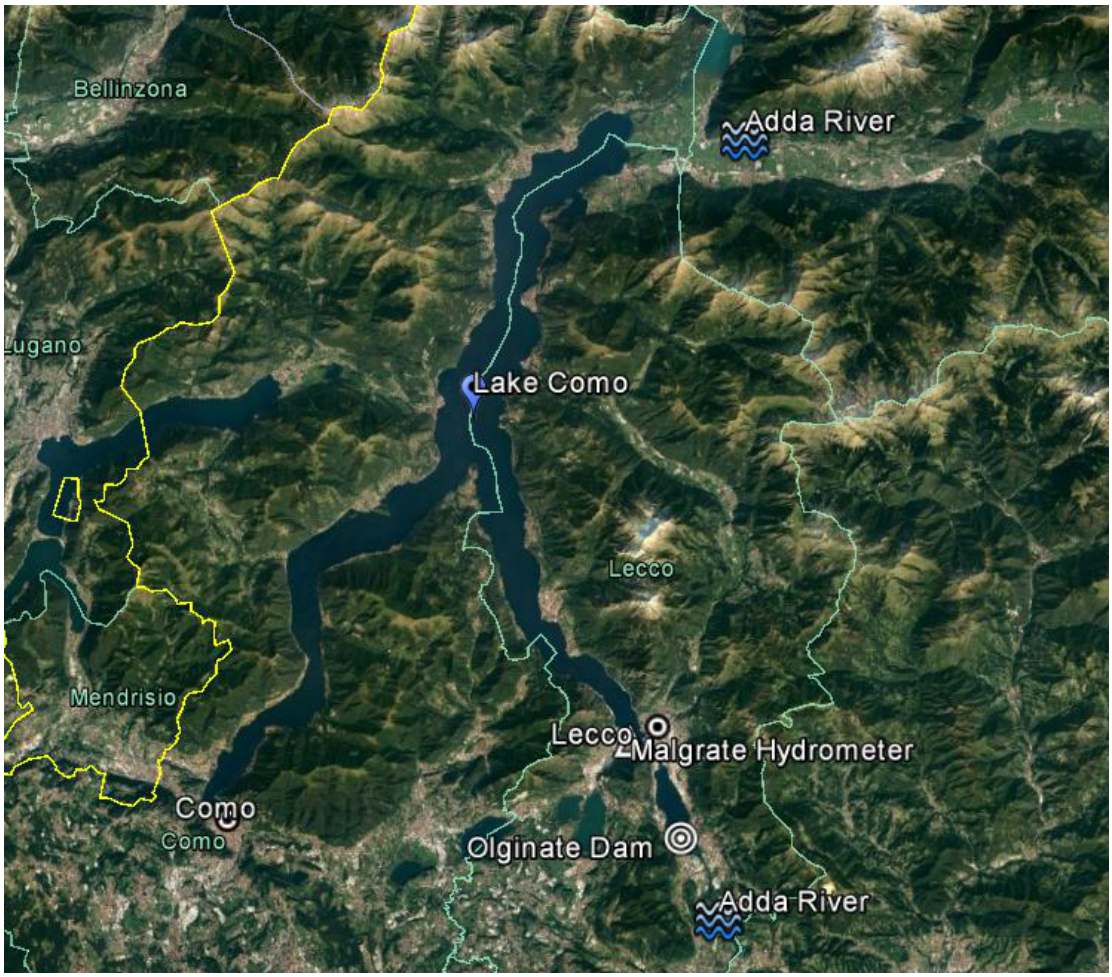


**Figure 4.1:** *Lake Como.*

of the lake is instead a dead end, suffering with floods (*Guariso et al.*, 1986) and water quality problems (*Mosello et al.*, 2010; *Binelli et al.*, 2001).
Since 1946, Lake Como is a regulated lake, thanks to the construction of the Olginate Dam, located between the lakes Garlate and Olginate. The dam has then been operated by the Adda Consortium to avoid floods (mostly in the city of Como), and to supply water to downstream users. The regulation can control a total volume of 254.3 $Mm^3$, of which 246.5 $Mm^3$ stored in Lake Como and the rest in Lake Garlate. The regulation is allowed between levels -0.4 m and +1.3 m, measured at the Malgrate hydrometer.
There are several artificial hydropower reservoirs and natural lakes upstream, with a total storing capacity of 545 $Mm^3$, more than twice the total active capacity of the lake (*Denaro et al.*, 2017).

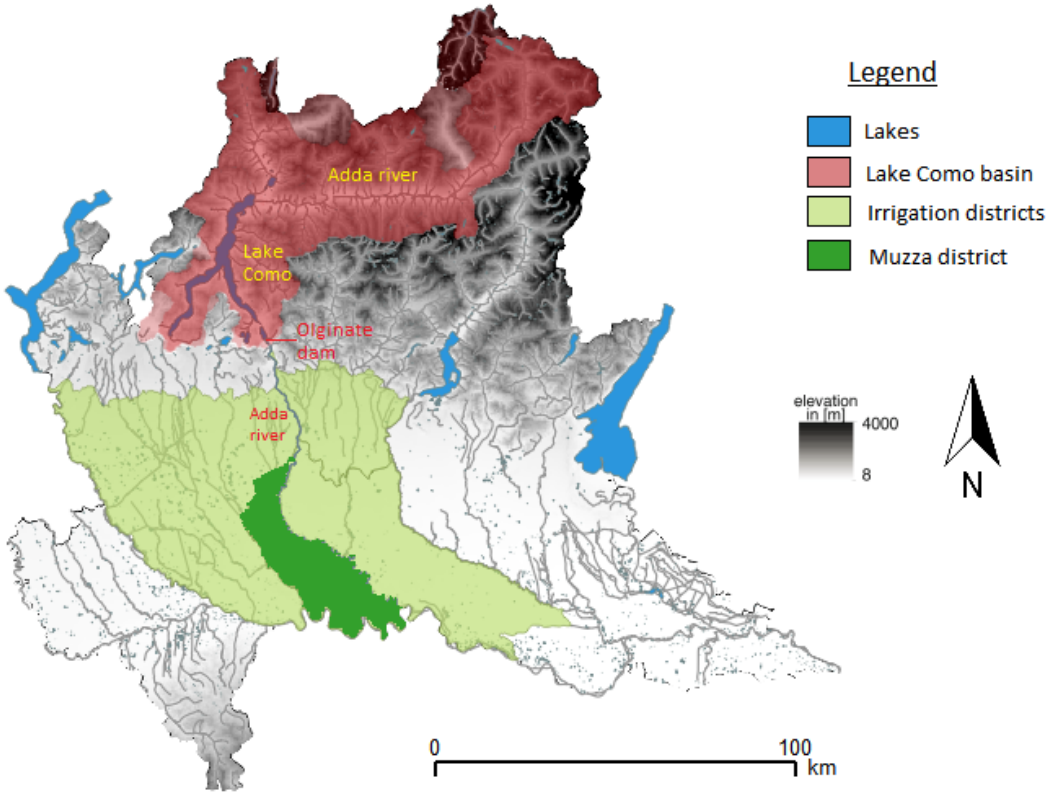


**Figure 4.2:** *Digital Elevation Model of Lombardy, including lakes, the main river network, Lake Como basin and irrigation districts.*

## 4.2 Hydrological regime

The pre-lacual Adda river, main tributary of Lake Como, is characterized by a snow-rainfall dominated hydrological regime, typical of Alpine catchments. The hydrograph (Figure 4.3) shows a snowmelt peak in late spring and a secondary rainfall peak in autumn. Winters and summers are characterized by low flows. Summers are typically dry in the region, while in winter a large portion of precipitation accumulates in the basin in the form of snow. Compared to the natural regime, the regulation shifts part of the spring volume to late summer in order to meet downstream irrigation demand. Nevertheless, Lake Como releases are not always capable to meet summer demand. Moreover, the effects of climate change on the system are expected to be extensive (*Anghileri et al.*, 2012) and to exacerbate the situation. Basins with a high average altitude like this (reaching 4049 m in Pizzo Bernina (*MeteoComo*, 2018)), are also the ones bound to suffer greater effects due to the temperature shifts ((*Bocchiola and Rosso*, 2007) and (*Rosso*, 2002)) caused by climate change. Droughts have already increased in frequency and intensity (e.g. 2003, 2005, 2006, 2012 and 2014

droughts)((*García-Herrera et al.*, 2010)) and the hydrological trends are changing, as illustrated in Figure 4.4. With respect to the past, and higher streamflow can be observed in winter, due to increasing temperatures that cause less precipitation to fall as snow and more to fall as rain and immediately flow.
As a consequence, spring peak is reduced and also anticipated, as snowmelt occurs earlier, due again to raising temperatures. This causes the reduction of water available in spring, and consequently a reduction of summer availability.

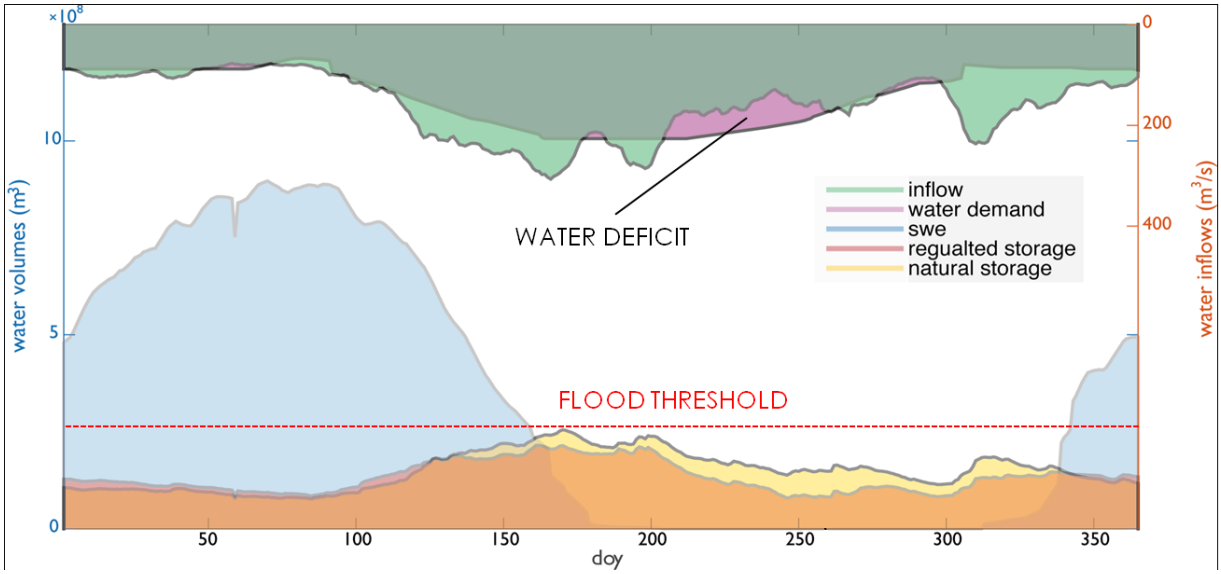


**Figure 4.3:** *Lake Como annual average hydrograph.*

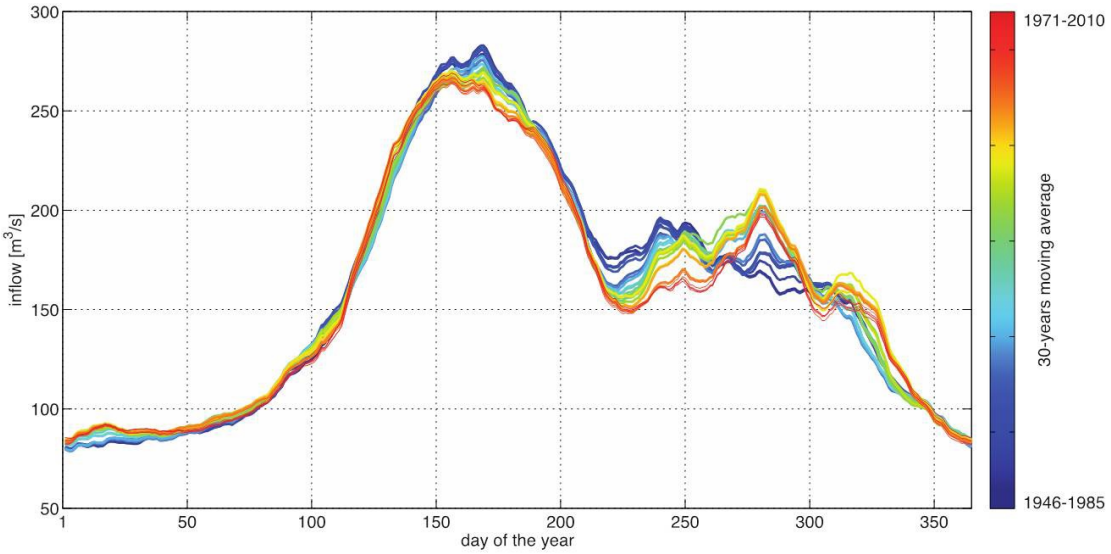


**Figure 4.4:** *Lake Como inflow. 30-years moving average between 1946 and 2010.*

## 4.3 Main stakeholders and interests

Lake Como and Adda river shores have historically been populated and their waters exploited in many different ways. The water has been used to feed agricultural districts since ancient times, as well as for fishing and sport activities. The Lake's geological conformation makes the south-western branch a dead end, and the city of Como subjected to floods. Also many important natural sites are located along the Adda course, e.g. Natural Reserve of Pian di Spagna Lake Mezzola, Parco Adda Nord, Parco Adda Sud and Parco Sud, all requiring particular hydrological conditions in order to survive.
Downstream to Lake Como, the Adda river serves four agricultural districts. Since the needs of the different stakeholders are seldom synchronized and very often conflicting, the lake has been operated as a multi-objective problem (*Guariso et al.*, 1986) in order to satisfy all the stakeholders.

### 4.3.1 Flood control

Flood risk management is one of the primary issues in the water governance of Lake Como. The most vulnerable part is the south-western branch of the lake (*Guariso et al.*, 1982), where the city of Como is located, with floods documented in the city since 1431. The floods happen mostly during autumn or late summer, when the basin is subject to the most intense rain. However, floods can happen also in late spring, due to intense snow-melt peaks (*Denaro et al.*, 2017). Since the construction of the Olginate dam, the number and intensity of floods has decreased, due to the introduction of DMV for the downstream river and the built of dykes in the city of Como (*Castelletti et al.*, 2010; *Anghileri et al.*, 2012). However the problem will still remain and may worsen due to a progressive phenomenon of subsidence registered in Cavour square, the commercial heart of the city of Como. The phenomena is known since 1955 and it is caused by the overuse of groundwater. It increases the vulnerability to flood of the city, although it has slowed down in recent years, from 12 mm/year in 1983 to the current trend of 2.5 mm/year.

### 4.3.2 Agricoltural districts

The river Adda, downstream from lake Como serves an approximate area of 1320 km$^2$ (Figure 4.2). Maize, with a 52% of the total cultivated area is the primary crop, with an annual production of about 1.5 Mton/year (*Li et al.*, 2017). Like most of the other crops in the area, it requires irrigation with water coming from the river during the growth season (spring to summer), as the rainfall is

not sufficient to cover its water needs.
The area is divided into 4 different irrigation districts, called Consorzi di Bonifica. The largest district, Muzza, has an area of 700 km² and an irrigation network of 4000 km.
The irrigation season goes from April to August, coinciding with the period of low flow of the river. Coming from a good condition, save for exceptionally dry years, this problem has worsened during all of 20th century and is expected to exacerbate in the future with increasing needs of water and climate change (*Giuliani and Castelletti*, 2016).

## 4.4 Data

### 4.4.1 Local hydrological data

The local data used in the thesis were:

- Precipitation Data: they come from the Euro4M-APGD (i.e. Alpine Precipitation Gridded Dataset) dataset, created by MeteoSwiss for the EURO4M (i.e. European Reanalysis and Observation for Monitoring deliverables) project. The EURO4M, is an European project aimed at providing timely, reliable information on the climate state in Europe. The dataset is based on a gridded analysis of daily precipitations, coming from an high resolution rain gauge networks which cover the entire Alpine region (Figure 4.5). It is composed by 8500 stations, spread across Austria, Croatia, France, Germany, Italy, Slovenia and Switzerland. The system considers rain, as well as the Snow Water Equivalent (SWE) [mm]. The quality checked data used for this thesis range from 01/01/1971 to 31/12/2008 with a $5 \times 5$ km resolution and a daily time step.

  These daily data, were then clipped over the Lake Como basin and aggregated monthly. Figure 4.6 shows the average trend of daily precipitations, calculated as daily mean on the basin from 1971 to 2008. Looking at any year, we can see a similar pattern. During summer, apart from anomalous values, the precipitations are generally low. During winter instead, the precipitations are slightly higher, but a large amount of it is snow. During spring and autumn there are two high peaks of precipitations.

- Temperature: the temperature is the one measured by the ARPA (i.e. Regional Agency for Environmental Protection ). The data range from year 1990 to 2013 and are averaged for the basin.

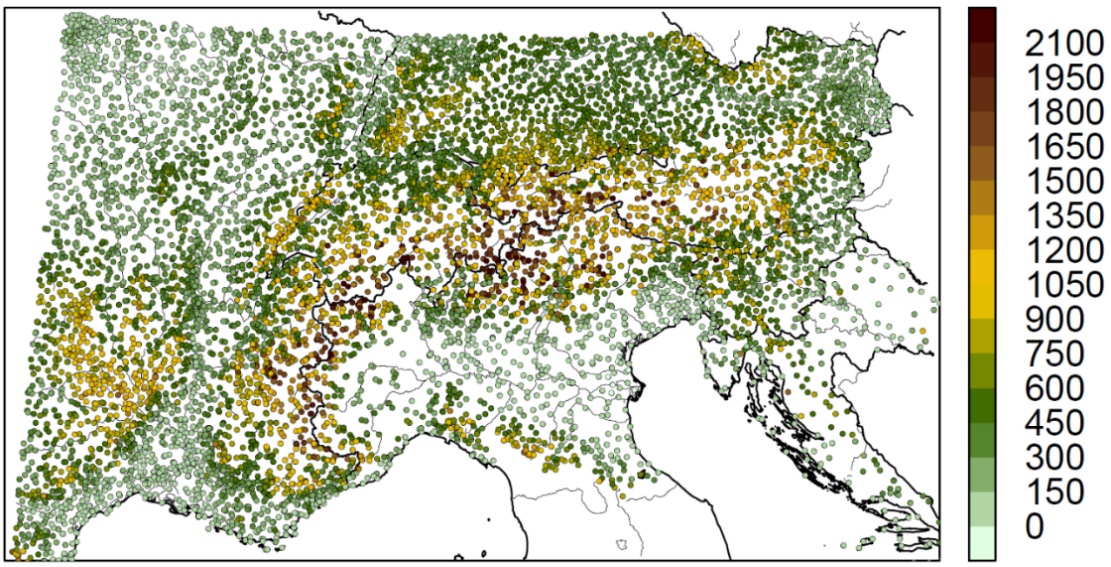


**Figure 4.5:** *Rain-gauge network. The color represents the height (m) of the station.*

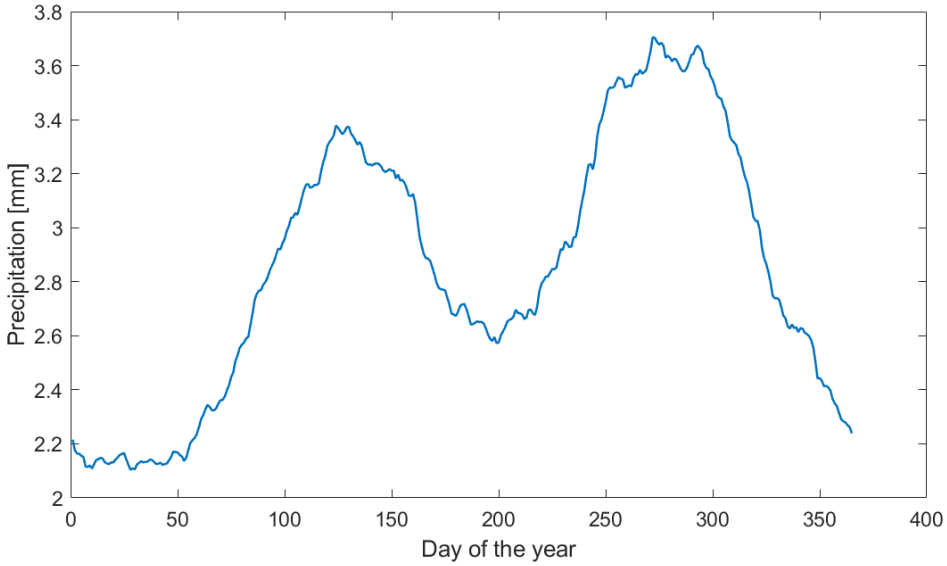


**Figure 4.6:** *Cyclostationary mean of the precipitations in Lake Como basin, from 1971 to 2008.*

Figure 4.7 shows the average daily temperature pattern, calculated as daily mean from 1971 to 2008, averaged in all the basin. The average temperature is 3.4 degrees. The pattern is that typical of the climatic region. It has hot summers, cold winters and intermediate springs and autumns.

- Lake inflow: daily data of inflow [ $m^3/s$ ] to Lake Como are measured and made available by the Consorzio Adda since 1946 [1]. Consorzio Adda is the company in charge of the management of the Olginate dam. Figure

[1] http://www.addaconsorzio.it/

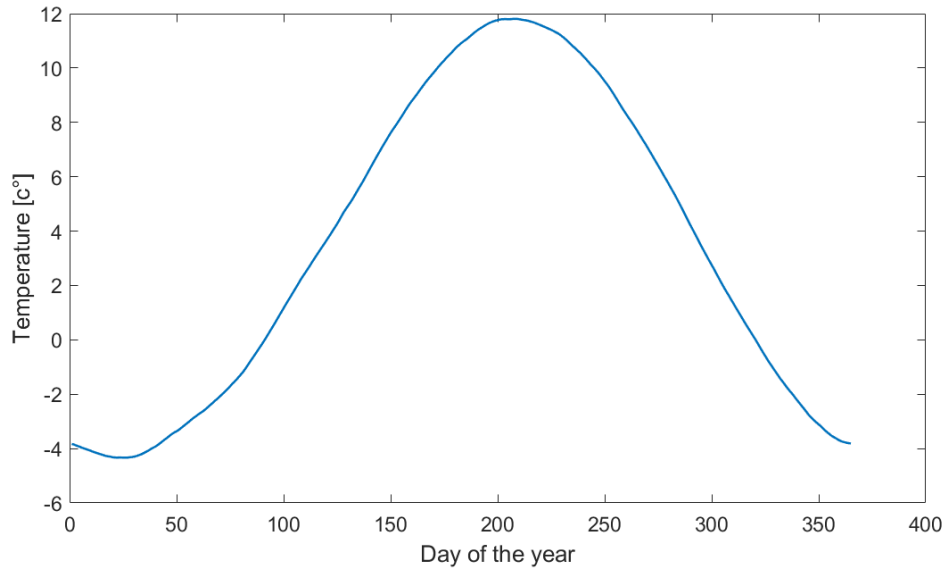


**Figure 4.7:** *Cyclostationary mean of the temperature in Lake Como basin, from 1971 to 2008.*

4.8, shows the cyclostationary mean of the inflow, calculated with data from 1971 to 2008.

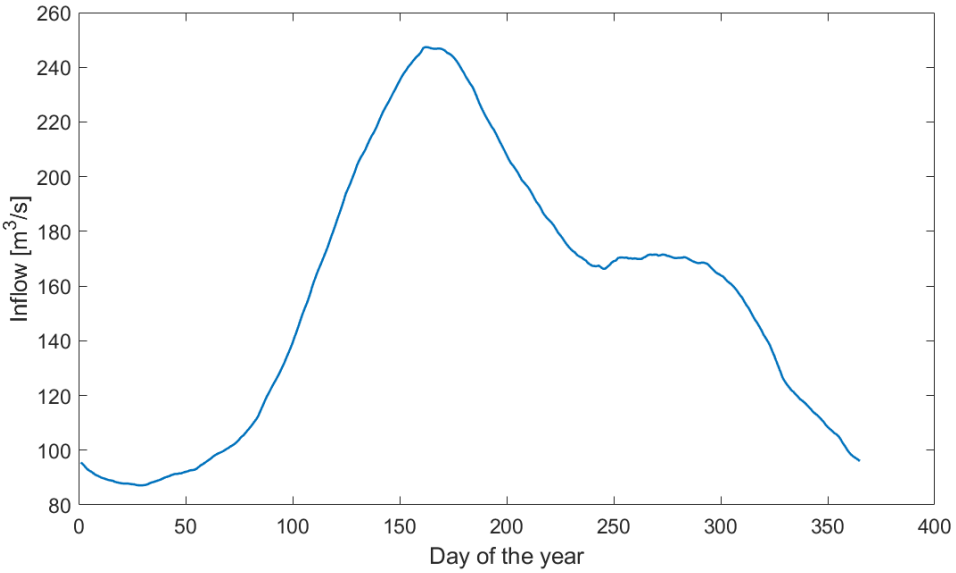


**Figure 4.8:** *Cyclostationary mean of the inflow to Lake Como, from 1971 to 2008.*

### 4.4.2 Global data

#### Sea Surface Temperatures

The global Sea Surface Temperatures (SSTs) come from the NOAA's Extended Reconstructed SST (ERSST) Version 3b dataset. It is a global dataset, with a monthly time resolution and 2.5 degrees spatial resolution. ERRST 3b version uses in situ SST data coming from the International Comprehensive Ocean-Atmosphere Dataset International Comprehensive Ocean-Atmosphere Dataset (IECOADS) and uses improved statistical methods to allow a stable reconstruction using sparse data. Version 3b is the newest available capable of excluding under-sampled regions for global averages. Unlike the previous versions, it doesn't consider satellite data, as they were observed to inject a a considerable bias in the analysis. A detailed description of the 3b version and a comparison to the prior ones can be found in (*Smith et al.*, 2008).

#### ENSO

Among the existing ENSO indexes, we selected the MEI index, as seen in chapter 2.2.1. Values for the index are available on the NOAA website from 1950 and to the present. The value of the index comes from a combination of sea level pressure, zonal and meridional components of the surface wind, sea surface temperature, surface air temperature, and total cloudiness fraction of the sky.
The index is calculated monthly considering two months at a time (January and February, February and March, ..., December and January). The index first filters the individual fields into clusters and then it is calculated as the first unrotated Principal Component (PC) of the six considered variables combined. To have comparable values of the MEI, all seasonal values are standardized with respect to average seasonal value for the 1950-1993 reference period.
Since 2011, an extended timeseries dating back to 1871 is available.

#### NAO

The selected NAO index is the station-based Hurrell NAO Index (see chapter 2.2.2 ). It is calculated using as inputs the difference of normalized Sea Level Pressure between Stykkisholmur in Iceland and Lisbon in Portugal. The National Center for Atmospheric Resource (NCAR) provides the the timeseries dating back from 1865, with a monthly resolution.

## 4.5 Models

The conceptual model for Lake Como assumes a 24 hours decision and modelling time-step. Its state dynamic is built as a mass balance equation of the storage $s$ [$m^3$]:

$$s_{t+1} = s_t + n_{t+1} - r_{t+1} \tag{4.1}$$

where $n_{t+1}$ is the net inflow to the lake, given by the difference between inflow, evaporation and other losses and $r_{t+1}$ is the outflow. The variables subscript indicates the time step when its value is deterministically known. The release is calculated as:

$$r_{t+1} = f(s_t, u_t, n_{t+1}) \tag{4.2}$$

where the function $f$ describes the nonlinear, stochastic relation between the decision $u_t$ and the actual release $r_{t+1}$ (*Piccardi and Soncini-Sessa* (1991)). Given an operating policy $p$, the daily release decision is obtained, using as inputs the day of the year and the reservoir storage:

$$u_t = p(t, s_t) \tag{4.3}$$

The policy is built in a way to produce a sequence of optimal decisions $u_t$ that maximize the stakeholders' needs, operationally defined by objective functions. These functions are formulated according to previous works (*Castelletti et al.*, 2010; *Culley et al.*, 2016; *Denaro et al.*, 2017) as follows: average annual number of flood days over the simulation horizon H, i.e.

$$J^{flood} = \frac{1}{H} \times \sum_{t=0}^{H} g_{t+1}^{flood} \tag{4.4}$$

where:

$$\begin{cases} 1 \, if \, h_{t+1} > h_{lim} \\ 0 \, else \end{cases} \tag{4.5}$$

where $h_{lim}$ = 1.24 m is the lake level threshold determining the occurence of a flood in Como. The objective for the irrigation deficit is defined as the quadratic daily average water deficit with respect to the water demand $w_t$, calculated as:

$$J^{irr} = \frac{1}{H} \times \sum_{t=0}^{H-1} g_{t+1}^{irr} \tag{4.6}$$

where:

$$g_{t+1}^{irr} = (\beta_t \times MAX(w_t - (r_{t+1} - q^{MEF}), 0))^2 \tag{4.7}$$

and $q^{MEF}$ = 5 $m^3/s$ is the minimum environmental flow, $\beta_t$ is a time-varying coefficient accounting for the different impacts of water deficit during the different crop growth stages. The quadratic formulation aims at penalizing severe deficits in a singe time step over more frequent, smaller ones.

## 4.6 Experimental settings

This section details the experimental settings used to adapt the procedures summarized in chapter 3 of the case study just presented.

NIPA is set to work binning years into two phases for each signal. Each can be either positive or negative. The model is set to predict, starting from SSTs data from three months, the next three ones and the minimal significance level threshold is set to be 95%.

For the calibration of multivariate rain prediction models, we used 4 neurons in the ANN, following the empirical rule where: $N_{neurons} = N_{inputs} + 1$. The number of neurons in the ELM model was set to 10, after a trial-and-error manual tuning.

For the policy optimization via Borg MOEA, the number of NFE was set to 2 millions, according to guidelines given by previous works on the systems. The optimization was repeated 20 times to filter the random components, and the final Pareto front is obtained by merging the results of the 20 repetitions.

# 5

# Results

This chapters presents the results of the procedures explained in chapter 3. Following a similar order, it shows the results for the detection of climate teleconnections (section 5.1), the multivariate seasonal meteorological forecast (section 5.2), the seasonal hydrological forecast (section 5.3) and valuation of forecast operational value (section 5.4).

## 5.1 Detection of climate teleconnections

This section is dedicated to the presentation of the results of the detection of climate teleconnection step, in which teleconnection indexes are employed to find significant correlations between the state of the large-scale climate signals, and the precipitation in the Lake Como basin. Following the NIPA procedure, detailed in section 3.1.2, we first bin the 12 triplet of consecutive months (JFM-FMA-MAM-AMJ-MJJ-JJA-JAS-ASO-SON-OND-NDJ-DJF) into meta-phases, according to the MEI index for ENSO and the NAO index for NAO. For each month triplet, four combinations of metaphases are possible, as shown in Table 5.1 for the JFM period.
After that, we perform a correlation analysis between the three months aggregated precipitations(e.g. JFM) and the average SSTs of the three previous months (e.g. OND SSTs) for each oceanic cell. Detected correlations with a significance level $\geq$ 95 % are retained.
An example of the results for the JFM precipitations and OND SSTs period can be seen in Figure 5.1. The complete set of results are reported in appendix A.

**Table 5.1:** *Years splitted into meta-phases according to MEI and NAO index: JFM period*

| MEI + NAO+ | MEI + NAO - | MEI - NAO + | MEI - NAO - |
|---|---|---|---|
| 1973 | 1978 | 1972 | 1971 |
| 1977 | 1979 | 1975 | 1974 |
| 1980 | 1981 | 1985 | 1976 |
| 1983 | 1988 | 1999 | 1982 |
| 1987 | 1998 | 2000 | 1984 |
| 1991 | 2003 | 2001 | 1986 |
| 1992 | 2004 | 2008 | 1989 |
| 1993 | | | 1990 |
| 1994 | | | 1996 |
| 1995 | | | 1997 |
| 2005 | | | 2002 |
| 2007 | | | 2006 |

For the JFM case, years with positive MEI index show many gridpoints where SSTs are negatively correlated with the precipitation, with a particularly high concentration in the Indian Ocean. For negative MEI index instead, there is a much smaller number of correlated points, all of them positively correlated, and located in the Atlantic Ocean.
The results are different for NAO where, for both phases, mixed negatively and positively correlated gridpoints of SSTs can be detected. For the positive NAO phase, most of the points are scattered without a prevalent location. For the negative NAO phase, instead, most of the points are concentrated in the Pacific Ocean.
Following the correlation analysis, a Principal Component Analysis (PCA) is performed for each combination of months' triplets and climate signal's phase on the significantly correlated cells. The first Principal Component (PC) obtained is finally retained as input for the subsequent multivariate modelling step.

## 5.2 Multivariate meteorological forecast

In this step, the previously obtained PCs are used as input to a multivariate prediction model that is calibrated and validated to reproduce the observed rainfall.
We test three model classes: linear models, ANNs and ELMs. All of them link the period's meta-phase, NAO PC and MEI PC to the precipitations in the Lake Como basin. As specified in chapter 3.2, a leave one out cross-validation is performed for each model, to limit the risk of over-fitting. The results for JFM season can be seen in Figure 5.2, while the rest are reported in appendix A.

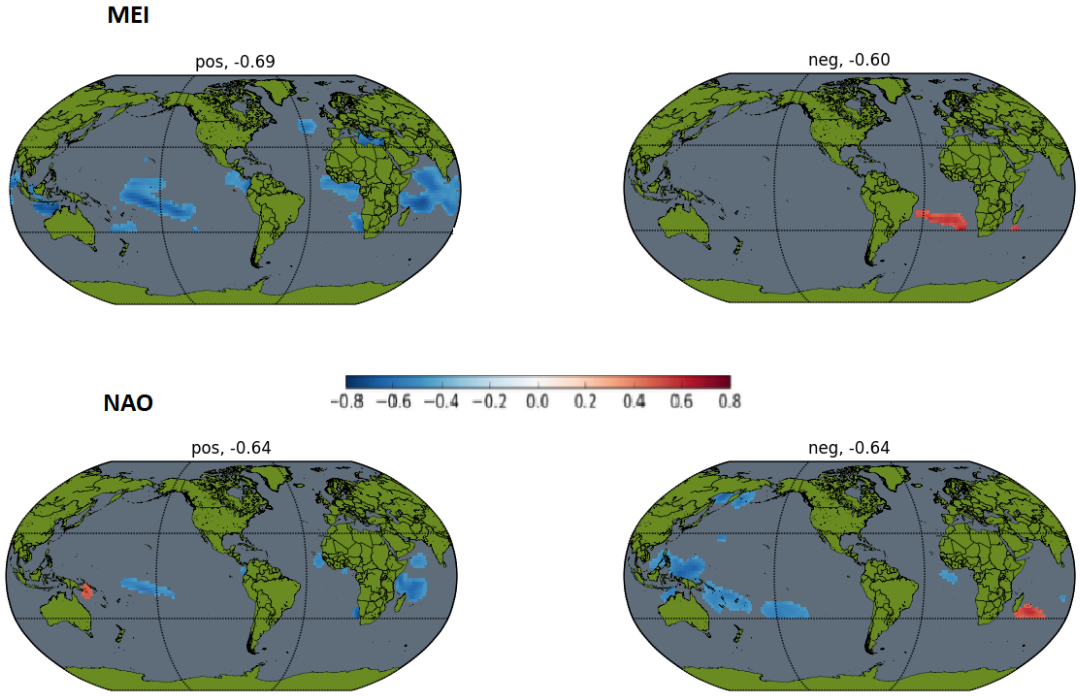


**Figure 5.1:** *Correlation maps between October, November, December SST anomalies and January, February, March precipitation in the Lake Como catchment for the two phases of ENSO (top panel) and NAO (bottom panel).*

Results show that, the ELM model clearly outperforms the other two. The linear model yields a very poor performance, even predicting highly negative precipitations in a few periods. In addition, the peaks are extremely emphasized, reaching extreme values out of the historic range for the area. The forecasted peaks are not even synchronized with the observed ones. Finally, also the average trend is not respected. We can clearly infer that the relationship between the PCs and the precipitations is not linear.
In comparison, the ANNs perform much better. No negative values nor unnaturally high peaks are present and they fairly reproduce the general trend. However, they poorly reproduce most of the highest peaks in both magnitude and timing.
Finally the ELMs show the best performances. They best reproduce peaks and generally perform better on the whole horizon. The observed trend is followed, without a large presence of time lag or anticipation. The performances seem to deteriorate a bit for the last years, but the error is still contained.
The conclusion we have drawn from the inspection of the predicted rainfall trajectories are numerically confirmed by the values of the Pearson coefficient $R$ and the coefficient of determination $R^2$ that can be seen in Table 5.2, which reports an $R = 0.9$ and an $R^2 = 0.76$ for the ELMs, which clearly outperform the

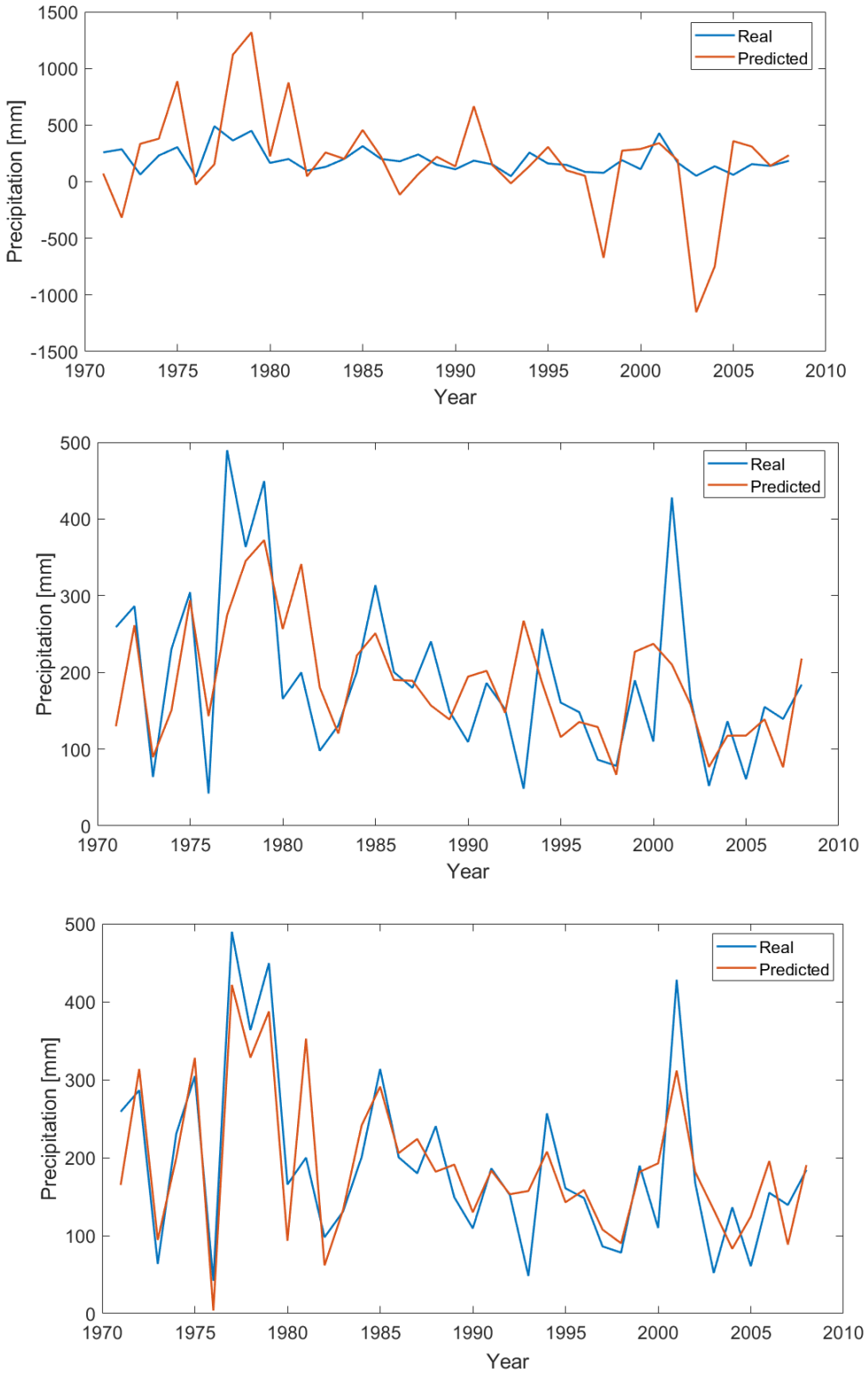


**Figure 5.2:** *Observed and predicted precipitation for JFM season: linear (top), ANN (center), ELM (bottom).*

**Table 5.2:** *Performances of Linear, ANN and ELM models: JFM case.*

| $R^2$ | Linear | ANN | ELM |
|---|---|---|---|
| $R$ | 0,50 | 0,63 | 0,90 |
| $R^2$ | -12,60 | 0,62 | 0,76 |

Linear and ANN models. Complete results for the $R$ and $R^2$ for ELM models can be seen in appendix A

With this procedure, we obtain the predicted precipitations for the three months following the three months of SSTs observations for each of the twelve months triplet. Figure 5.3 illustrates a scatterplot of observed vs ELM-predicted values of the three months cumulated precipitations, which gives an idea of the consistently good performance of ELMs, for all the twelve months triplet.

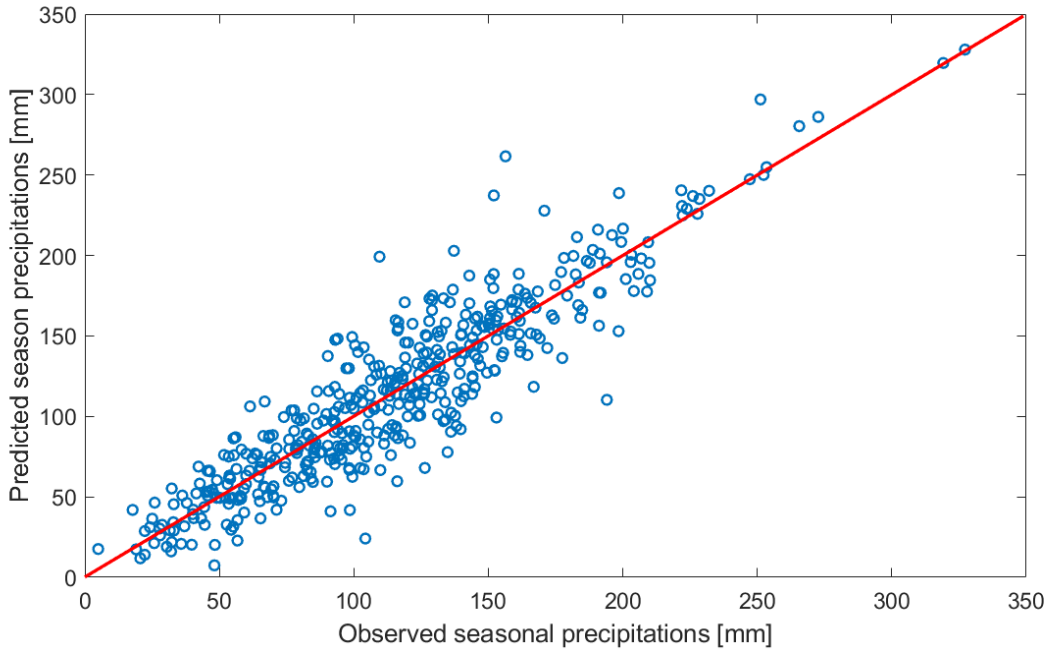


**Figure 5.3:** *Scatterplot between observed and predicted precipitation for all the three-month triplets.*

The points look aligned to the diagonal line splitting the plane in two equal halves, with no apparent deterministic trend in the disposition of the outliers. The Person's correlation coefficient $R$ is equal to 0.91 and $R^2$ to 0.83, further confirming the very satisfactory results. So, in the end, we use the seasonal precipitations predictions calculated with ELM models to proceed to the next step.

## 5.3 Seasonal hydrological forecast

Once we have the predicted seasonal precipitations, the next step is to transform them into daily precipitations and finally into daily streamflows.
The K- Nearest Neighbour procedure is first employed to obtain the daily precipitation data. Figure 5.4 shows an example of the results, for the JFM season. We used a k=6, to have enough variability and at the same time avoid using season with big differences in total value.

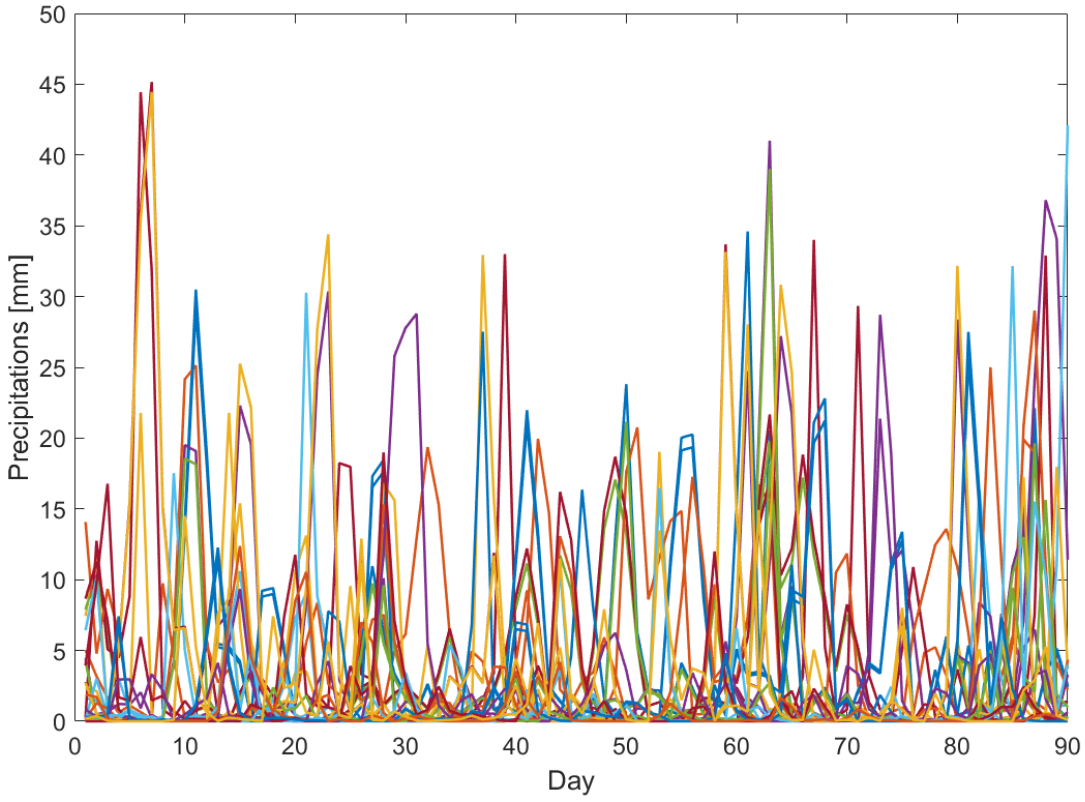


**Figure 5.4:** *Disaggregation of seasonal precipitation values into daily ones: JFM case. The different colours represent different years.*

KNN does not try to reproduce the exact values of historical daily precipitations, but only to construct an appropriate daily distribution by capturing a plausible seasonal precipitation pattern. In fact, for our purpose, it is not particularly important to get a precise day prediction as long as cumulated precipitation is accurate enough, considering that our aim is to make long term prediction, as opposed to short term predictions. Short term predictions need to accurately reproduce daily magnitudes and follow the fast flood dynamics; long term predictions need to give an indication of season ahead water availability, necessary to trigger effective hedging strategies in water supply opera-

tions.

The obtained daily precipitations, along with cyclostationary average the temperatures, are then used as inputs for the hydrological model HBV to get the corresponding daily streamflow. Lastly, according to the findings of (*Denaro et al.*, 2017), daily predicted inflows will be cumulated over a lead time of 51 days to inform the lake operating policy.
From Figure 5.5 we can see that the hydrological predictions tend to present a wet bias, caused by the imperfect reproduction within the HBV model of some of the physical processes taking place in the catchment. In particular, the largest bias can be observed on low flow conditions,where the values of predicted inflow are much higher than the real ones. Analysing these points, we find out that they are mostly located during the dry summer season. This error could be explained by the fact that the HBV model doesn't take into account the multiple hydropower reservoirs located in the upstream the catchment. These reservoirs are operated with only the maximization of the profit from hydropower electricity production as objective. During the summer period, the demand for electricity is generally low (*Bianco et al.*, 2009) and so is the price of sold energy, due to the market's dynamics. So, in this period, the hydropower companies have little to no interest in releasing water that wouldn't bring profit and so they lower their releases. The HBV doesn't model explicitly this part of the system and so it can't accurately simulate these dynamics.
Anyway, apart from those low flow values, the model's performance seem sufficiently accurate, with the Pearson coefficient still attaining a satisfying value of 0.71. Yet, it is worth noticing that the transformation from precipitation to streamflow forecasts introduces a 0.2 degradation of forecast accuracy.

At the end of this step, we have the predicted inflows to Lake Como to be used in the next step to condition the control policy.

## 5.4 Quantification of forecast skill and operational value

After obtaining the streamflow we feed use this information in the design of the the control policies for the operations of Lake Como. Formally we solve the following multi-objective optimal control problem:

$$p^{\star} = argmin_p |J^{flood}, J^{irr}| \tag{5.1}$$

where the two objectives are defined as in eqs. 4.7 and 4.6.s a baseline operating policy (BOP) we consider to condition the lake operations over the day of

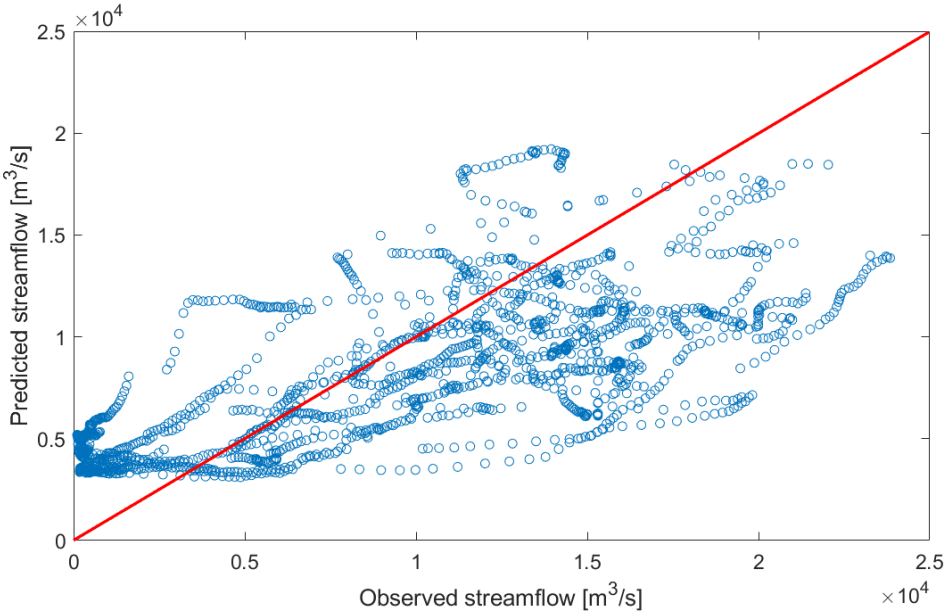


**Figure 5.5:** *Scatterplot of observed and predicted inflows cumulated over a leadtime of 51 days.*

the year and the lake level (*Denaro et al.*, 2017). Enlarging this basic information set by including the 51 days ahead predicted inflows represent a promising option for increasing the overall system performances and reliability (*Tejada-Guibert et al.*, 1995; *Galelli et al.*, 2010; *Gelati et al.*, 2010; *Denaro et al.*, 2017), especially in terms of irrigation supply. In particular, we build three different sets of Pareto optimal policies:

1. Perfect Operating Policy (POP): POP is designed using Deterministic Dynamic Programming, assuming to have perfect knowledge of all the future information at he time the decision is taken. All the future inflow is deterministically known over the entire horizon $H$. This set of solutions serve as an upper bound reference of the best (ideal) system performance.

2. Baseline Operating Policy (BOP): BOP is designed via EMODPS to approximate the historical lake regulation. BOP decisions depend only on the day of the year and on the lake level, i.e. $u_t = p(t, h_t)$.

3. Informed Operating Policy (IOP): IOP is also designed using EMODPS, but it includes the information coming from our study. So the decision is calculated as $u_t = P(t, h_t, \hat{q}_5 1)$.

Figure 5.6 shows the performances of the three alternatives in terms of objective values. Both objectives are described as cost functions and so both should be minimized, meaning that the perfect solution would lay on the bottom left

corner. The Figure shows the reference set identified for each of the three alternative policy structures, obtained as the set of non-dominated solutions across the 20 optimization trials performed.

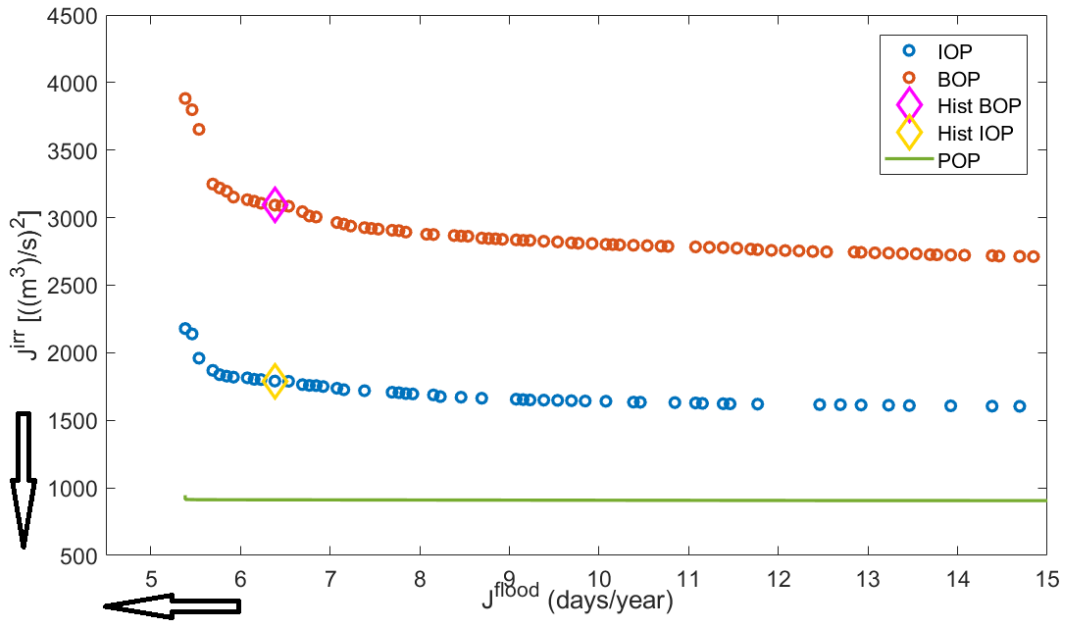


**Figure 5.6:** *Performance comparison between Baseline Operating Policy (BOP), Informed Operating Policy (IOP) and Perfect Operating Policy (POP). The two rhombi represent the policies with 6.3 days of floods per year, corresponding to the historical lake operations, which are analyzed in detail in Figures 5.7 and 5.11.*

From the observation of the three Pareto fronts, a clear ranking can be made, since there are no intersections between the three classes of policies.
The POP, represented by the green line clearly outperforms the other two. This because perfect knowledge allows to take the best possible decisions at any time step. It is interesting to note that the bottom left part of the POP is sharp edged. This means that with a perfect forecast of the future conditions, the conflict between irrigation and flooding wouldn't exist. In fact, using the solution in the bottom left corner would mean that giving a slight advantage to one of the two stakeholders would cause a massive disadvantage for the other and vice-versa. So an agreement on using that specific solution could be easily accepted by both parts and this would eliminate the conflict. However, with the current time technology and knowledge, it is not possible to gain perfect knowledge about the future and the conflict will remain. Anyway, the use of additional information could help mitigate it.
This can be seen looking at the performances of the IOP. We can see that the IOP

**Table 5.3:** *Results of the Hypervolume Indicator for the three Pareto Fronts in Figure 5.6. The POP Pareto front assumes value 1 as it is the reference performance.*

| Pareto front | Hypervolume |
|---|---|
| POP | 1 |
| BOP | 0.21 |
| IOP | 0.69 |

Pareto front looks down-shifted compared to the BOP one. This is due to the fact that the information we give is a long term one which useful for irrigation, while the leadtime should be much shorter to be useful for flood control. So, the information we give about future expected inflow is particularly valuable to improve the water supply strategy rather than flood control.
But the fact that largest improvement is shown by $J^{irr}$ doesn't mean that the information is not helpful also for $J^{flo}$. We can in fact improve $J^{irr}$ at no cost for $J^{flo}$, meaning a mitigation of the conflict.

To get a better understanding of the results, beside looking at Figure 5.6, we can use the hypervolume, already introduced in chapter 3.4.2, to quantify the quality of the different Pareto fronts. The hypervolume (HV) can assume values from 1 (best performance) to 0 (worst performance). The value 1 is given to the POP and used as reference to calculate the performances of BOP and IOP, as reported in Table 5.3. The value assumed by BOP is 0.21 and its difference compared to that of IOP confirms the large potential improvement provided by the use of the 51 days ahead inflow prediction. In fact, the introduction of the information coming from the MV-forecast helps achieving an HV of 0.69. This means a 48% improvement compared to the BOP, demonstrating that it represents an extremely valuable information.

### 5.4.1 Policy trajectory analysis

This section deepens the analysis, by comparing Lake Como levels and releases in the case of baseline and informed policy. In particular, we choose to study the case where we have a number of flood days equal to the average historic one (6.3 days/year). These two points can be seen in Figure 5.6 circled by the two diamonds. In this way, we can focus on how much IOP improves the BOP's $J^{irr}$ performance while maintaining the same value for $J^{flo}$.
Figure 5.7 shows the level at the Malgrate hydrometer trend for the two policies, compared to the flooding threshold.

The most evident trend of the IOP compared to the BOP is that the level is

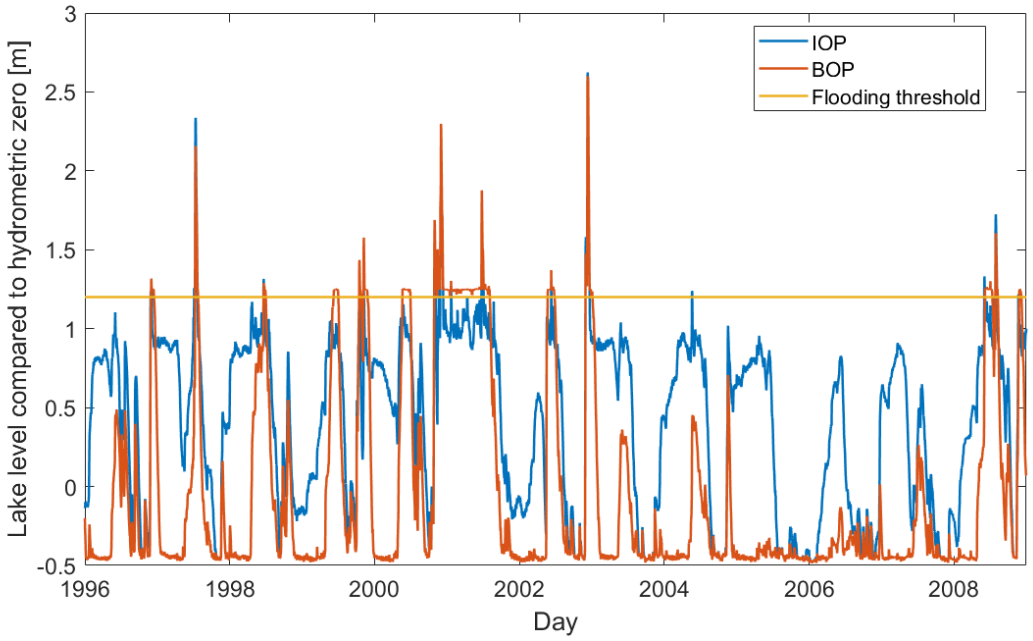


**Figure 5.7:** *Lake Como level from 1996 to 2008: BOP, IOP and flood threshold comparison.*

generally higher throughout the whole year, except for the end of summer and winter period, where they both reach their minima. In particular IOP keeps the level just below the flood threshold for a long period. This is possible due to the information provided by the forecast about the expectedinflow in the next period. This knowledge about the expected inflow allows evaluating the flood risk and keeping the lake at higher levels. As a consequence, irrigation can be better satisfied. Figure 5.8 helps visualizing this trend. It shows the cyclostationary daily mean of the Lake level for the two different policies. From the Figure, we can see that the IOP clearly stays above the BOP for all the year on average, confirming what was said before. The difference between the two policies is particularly large during spring to summer, while the gap reduces in autumn.

Among the considered horizon, two particular periods are interesting to look at. The first one can be seen in Figure 5.9. The Figure shows the level for IOP and BOP for the period from the end of year 2000 to autumn 2001. This is one of the few periods where the IOP is below the BOP. We can clearly see that BOP's level is over the threshold for a very long period while IOP manages to keep it just below for most of the time. In this case the IOP works correctly and actively helps in avoiding floods. This is possible for the IOP because the anomalies for that period all show above average inflows and so the policy can release a considerate amount of water to avoid flooding, while also covering

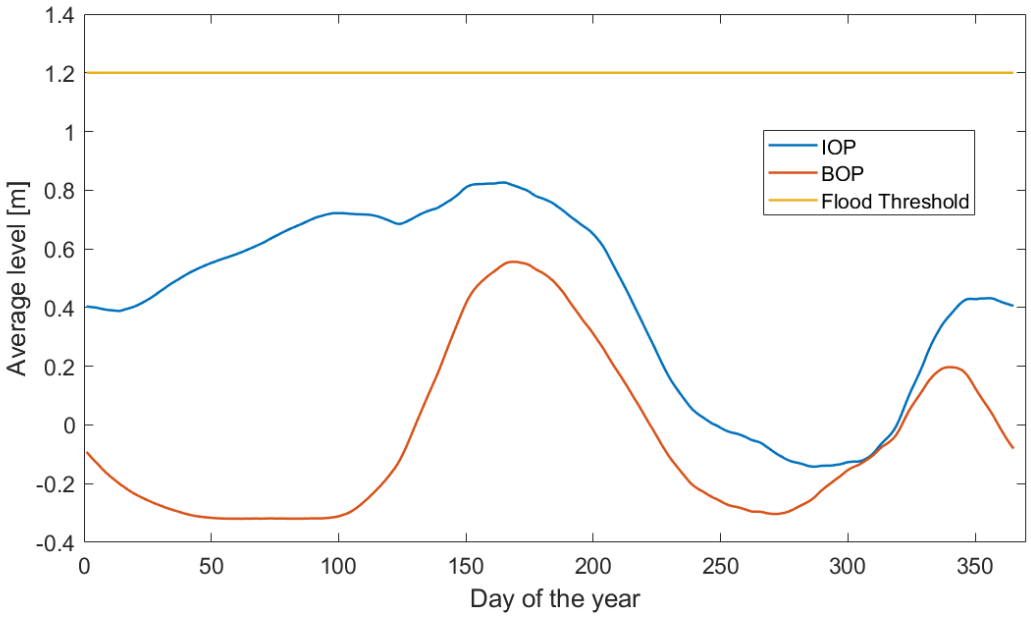


**Figure 5.8:** *Cyclostationary mean of the lake level from 1996 to 2008 for BOP and IOP.*

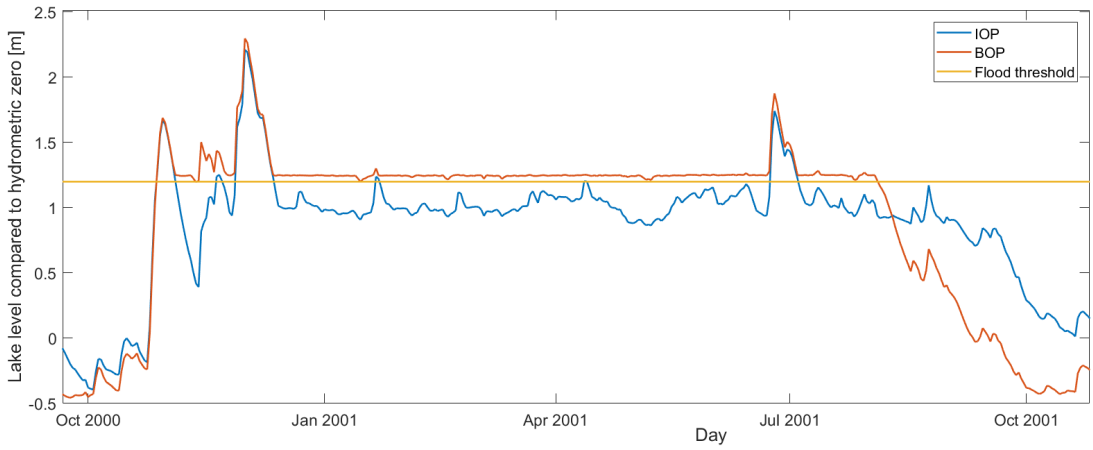


**Figure 5.9:** *BOP and IOP Lake level from fall 2000 to fall 2001, compared with the flood treshold.*

future irrigation demand.

Figure 5.10 shows another example of the IOP's good management. In particular we can notice that for a very long period, starting at September 2004 and ending in August 2005, the IOP is able to maintain a higher lake level despite the intense drought of 2005. Conversely, the BOP almost empties the lake.
These two examples further confirm the advantages gained in terms of $J^{irr}$ that IOP can bring when compared with BOP and the downshifting of the Pareto fronts, in favour of the irrigation objective. This is made possible by the fact

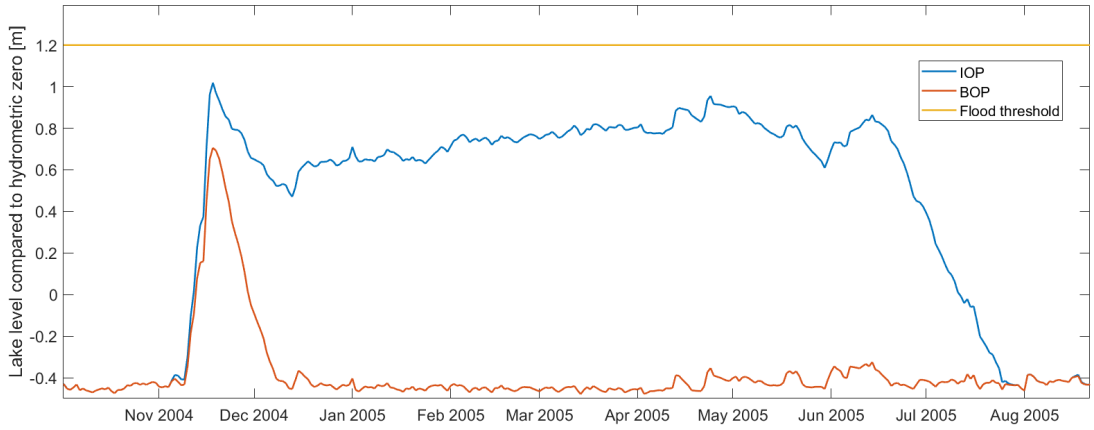


**Figure 5.10:** *BOP and IOP Lake level from fall 2004 and end of summer 2005.*

that the introduction of the forecast into the control policy arguments, brings information about next season's expected streamflow. .

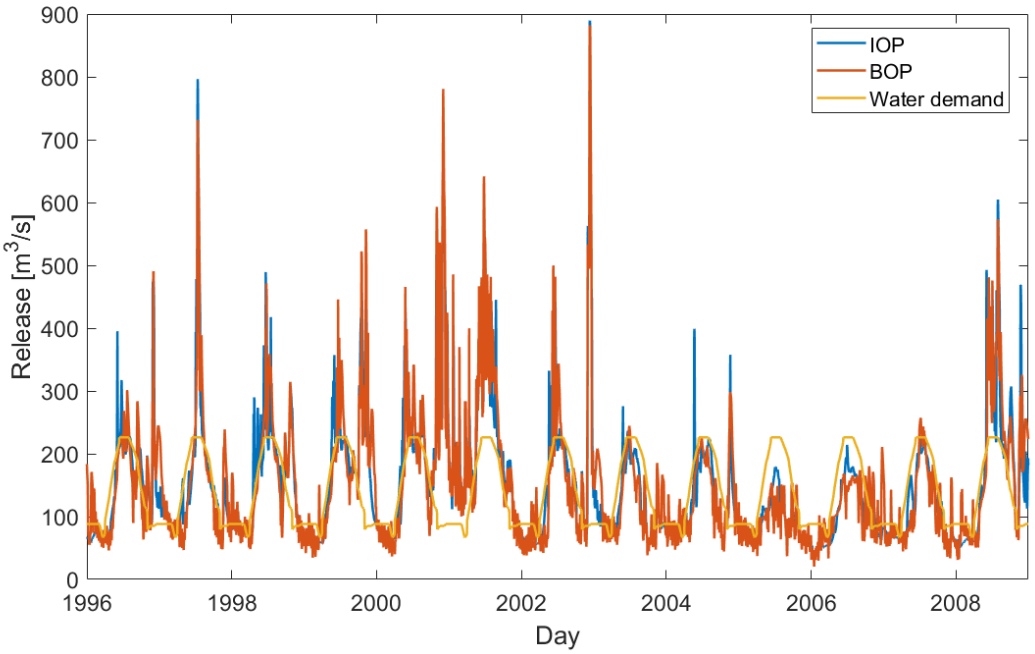


**Figure 5.11:** *Lake Como release from 1996 to 2008: BOP vs IOP management for the 6.3 flood days policies.*

Figure 5.11 shows the release trajectories for the two selected policies, along with the water demand. The water demand has a time varying pattern, reaching its peak during summer and late spring, when crops are growing most, and its minima in winter, when the crop is still to be planted. By looking at the Figure, we can make a visual analysis of the timing and magnitude of the

water deficit for the two cases. We can see that the release values for IOP are slightly smaller that the release from BOP during the winter period. This is done to accumulate more water to be used during spring and summer. Indeed the release from IOP during spring is very often higher than that from BOP and follows more closely the pattern of water demand, minimizing the deficit and improving the performances in terms of $J^{irr}$.

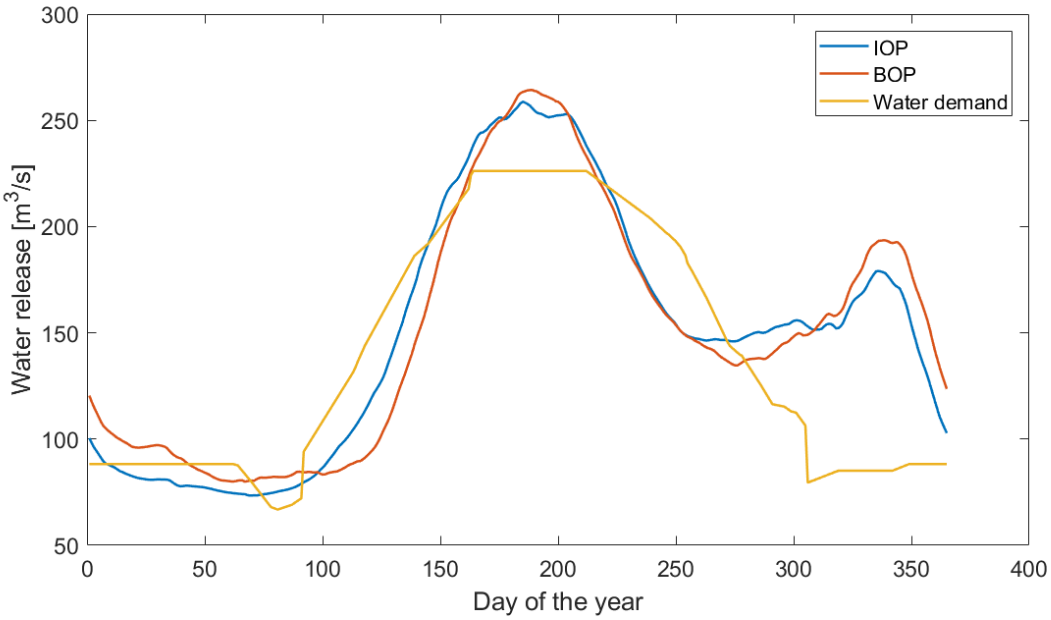


**Figure 5.12:** *Releases cyclostationary means for BOP and IOP, compared to water demand.*

The trend just described is confirmed when looking at Figure 5.12, which shows the cyclostationary mean of the release for BOP and IOP, compared with water demand. In particular we can see that the release is higher for IOP during all the period with the highest water demand, from late spring to autumn, with the exception of the peak. The opposite happens during winter and early spring, where IOP releases less in order to save water for the summer period.

Figure 5.13 shows the releases corresponding to the lake levels in Figure 5.9. Where we can see that the release from IOP is slightly higher than that from BOP. Figure 5.14 , instead, shows the releases corresponding to the lake levels in Figure 5.10. A part from the higher peak at the end of November 2004, with the IOP policy, the release is kept at a lower level than that coming from BOP. This is what allows the lake to accumulate the water volume, necessary to better satisfy the water demand in spring 200.

To resume, what we have found is that IOP's next season's forecast, allows it to perform better compared to BOP. This because the release in one season

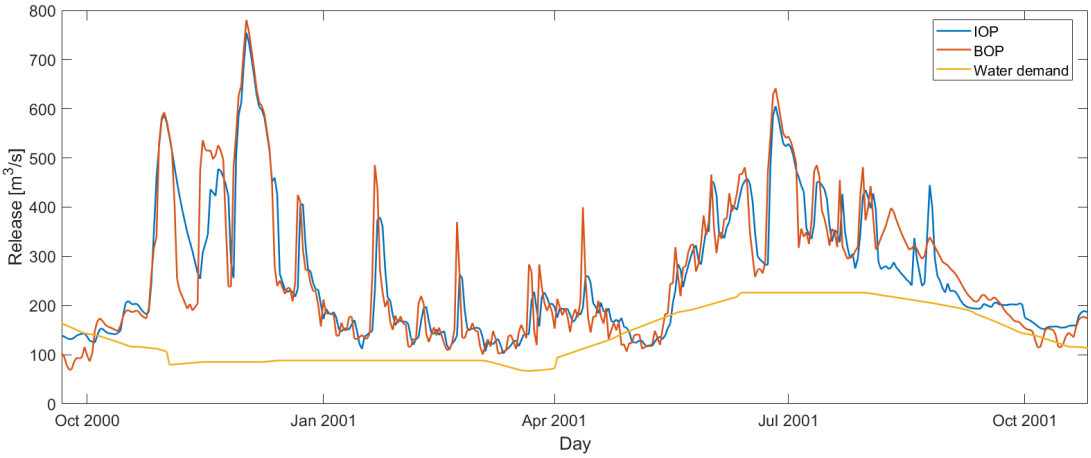


**Figure 5.13:** *BOP and IOP release from fall 2000 to end of fall 2001, compared to water demand.*

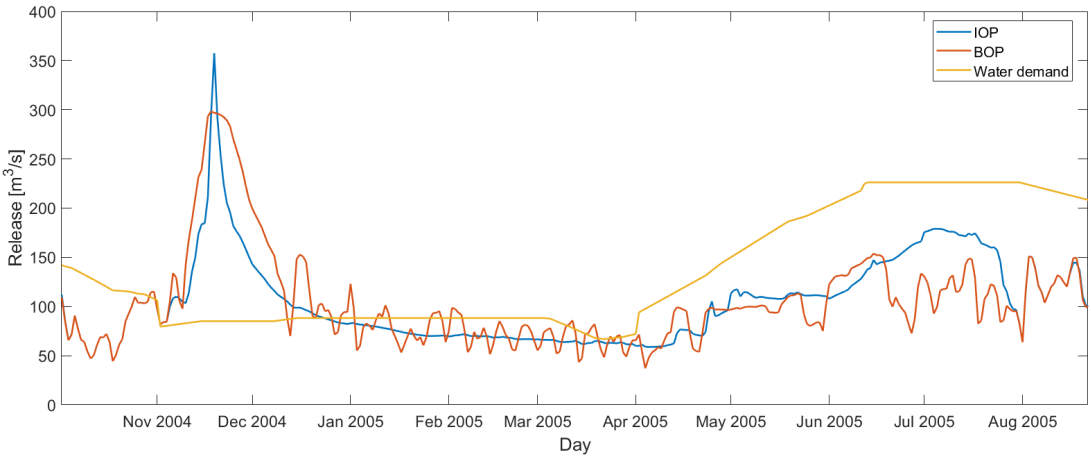


**Figure 5.14:** *BOP and IOP release from fall 2004 to end of summer 2005, compared to the water demand.*

can be regulated according to the next one's expected conditions. So, if the following season is expected to be dryer than usual, more water will be stored by lowering the release. In the opposite case, instead, the release will be promptly raised to avoid floods.

# 6

# Conclusions and future research

This work's aim is to investigate the possibility of using information coming from teleconnections to improve the operations of water systems, trough the use of long term forecast models of local hydrological variables. In particular, this thesis analyses the main teleconnection patterns to construct long term forecasts of precipitation and inflow for the Lake Como basin, and redesigns the lake operations including such information to mitigate the existing conflicts between water users.

Lake Como is a regulated system located in Northern Italy. The management of its storage is cause of many conflicts, with the one between agricultural districts and flood protection as the most important. In particular, agriculture needs the lake volume to be as high as possible, to have enough water to satisfy summer demands. On the contrary, flood protection is interested in keeping Lake Como's level as low as possible, to prevent flooding for those living on its shores. So, the demands of the two are opposite and difficult to satisfy at the same time. A better management, coming from a larger set of information, could help mitigating this conflict.

To achieve that, we first apply the NIPA procedure, binning the years in different phases according to both ENSO and NAO oscillations, creating correlation maps and finding Principal Components aggregating the pre-seasons SSTs significantly correlated with the local precipitations. Those PCs, are then combined in MV-forecast ELM models, to predict the precipitation in the following three months. The results show that a correlation between teleconnections and precipitations in the area exist, and that ELM models are able to use it for de-

livering skilful forecast. In particularthe comparison between observations and resulting hindcast provides a Pearson coefficient $R = 0.9$ and the determination coefficient $R^2 = 0.76$.

These seasonal precipitation forecast are then transformed into daily forecasts, by means of a KNN procedure, and a basin hydrological model produces the daily inflow to Lake Como. The procedure to get daily inflows from seasonal precipitations performs sufficiently well, attaining an $R = 0.71$, although introducing some biases with respect to the precipitation forecasts. The forecasted inflows are then aggregated into 51 days cumulated inflow forecast. Finally, the last part of the work focuses on exploring the potential of informing Lake Como operating policy with the produced teleconnection based long term forecast. Three policies were designed:

1. Perfect Operating Policy (POP): POP assumes perfect foresight of the future inflow and is taken as a reference for the other policies;
2. Baseline Operating Policy (BOP): BOP approximates the historical lake regulation
3. Informed Operating Policy (IOP): IOP is conditioned upon basic information and the long term forecast

The performance improvement provided by the forecast is very notable, and can be quantified with an increase of the Hypervolume metric of 48%. A comparative analysis of the trajectories of the lake level and releases under BOP and IOP shows that the informed policy tends to maintain the lake level higher during the whole year, except for the winter months, thus generally counting on larger storages on irrigation months.

The conclusion we can draw from this is that a clear correlation between teleconnections and local hydrological variables can exist and can help bringing massive advantages in water systems management. This is true in particular for those objectives requiring a long term forecast to improve their performances, like for example irrigation supply, while the effects are limited on some others that would benefit more from a short term forecast, like flood control.
Future researches could build on these results and extend the analysis to combine short and long term forecast to inform the lake operating policy on fast and slow upcoming hydrological dynamics, for the benefit of both objectives.

A possible improvement could be also achieved by using forecast also for temperatures. In this thesis, as input to the HBV model, we use climatology temperatures, i.e. the cyclostationary average of the mean temperatures in the basin from 1990 to 2003. This timeseries could be one of the causes of the loss of performances that we observe in this stepas they affect both snow dynamics and evapotranspiration processes. Using a forecast model also for temperature could help improving the performances of the resulting hydrological forecast, which has proven to be one of the most critical in the framework.
More specifically for the Lake Como system, a different model for transforming rainfall into inflow, which considers also the many upstream reservoirs, could further improve the hydrological forecast accuracy. By including them, the errors could be minimized and some benefits could be provided to the overall procedure.

# Bibliography


Abraham, A. (2005), Artificial neural networks, *handbook of measuring system design*.

Abtew, W., and P. Trimble (2010), El niño–southern oscillation link to south florida hydrology and water management applications, *Water resources management*, *24*(15), 4255–4271.

Anghileri, D., A. Castelletti, F. Pianosi, R. Soncini-Sessa, and E. Weber (2012), Optimizing watershed management by coordinated operation of storing facilities, *Journal of Water Resources Planning and Management*, *139*(5), 492–500.

Banihabib, M. E., A. Ahmadian, and F. S. Jamali (2017), Hybrid darima-narx model for forecasting long-term daily inflow to dez reservoir using the north atlantic oscillation (nao) and rainfall data, *GeoResJ*, *13*, 9–16.

Barcikowska, M. J., S. B. Kapnick, and F. Feser (2017), Impact of large-scale circulation changes in the north atlantic sector on the current and future mediterranean winter hydroclimate, *Climate Dynamics*, pp. 1–21.

Bartolini, E., P. Claps, and P. D'odorico (2009), Interannual variability of winter precipitation in the european alps: relations with the north atlantic oscillation., *Hydrology and Earth System Sciences*, *13*(1), 17–25.

Baxter, J., and P. L. Bartlett (2001), Infinite-horizon policy-gradient estimation, *Journal of Artificial Intelligence Research*, *15*, 319–350.

Bellman, R. (1957), Dynamic programming (dp).

Bellman, R. (1958), Dynamic programming and stochastic control processes, *Information and control*, *1*(3), 228–239.

Beltrame, L., and D. Carbonin (2013), Enso teleconnection patterns on large scale water resources systems.

Beltrame, L., D. Carbonin, S. Galelli, A. Castelletti, and M. Giuliani (2014), Quantifying ENSO impacts at the basin scale using the Iterative Input variable Selection algorithm, in *Proceedings of the 7th International Congress on Environmental Modeling and Software (iEMSs 2014)*, San Diego (CA).

Beniston, M. (1997), Variations of snow depth and duration in the swiss alps over the last 50 years: links to changes in large-scale climatic forcings, in *Climatic change at high elevation sites*, pp. 49–68, Springer.

Beniston, M. (2005a), Mountain climates and climatic change: an overview of processes focusing on the european alps, *Pure and Applied Geophysics*, *162*(8-9), 1587–1606.

Beniston, M. (2005b), Warm winter spells in the swiss alps: Strong heat waves in a cold season? a study focusing on climate observations at the saentis high mountain site, *Geophysical Research Letters*, *32*(1).

Bergstrom, S. (1976), Development and application of a conceptual runoff model for scandinavian catchments.

Bergström, S. (1992), *The HBV model: Its structure and applications*, Swedish Meteorological and Hydrological Institute.

Bianco, V., O. Manca, and S. Nardini (2009), Electricity consumption forecasting in italy using linear regression models, *Energy*, *34*(9), 1413–1421.

Bierkens, M., and L. Van Beek (2009), Seasonal predictability of european discharge: Nao and hydrological response time, *Journal of Hydrometeorology*, *10*(4), 953–968.

Binelli, A., S. Galassi, and A. Provini (2001), Factors affecting the use of dreissena polymorpha as a bioindicator: the pcb pollution in lake como (n. italy), *Water, Air, and Soil Pollution*, *125*(1), 19–32.

Block, P. (2016), Tailoring seasonal climate forecasts for hydropower operations, *Meteorology and Energy Security: Simulations, Projections, and Management*, p. 179.

Block, P., and L. Goddard (2011), Statistical and dynamical climate predictions to guide water resources in ethiopia, *Journal of Water Resources Planning and Management*, *138*(3), 287–298.

Block, P., and B. Rajagopalan (2007), Interannual variability and ensemble forecast of upper blue nile basin kiremt season precipitation, *Journal of Hydrometeorology*, *8*(3), 327–343.

Bocchiola, D., and R. Rosso (2007), The distribution of daily snow water equivalent in the central italian alps, *Advances in water resources*, *30*(1), 135–147.

Bojariu, R., and D.-M. Paliu (2001), North atlantic oscillation projection on romanian climate fluctuations in the cold season, in *Detecting and Modelling Regional Climate Change*, pp. 345–356, Springer.

Bouvy, M., S. M. Nascimento, R. J. Molica, A. Ferreira, V. Huszar, and S. M. Azevedo (2003), Limnological features in tapacurá reservoir (northeast brazil) during a severe drought, *Hydrobiologia*, *493*(1-3), 115–130.

Brandimarte, L., G. Di Baldassarre, G. Bruni, P. D,ÄôOdorico, and A. Montanari (2011), Relation between the north-atlantic oscillation and hydroclimatic conditions in mediterranean areas, *Water Resources Management*, *25*(5), 1269–1279.

Brönnimann, S., E. Xoplaki, C. Casty, A. Pauling, and J. Luterbacher (2007), Enso influence on europe during the last centuries, *Climate Dynamics*, *28*(2-3), 181–197.

Busa-Fekete, R., B. Szörényi, P. Weng, W. Cheng, and E. Hüllermeier (2014), Preference-based reinforcement learning: evolutionary direct policy search using a preference-based racing algorithm, *Machine Learning*, *97*(3), 327–351.

Callegari, M., P. Mazzoli, L. de Gregorio, C. Notarnicola, L. Pasolli, M. Petitta, and A. Pistocchi (2015), Seasonal river discharge forecasting using support vector regression: a case study in the italian alps, *Water*, *7*(5), 2494–2515.

Castelletti, A., S. Galelli, M. Restelli, and R. Soncini-Sessa (2010), Tree-based reinforcement learning for optimal water reservoir operation, *Water Resources Research*, *46*(9).

Castro-Díez, Y., D. Pozo-Vázquez, F. Rodrigo, and M. Esteban-Parra (2002), Nao and winter temperature variability in southern europe, *Geophysical Research Letters*, *29*(8).

Casty, C., H. Wanner, J. Luterbacher, J. Esper, and R. Böhm (2005), Temperature and precipitation variability in the european alps since 1500, *International Journal of Climatology*, *25*(14), 1855–1880.

Ceglar, A., M. Turco, A. Toreti, and F. J. Doblas-Reyes (2017), Linking crop yield anomalies to large-scale atmospheric circulation in europe, *Agricultural and forest meteorology*, *240*, 35–45.

Chandimala, J., and L. Zubair (2007), Predictability of stream flow and rainfall based on enso for water resources management in sri lanka, *Journal of Hydrology*, *335*(3-4), 303–312.

Chandrasekara, S., V. Prasanna, and H.-H. Kwon (2017), Monitoring water resources over the kotmale reservoir in sri lanka using enso phases, *Advances in Meteorology*, *2017*.

Chen, C.-C., D. Gillig, B. A. McCarl, and R. L. Williams (2005), Enso impacts on regional water management: Case study of the edwards aquifer (texas, usa), *Climate Research*, *28*(2), 175–181.

Chen, T., and H. Chen (1995), Universal approximation to nonlinear operators by neural networks with arbitrary activation functions and its application to dynamical systems, *IEEE Transactions on Neural Networks*, *6*(4), 911–917.

Chen, W. (1982), Assessment of southern oscillation sea-level pressure indices, *Monthly Weather Review*, *110*(7), 800–807.

Chiew, F. H., and T. A. McMahon (2002), Global enso-streamflow teleconnection, streamflow forecasting and interannual variability, *Hydrological Sciences Journal*, *47*(3), 505–522.

Cullen, H. M., A. Kaplan, P. A. Arkin, et al. (2002), Impact of the north atlantic oscillation on middle eastern climate and streamflow, *Climatic Change*, *55*(3), 315–338.

Culley, S., S. Noble, A. Yates, M. Timbs, S. Westra, H. Maier, M. Giuliani, and A. Castelletti (2016), A bottom-up approach to identifying the maximum operational adaptive capacity of water resource systems to a changing climate, *Water Resources Research*, *52*(9), 6751–6768.

Cybenko, G. (1989), Approximation by superpositions of a sigmoidal function, *Mathematics of control, signals and systems*, *2*(4), 303–314.

Daniels, L. D., and T. T. Veblen (2000), Enso effects on temperature and precipitation of the patagonian-andean region: implications for biogeography, *Physical Geography*, *21*(3), 223–243.

Dayan, U. (2011), Impacts of the nao on atmospheric pollution in the mediterranean basin, in *Hydrological, Socioeconomic and Ecological Impacts of the North Atlantic Oscillation in the Mediterranean Region*, pp. 171–181, Springer.

Denaro, S., D. Anghileri, M. Giuliani, and A. Castelletti (2017), Informing the operations of water reservoirs over multiple temporal scales by direct use of hydro-meteorological data, *Advances in water resources*, *103*, 51–63.

Diaz, H. F., and V. Markgraf (2000), *El Niño and the Southern Oscillation: multiscale variability and global and regional impacts*, Cambridge University Press.

Durand, Y., G. Giraud, M. Laternser, P. Etchevers, L. Mérindol, and B. Lesaffre (2009), Reanalysis of 47 years of climate in the french alps (1958–2005): climatology and trends for snow cover, *Journal of applied meteorology and climatology*, *48*(12), 2487–2512.

Efthymiadis, D., P. D. Jones, K. R. Briffa, R. Böhm, and M. Maugeri (2007), Influence of large-scale atmospheric circulation on climate variability in the greater alpine region of europe, *Journal of Geophysical Research: Atmospheres*, *112*(D12).

Everingham, Y. L., N. E. Stoeckl, J. Cusack, and J. A. Osborne (2012), Quantifying the benefits of a long-lead enso prediction model to enhance harvest management,Äîa case study for the herbert sugarcane growing region, australia, *International Journal of Climatology*, *32*(7), 1069–1076.

Fiedler, P. C. (2002), Environmental change in the eastern tropical pacific ocean: review of enso and decadal variability, *Marine Ecology Progress Series*, *244*, 265–283.

Folland, C. K., J. Knight, H. W. Linderholm, D. Fereday, S. Ineson, and J. W. Hurrell (2009), The summer north atlantic oscillation: past, present, and future, *Journal of Climate*, *22*(5), 1082–1103.

Fraedrich, K., and K. Müller (1992), Climate anomalies in europe associated with enso extremes, *International Journal of Climatology*, *12*(1), 25–31.

François, B. (2016), Influence of winter north-atlantic oscillation on climate-related-energy penetration in europe, *Renewable Energy*, *99*, 602–613.

Galelli, S., C. Gandolfi, R. Soncini-Sessa, and D. Agostani (2010), Building a metamodel of an irrigation district distributed-parameter model, *Agricultural water management*, *97*(2), 187–200.

García-Herrera, R., J. Díaz, R. M. Trigo, J. Luterbacher, and E. M. Fischer (2010), A review of the european summer heat wave of 2003, *Critical Reviews in Environmental Science and Technology*, *40*(4), 267–306.

Gelati, E., H. Madsen, and D. Rosbjerg (2010), Reservoir optimisation using el niño information. case study of daule peripa (ecuador), in *EGU General Assembly Conference Abstracts*, vol. 12, p. 10112.

Gelati, E., H. Madsen, and D. Rosbjerg (2014), Reservoir operation using el niño forecasts,Äîcase study of daule peripa and baba, ecuador, *Hydrological Sciences Journal*, *59*(8), 1559–1581.

Giacomelli, P., A. Rossetti, and M. Brambilla (2008), Adapting water allocation management to drought scenarios, *Natural Hazards and Earth System Science*, *8*(2), 293–302.

Giuliani, M., and A. Castelletti (2016), Is robustness really robust? how different definitions of robustness impact decision-making under climate change, *Climatic change*, *135*(3-4), 409–424.

Giuliani, M., J. Herman, A. Castelletti, and P. Reed (2014a), Many-objective reservoir policy identification and refinement to reduce policy inertia and myopia in water management, *Water Resources Research*, *50*(4), 3355–3377.

Giuliani, M., E. Mason, A. Castelletti, F. Pianosi, and R. Soncini-Sessa (2014b), Universal approximators for direct policy search in multi-purpose water reservoir management: A comparative analysis, *IFAC Proceedings Volumes*, *47*(3), 6234–6239.

Giuliani, M., A. Castelletti, F. Pianosi, E. Mason, and P. M. Reed (2015), Curses, tradeoffs, and scalable management: Advancing evolutionary multiobjective direct policy search to improve water reservoir operations, *Journal of Water Resources Planning and Management*, *142*(2), 04015,050.

Giuliani, M., D. Anghileri, A. Castelletti, P. N. Vu, and R. Soncini-Sessa (2016), Large storage operations under climate change: expanding uncertainties and evolving tradeoffs, *Environmental Research Letters*, *11*(3), 035,009.

Giuliani, M., J. D. Quinn, J. D. Herman, A. Castelletti, and P. M. Reed (2017), Scalable multiobjective control for large-scale water resources systems under uncertainty, *IEEE Transactions on Control Systems Technology*.

Gleick, P. (1998), Water and conflict (see chronologies a and b.), *The World,Äòs Water*, *1999*, 105–135.

Gleick, P. H. (1994), Water, war & peace in the middle east, *Environment: science and policy for sustainable development*, *36*(3), 6–42.

Goddard, L., S. J. Mason, S. E. Zebiak, C. F. Ropelewski, R. Basher, and M. A. Cane (2001), Current approaches to seasonal to interannual climate predictions, *International Journal of Climatology*, *21*(9), 1111–1152.

Gordo, O., C. Barriocanal, and D. Robson (2011), Ecological impacts of the north atlantic oscillation (nao) in mediterranean ecosystems, in *Hydrological, socioeconomic and ecological impacts of the North Atlantic Oscillation in the Mediterranean region*, pp. 153–170, Springer.

Guariso, G., S. Rinaldi, and R. Soncini-Sessa (1982), The management of lake como.

Guariso, G., S. Rinaldi, and R. Soncini-Sessa (1986), The management of lake como: A multiobjective analysis, *Water Resources Research*, *22*(2), 109–120.

Hadka, D., and P. Reed (2013), Borg: An auto-adaptive many-objective evolutionary computing framework, *Evolutionary computation*, *21*(2), 231–259.

Hafez, Y. (2017), On the relationship between heat waves over the western and central europe and nao, soi, el-nino 3.4 in summer 2015, *Journal of Geoscience and Environment Protection*, *5*(04), 31.

Hamon, W. R. (1960), Estimating potential evapotranspiration, Ph.D. thesis, Massachusetts Institute of Technology.

Hanley, D. E., M. A. Bourassa, J. J. O'Brien, S. R. Smith, and E. R. Spade (2003), A quantitative evaluation of enso indices, *Journal of Climate*, *16*(8), 1249–1258.

Harger, J. (1995), Air-temperature variations and enso effects in indonesia, the philippines and el salvador. enso patterns and changes from 1866–1993, *Atmospheric Environment*, *29*(16), 1919–1942.

Harrison, D., and N. Larkin (1998), Seasonal us temperature and precipitation anomalies associated with el niño: Historical results and comparison with 1997-98, *Geophysical Research Letters*, *25*(21), 3959–3962.

Holmgren, M., et al. (2006), A synthesis of enso effects on drylands in australia, north america and south america, *Advances in Geosciences*, *6*, 69–72.

Huang, G.-B., Q.-Y. Zhu, and C.-K. Siew (2004), Extreme learning machine: a new learning scheme of feedforward neural networks, in *Neural Networks, 2004. Proceedings. 2004 IEEE International Joint Conference on*, vol. 2, pp. 985–990, IEEE.

Huang, G.-B., Q.-Y. Zhu, and C.-K. Siew (2006), Extreme learning machine: theory and applications, *Neurocomputing*, *70*(1-3), 489–501.

Hurrell, J. W. (1995), Decadal trends in the north atlantic oscillation: regional temperatures and precipitation, *Science*, *269*(5224), 676–679.

Hurrell, J. W. (2005), North atlantic oscillation, *Encyclopedia of World Climatology*, pp. 536–539.

Hurrell, J. W., and H. Van Loon (1997), Decadal variations in climate associated with the north atlantic oscillation, in *Climatic change at high elevation sites*, pp. 69–94, Springer.

Hurrell, J. W., Y. Kushnir, G. Ottersen, and M. Visbeck (2003), An overview of the north atlantic oscillation, *The North Atlantic Oscillation: climatic significance and environmental impact*, pp. 1–35.

Jin, F.-F., and S.-I. An (1999), Thermocline and zonal advective feedbacks within the equatorial ocean recharge oscillator model for enso, *Geophysical research letters*, *26*(19), 2989–2992.

Joliffe, I. (2002), Principle component analysis. 2nd.

Kahya, E. (2011), The impacts of nao on the hydrology of the eastern mediterranean, in *Hydrological, Socioeconomic and Ecological Impacts of the North Atlantic Oscillation in the Mediterranean Region*, pp. 57–71, Springer.

Kahya, E., and J. A. Dracup (1993), Us streamflow patterns in relation to the el niño/southern oscillation, *Water Resources Research*, *29*(8), 2491–2503.

Kamil, S., M. Almazroui, F. Kucharski, and I.-S. Kang (2017), Multidecadal changes in the relationship of storm frequency over euro-mediterranean region and enso during boreal winter, *Earth Systems and Environment*, *1*(1), 6.

Kohavi, R., et al. (1995), A study of cross-validation and bootstrap for accuracy estimation and model selection, in *Ijcai*, vol. 14, pp. 1137–1145, Montreal, Canada.

Larkin, N. K., and D. Harrison (2002), Enso warm (el niño) and cold (la niña) event life cycles: Ocean surface anomaly patterns, their symmetries, asymmetries, and implications, *Journal of Climate*, *15*(10), 1118–1140.

Li, Y., M. Giuliani, and A. Castelletti (2017), A coupled human–natural system to assess the operational value of weather and climate services for agriculture, *Hydrology and Earth System Sciences*, *21*(9), 4693.

Lindström, G., B. Johansson, M. Persson, M. Gardelin, and S. Bergström (1997), Development and test of the distributed hbv-96 hydrological model, *Journal of hydrology*, *201*(1-4), 272–288.

Lloyd-Hughes, B., and M. A. Saunders (2002), Seasonal prediction of european spring precipitation from el niño–southern oscillation and local sea-surface temperatures, *International Journal of Climatology*, *22*(1), 1–14.

López, J., and F. Francés (2013), Non-stationary flood frequency analysis in continental spanish rivers, using climate and reservoir indices as external covariates, in *Hydrology and Earth System Sciences Discussions*, vol. 17, pp. 3103–3142, European Geosciences Union (EGU).

López-Moreno, J. I., S. Beguería, S. M. Vicente-Serrano, and J. M. García-Ruiz (2007), Influence of the north atlantic oscillation on water resources in central iberia: Precipitation, streamflow anomalies, and reservoir management strategies, *Water Resources Research*, *43*(9).

López-Moreno, J. I., S. M. Vicente-Serrano, E. Morán-Tejeda, J. Lorenzo-Lacruz, J. Zabalza, A. El Kenawy, and M. Beniston (2011), Influence of winter north atlantic oscillation index (nao) on climate and snow accumulation in the mediterranean mountains, in *Hydrological, Socioeconomic and Ecological Impacts of the North Atlantic Oscillation in the Mediterranean Region*, pp. 73–89, Springer.

MacCarthy, D. S., S. G. Adiku, B. S. Freduah, F. Gbefo, et al. (2017), Using ceres-maize and enso as decision support tools to evaluate climate-sensitive farm management practices for maize production in the northern regions of ghana, *Frontiers in plant science*, *8*, 31.

Maier, H. R., et al. (2014), Evolutionary algorithms and other metaheuristics in water resources: Current status, research challenges and future directions, *Environmental Modelling & Software*, *62*, 271–299.

Maity, R., and D. Nagesh Kumar (2009), Hydroclimatic influence of large-scale circulation on the variability of reservoir inflow, *Hydrological processes*, *23*(6), 934–942.

Maynou, F. (2011), Impact of nao on mediterranean fisheries, in *Hydrological, Socioeconomic and Ecological Impacts of the North Atlantic Oscillation in the Mediterranean Region*, pp. 91–102, Springer.

McCulloch, W. S., and W. Pitts (1943), A logical calculus of the ideas immanent in nervous activity, *The bulletin of mathematical biophysics*, *5*(4), 115–133.

MeteoComo (2018), Previsioni meteo per como e dintorni, available on line.

Mosello, R., et al. (2010), Evoluzione recente della qualità delle acque dei laghi profondi sudalpini (maggiore, lugano, como, iseo e garda) in risposta alle pressioni antropiche e alle variazioni climatiche, *Biologia Ambientale*, *24*(1), 167–177.

Nesje, A., Ø. Lie, and S. O. Dahl (2000), Is the north atlantic oscillation reflected in scandinavian glacier mass balance records?, *Journal of quaternary science*, *15*(6), 587–601.

Ng, J. Y., S. W. Turner, and S. Galelli (2017), Influence of el niño southern oscillation on global hydropower production, *Environmental Research Letters*, *12*(3), 034,010.

NOAA (2018a), Climate change and variability, available on line.

NOAA (2018b), Teleconnections introduction, available on line.

Nobre, G. G., B. Jongman, J. Aerts, and P. J. Ward (2017), The role of climate variability in extreme floods in europe, *Environmental Research Letters*, *12*(8), 084,012.

Nowak, K., J. Prairie, B. Rajagopalan, and U. Lall (2010), A nonparametric stochastic approach for multisite disaggregation of annual to daily streamflow, *Water Resources Research*, *46*(8).

Orlandini, S., A. Dalla Marta, M. Mancini, and D. Grifoni (2011), Impacts of the nao on mediterranean crop production, in *Hydrological, Socioeconomic and Ecological Impacts of the North Atlantic Oscillation in the Mediterranean Region*, pp. 103–112, Springer.

PacificInstitute (2018), Water conflicts, available on line.

Park, J., and I. W. Sandberg (1991), Universal approximation using radial-basis-function networks, *Neural computation*, *3*(2), 246–257.

Pavia, E. G., F. Graef, and J. Reyes (2006), Pdo–enso effects in the climate of mexico, *Journal of Climate*, *19*(24), 6433–6438.

Phillips, J., and B. McIntyre (2000), Enso and interannual rainfall variability in uganda: implications for agricultural management, *International Journal of Climatology*, *20*(2), 171–182.

Picaut, J., M. Ioualalen, C. Menkès, T. Delcroix, and M. J. Mcphaden (1996), Mechanism of the zonal displacements of the pacific warm pool: Implications for enso, *Science*, *274*(5292), 1486–1489.

Piccardi, C., and R. Soncini-Sessa (1991), Stochastic dynamic programming for reservoir optimal control: dense discretization and inflow correlation assumption made possible by parallel computing, *Water Resources Research*, *27*(5), 729–741.

Powell, W. B. (2007), *Approximate Dynamic Programming: Solving the curses of dimensionality*, vol. 703, John Wiley & Sons.

Pulwarty, R. S., and T. S. Melis (2001), Climate extremes and adaptive management on the colorado river: lessons from the 1997–1998 enso event, *Journal of Environmental Management*, *63*(3), 307–324.

Rajagopalan, B., U. Lall, D. G. Tarboton, and D. Bowles (1997), Multivariate nonparametric resampling scheme for generation of daily weather variables, *Stochastic Hydrology and Hydraulics*, *11*(1), 65–93.

Ranković, V., J. Radulović, I. Radojević, A. Ostojić, and L. Čomić (2010), Neural network modeling of dissolved oxygen in the gruža reservoir, serbia, *Ecological Modelling*, *221*(8), 1239–1244.

Rasmusson, E. M., and J. M. Wallace (1983), Meteorological aspects of the el nino/southern oscillation, *Science*, *222*(4629), 1195–1202.

Refaeilzadeh, P., L. Tang, and H. Liu (2009), Cross-validation, in *Encyclopedia of database systems*, pp. 532–538, Springer.

Robertson, A. W., E. R. Cook, M. Ghil, A. M. Greene, D. A. Kondrashov, U. Lall, and M. Lu (2013), Diagnostics of interannual-to-interdecadal climate and streamflow variability: Applications to reservoir management over nw india, in *AGU Fall Meeting Abstracts*.

Rodó, X., E. Baert, and F. Comin (1997), Variations in seasonal rainfall in southern europe during the present century: relationships with the north atlantic oscillation and the el niño-southern oscillation, *Climate Dynamics*, *13*(4), 275–284.

Rodwell, M. J., D. P. Rowell, and C. K. Folland (1999), Oceanic forcing of the wintertime north atlantic oscillation and european climate, *Nature*, *398*(6725), 320.

Rogers, J. C. (1997), North atlantic storm track variability and its association to the north atlantic oscillation and climate variability of northern europe, *Journal of Climate*, *10*(7), 1635–1647.

Rohrer, M., M. Croci-Maspoli, and C. Appenzeller (2017), Climate change and circulation types in the alpine region, *Meteorologische Zeitschrift*, *26*(1), 83–92.

Ropelewski, C. F., and M. S. Halpert (1986), North american precipitation and temperature patterns associated with the el niño/southern oscillation (enso), *Monthly Weather Review*, *114*(12), 2352–2362.

Ropelewski, C. F., and M. S. Halpert (1987), Global and regional scale precipitation patterns associated with the el niño/southern oscillation, *Monthly weather review*, *115*(8), 1606–1626.

Rosso, R. (2002), *Manuale di protezione idraulica del territorio. Appendice sulla normativa italiana in materia di difesa del suolo, protezione civile e dighe*, CUSL (Milano).

Salazar, J. Z., P. M. Reed, J. D. Herman, M. Giuliani, and A. Castelletti (2016), A diagnostic assessment of evolutionary algorithms for multi-objective surface water reservoir control, *Advances in water resources*, *92*, 172–185.

Samale, C., B. Zimmerman, M. Giuliani, A. Castelletti, and P. Block (2017), Improving seasonal forecast through the state of large-scale climate signals, in *Geophysical Research Abstracts of EGU General Assembly*, vol. 19.

Sandweiss, D. H., K. A. Maasch, F. Chai, C. F. T. Andrus, and E. J. Reitz (2004), Geoarchaeological evidence for multidecadal natural climatic variability and ancient peruvian fisheries, *Quaternary Research*, *61*(3), 330–334.

Sarachik, E. S., and M. A. Cane (2010), *The El Nino-southern oscillation phenomenon*, Cambridge University Press.

Scherrer, S. C., C. Appenzeller, and M. Laternser (2004), Trends in swiss alpine snow days: The role of local-and large-scale climate variability, *Geophysical Research Letters*, *31*(13).

Sellars, C. D., M. Garrett, and S. Woods (2008), Influence of the pacific decadal oscillation and el nino southern oscillation on operation of the capilano water supply reservoir, vancouver, british columbia, *Canadian Water Resources Journal*, *33*(2), 155–164.

Shaman, J. (2014), The seasonal effects of enso on european precipitation: Observational analysis, *Journal of Climate*, *27*(17), 6423–6438.

Sharma, A. (2000), Seasonal to interannual rainfall probabilistic forecasts for improved water supply management: Part 1,Äîa strategy for system predictor identification, *Journal of Hydrology*, *239*(1-4), 232–239.

Simpson, H., M. Cane, A. Herczeg, S. Zebiak, and J. Simpson (1993), Annual river discharge in south-eastern australia related to el nino-southern oscillation forecasts of sea surface temperatures, *Water Resources Research*, *29*(11), 3671–3680.

Smith, T. M., R. W. Reynolds, T. C. Peterson, and J. Lawrimore (2008), Improvements to noaa,Äôs historical merged land–ocean surface temperature analysis (1880–2006), *Journal of Climate*, *21*(10), 2283–2296.

Steirou, E., L. Gerlitz, H. Apel, and B. Merz (2017), Links between large-scale circulation patterns and streamflow in central europe: A review, *Journal of Hydrology*, *549*, 484–500.

Stenseth, N. C., G. Ottersen, J. W. Hurrell, A. Mysterud, M. Lima, K.-S. Chan, N. G. Yoccoz, and B. Ådlandsvik (2003), Studying climate effects on ecology through the use of climate indices: the north atlantic oscillation, el nino southern oscillation and beyond, *Proceedings of the Royal Society of London B: Biological Sciences*, *270*(1529), 2087–2096.

Tejada-Guibert, J. A., S. A. Johnson, and J. R. Stedinger (1995), The value of hydrologic information in stochastic dynamic programming models of a multireservoir system, *Water resources research*, *31*(10), 2571–2579.

Terray, P., S. Masson, C. Prodhomme, M. K. Roxy, and K. Sooraj (2016), Impacts of indian and atlantic oceans on enso in a comprehensive modeling framework, *Climate dynamics*, *46*(7-8), 2507–2533.

Trenberth, K. E. (1997), The definition of el nino, *Bulletin of the American Meteorological Society*, *78*(12), 2771–2777.

Trigo, R. M., D. Pozo-Vázquez, T. J. Osborn, Y. Castro-Díez, S. Gámiz-Fortis, and M. J. Esteban-Parra (2004), North atlantic oscillation influence on precipitation, river flow and water resources in the iberian peninsula, *International Journal of Climatology*, *24*(8), 925–944.

Tsitsiklis, J. N., and B. Van Roy (1996), Feature-based methods for large scale dynamic programming, *Machine Learning*, *22*(1-3), 59–94.

Turner, S., and S. Galelli (2016), Regime-shifting streamflow processes: Implications for water supply reservoir operations, *Water Resources Research*, *52*(5), 3984–4002.

Uvo, C. B. (2003), Analysis and regionalization of northern european winter precipitation based on its relationship with the north atlantic oscillation, *International Journal of Climatology*, *23*(10), 1185–1194.

Uvo, C. B., and R. Berndtsson (2002), North atlantic oscillation; a climatic indicator to predict hydropower availability in scandinavia, *Hydrology Research*, *33*(5), 415–424.

Veldkamp, T. I., S. Eisner, Y. Wada, J. C. Aerts, and P. J. Ward (2015), Sensitivity of water scarcity events to enso-driven climate variability at the global scale, *Hydrology and Earth System Sciences*, *19*(10), 4081.

Vicente-Serrano, S. M., and R. M. Trigo (2011), *Hydrological, socioeconomic and ecological impacts of the North Atlantic Oscillation in the Mediterranean region*, vol. 46, Springer Science & Business Media.

Vincent, C., P. Ribstein, V. Favier, P. Wagnon, B. Francou, E. Le Meur, and D. Six (2005), Glacier fluctuations in the alps and in the tropical andes, *Comptes Rendus Geoscience*, *337*(1-2), 97–106.

Walker, G. T. (1932), World weather v memories r., *Meteor. Soc.*, *4*, 53–84.

Waluda, C. M., C. Yamashiro, and P. G. Rodhouse (2006), Influence of the enso cycle on the light-fishery for dosidicus gigas in the peru current: an analysis of remotely sensed data, *Fisheries Research*, *79*(1-2), 56–63.

Wanner, H., S. Brönnimann, C. Casty, D. Gyalistras, J. Luterbacher, C. Schmutz, D. B. Stephenson, and E. Xoplaki (2001), North atlantic oscillation–concepts and studies, *Surveys in geophysics*, *22*(4), 321–381.

Ward, P. J., W. Beets, L. M. Bouwer, J. C. Aerts, and H. Renssen (2010), Sensitivity of river discharge to enso, *Geophysical Research Letters*, *37*(12).

Ward, P. J., B. Jongman, M. Kummu, M. D. Dettinger, F. C. S. Weiland, and H. C. Winsemius (2014), Strong influence of el niño southern oscillation on flood risk around the world, *Proceedings of the National Academy of Sciences*, *111*(44), 15,659–15,664.

Wei, W., Y. Chang, and Z. Dai (2014), Streamflow changes of the changjiang (yangtze) river in the recent 60 years: Impacts of the east asian summer monsoon, enso, and human activities, *Quaternary International*, *336*, 98–107.

Whateley, S., S. Steinschneider, and C. Brown (2014), A climate change range-based method for estimating robustness for water resources supply, *Water Resources Research*, *50*(11), 8944–8961.

WMO (2018), What is climate variability, available on line.

Wolter, K. (1993), Monitoring enso in coads with a seasonally adjusted principal component index, in *Proc. of the 17th Climate Diagnostics Workshop, 1993*.

Wolter, K., and M. S. Timlin (), Monitoring enso in coads with a seasonally adjusted principal.

Wolter, K., and M. S. Timlin (1998), Measuring the strength of enso events: How does 1997/98 rank?, *Weather*, *53*(9), 315–324.

Yeh, W. W.-G. (1985), Reservoir management and operations models: A state-of-the-art review, *Water resources research*, *21*(12), 1797–1818.

Zhang, R., A. Sumi, and M. Kimoto (1999), A diagnostic study of the impact of el nino on the precipitation in china, *Advances in Atmospheric Sciences*, *16*(2), 229–241.

Zimmerman, B. G., D. J. Vimont, and P. J. Block (2016), Utilizing the state of enso as a means for season-ahead predictor selection, *Water resources research*, *52*(5), 3761–3774.

Zitzler, E., L. Thiele, M. Laumanns, C. M. Fonseca, and V. G. Da Fonseca (2003), Performance assessment of multiobjective optimizers: An analysis and review, *IEEE Transactions on evolutionary computation*, *7*(2), 117–132.

Zoppoli, R., M. Sanguineti, and T. Parisini (2002), Approximating networks and extended ritz method for the solution of functional optimization problems, *Journal of Optimization Theory and Applications*, *112*(2), 403–440.

# A

# Additional material

In this chapter we show the complete results of the procedure.

**Table A.1:** *Performance of ELM model for the three differently constructed years.*

| | | | | | |
|---|---|---|---|---|---|
| | JFM | AMJ | JAS | OND | Total |
| $R^2$ | 0,7614 | 0,7072 | 0,7598 | 0,6562 | 0,72115 |
| | FMA | MJJ | ASO | NDJ | Total |
| $R^2$ | 0,7262 | 0,5518 | 0,6116 | 0,6813 | 0,642725 |
| | MAM | JJA | SON | DJF | Total |
| $R^2$ | 0,7371 | 0,6933 | 0,6242 | 0,5035 | 0,639525 |

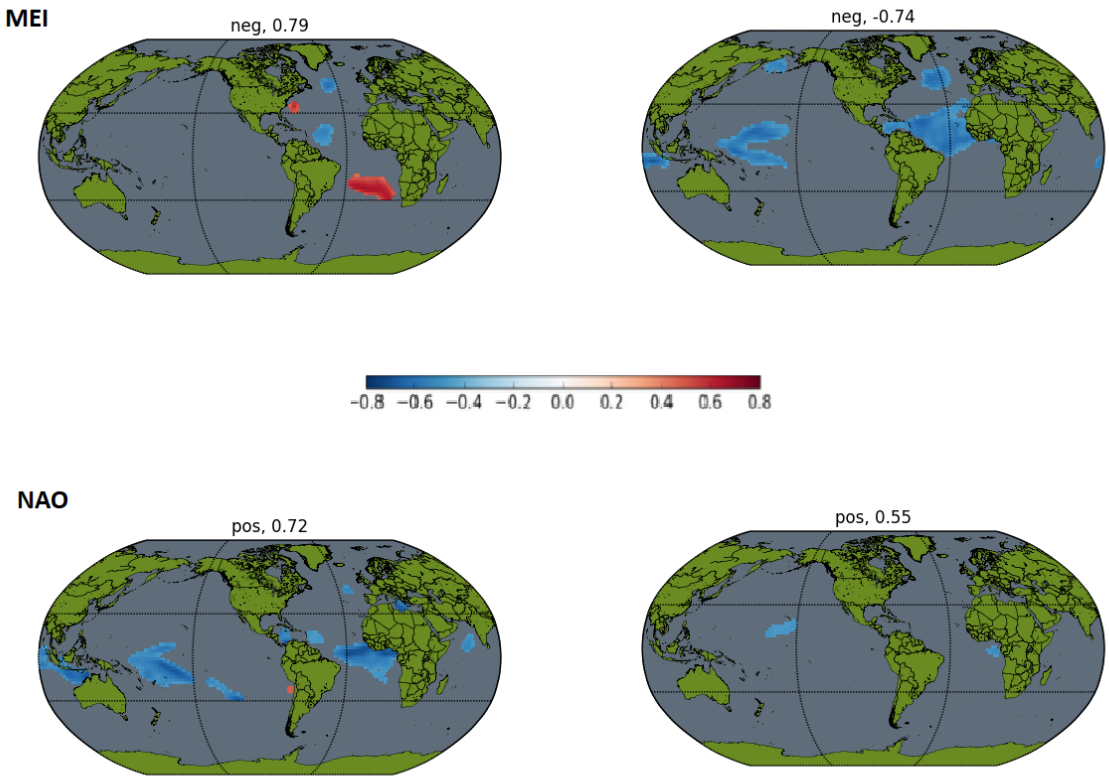


**Figure A.1:** *Correlation maps between pre-season SST anomalies and FMA precipitation for the two phases of ENSO (top panel) and NAO (bottom panel).*

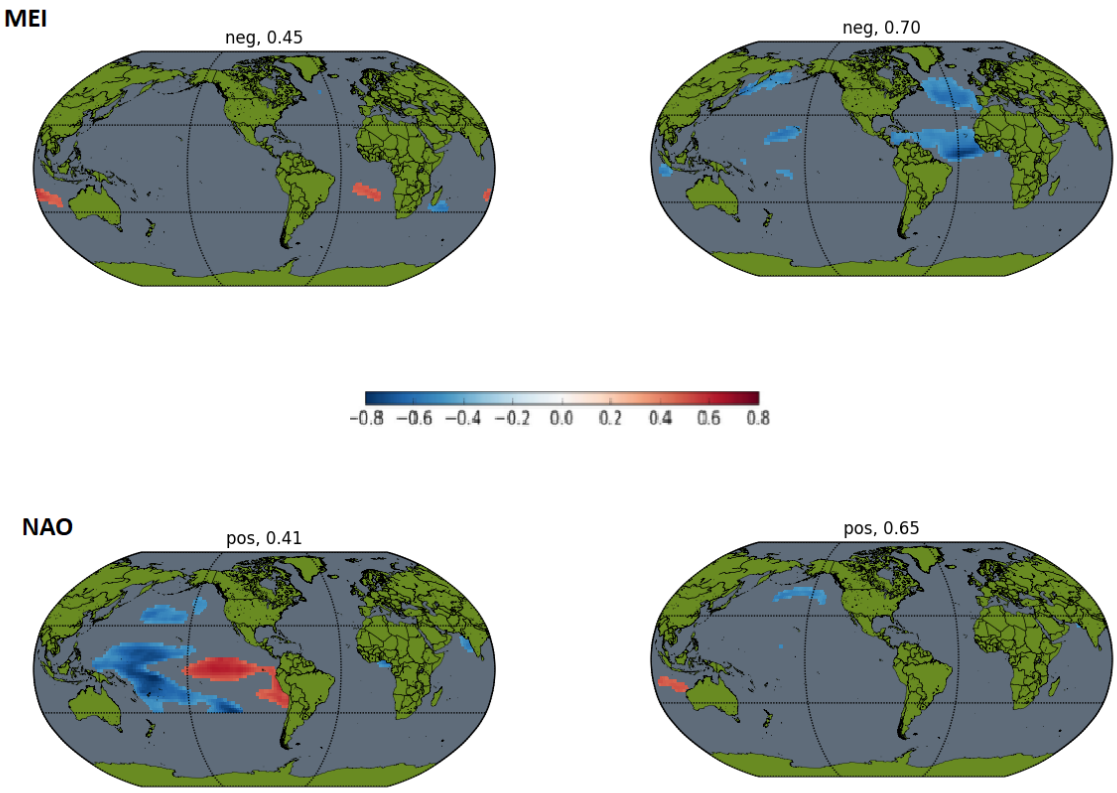


**Figure A.2:** *Correlation maps between pre-season SST anomalies and MAM precipitation for the two phases of ENSO (top panel) and NAO (bottom panel).*

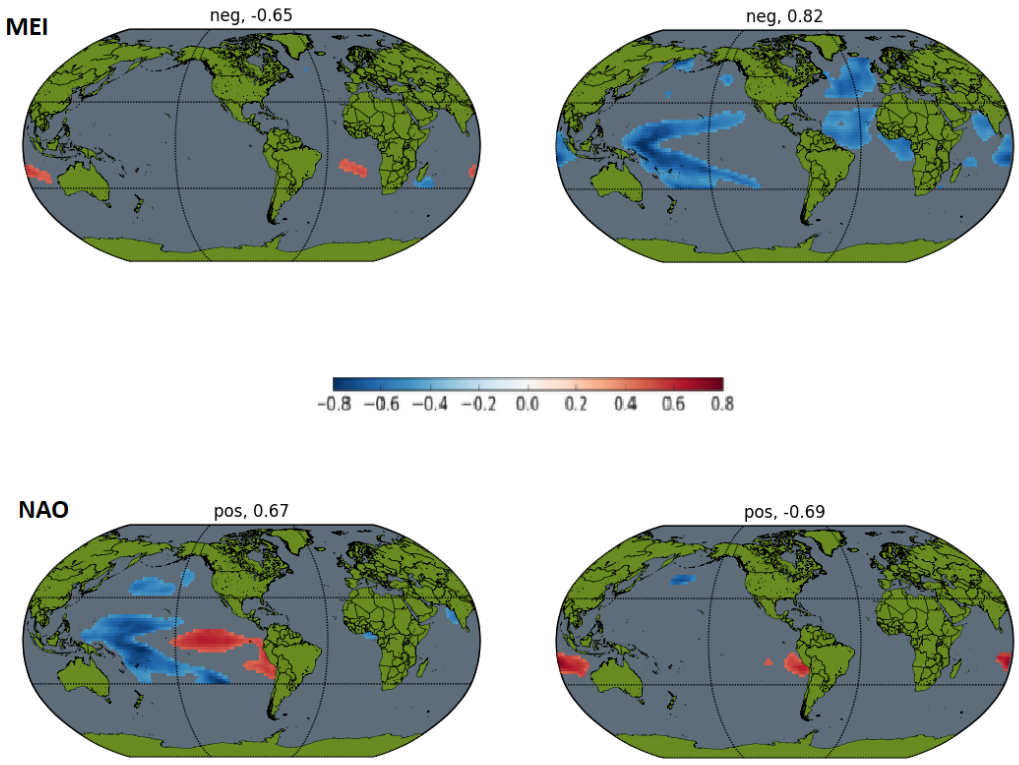


**Figure A.3:** *Correlation maps between pre-season SST anomalies and AMJ precipitation for the two phases of ENSO (top panel) and NAO (bottom panel).*

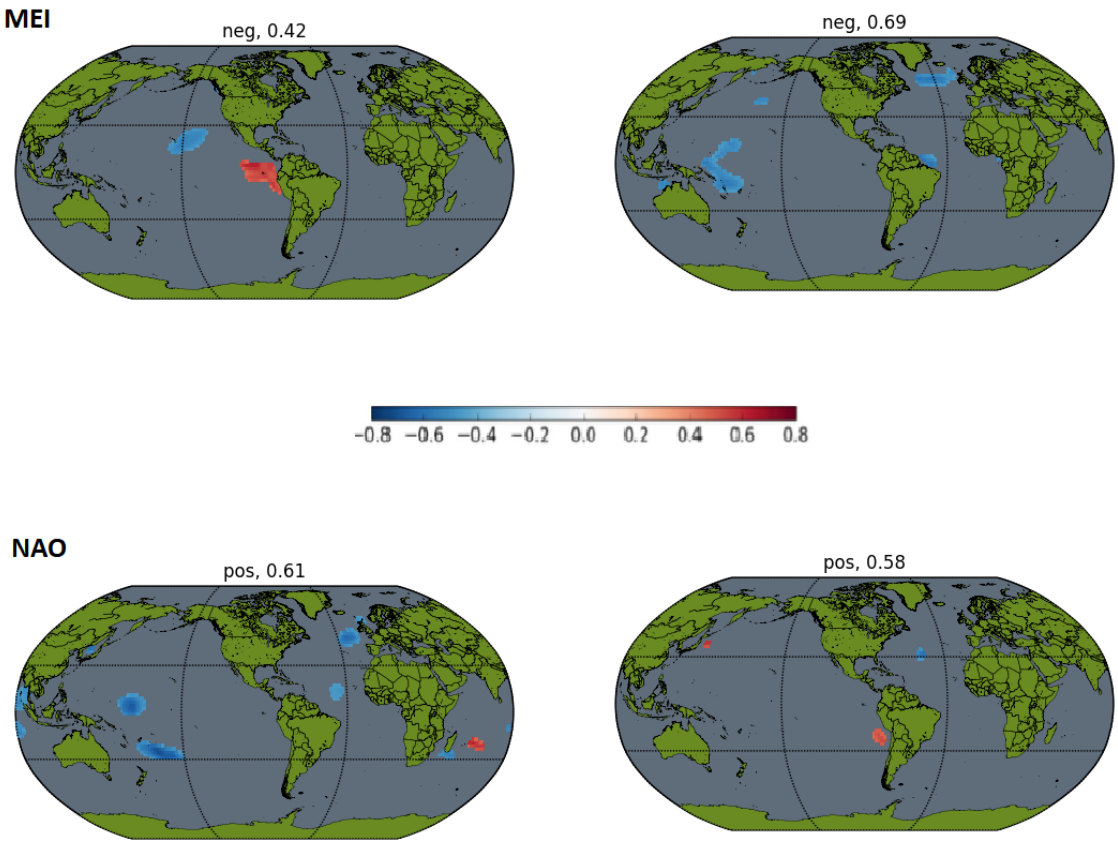


**Figure A.4:** *Correlation maps between pre-season SST anomalies and MJJ precipitation for the two phases of ENSO (top panel) and NAO (bottom panel).*

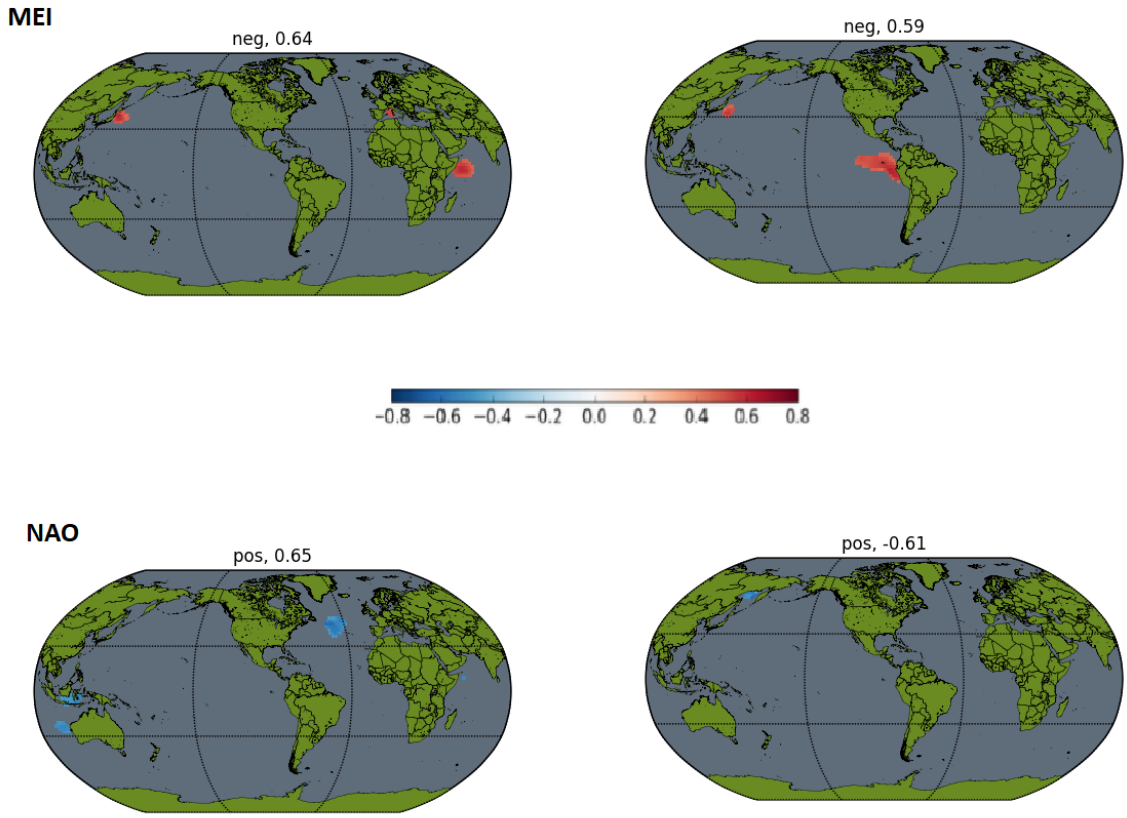


**Figure A.5:** *Correlation maps between pre-season SST anomalies and JJA precipitation for the two phases of ENSO (top panel) and NAO (bottom panel).*

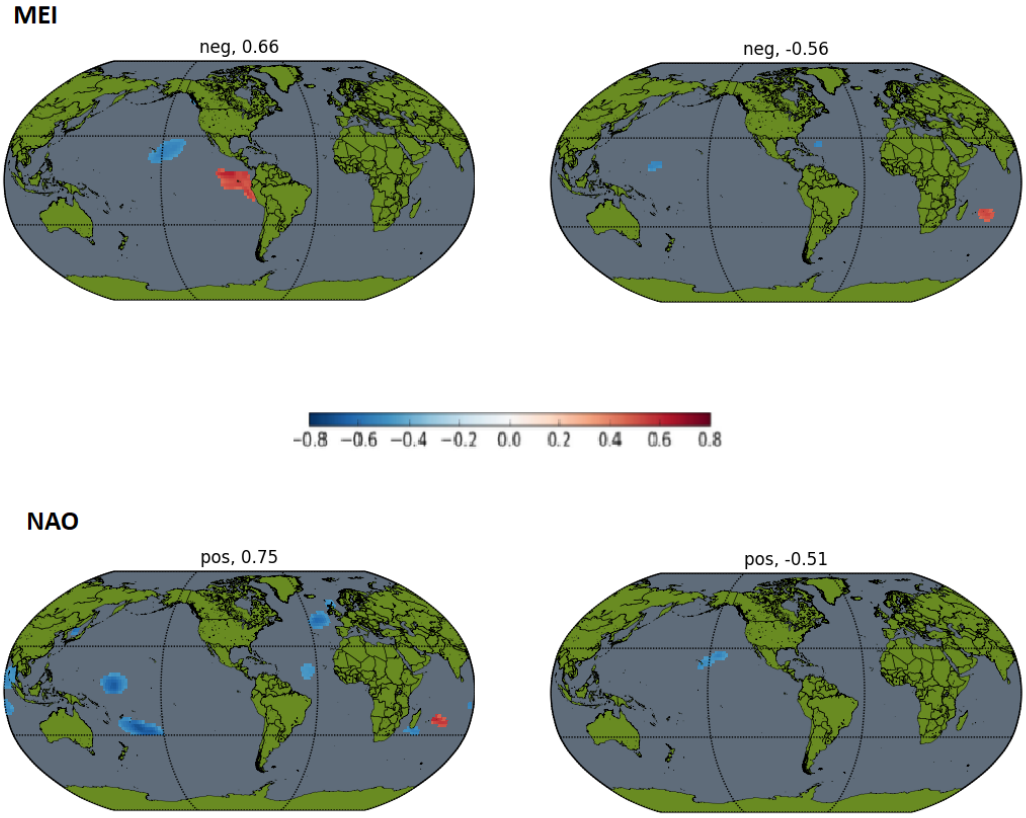


**Figure A.6:** *Correlation maps between pre-season SST anomalies and JAS precipitation for the two phases of ENSO (top panel) and NAO (bottom panel).*

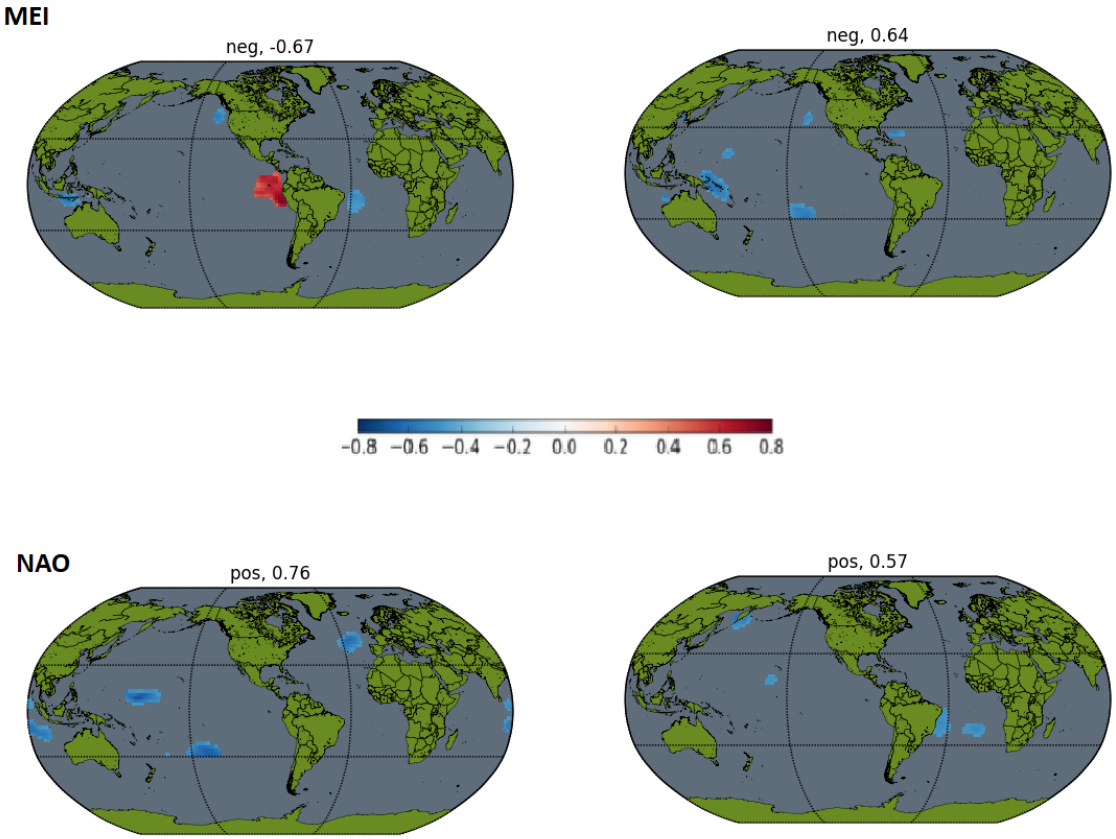


**Figure A.7:** *Correlation maps between pre-season SST anomalies and ASO precipitation for the two phases of ENSO (top panel) and NAO (bottom panel).*

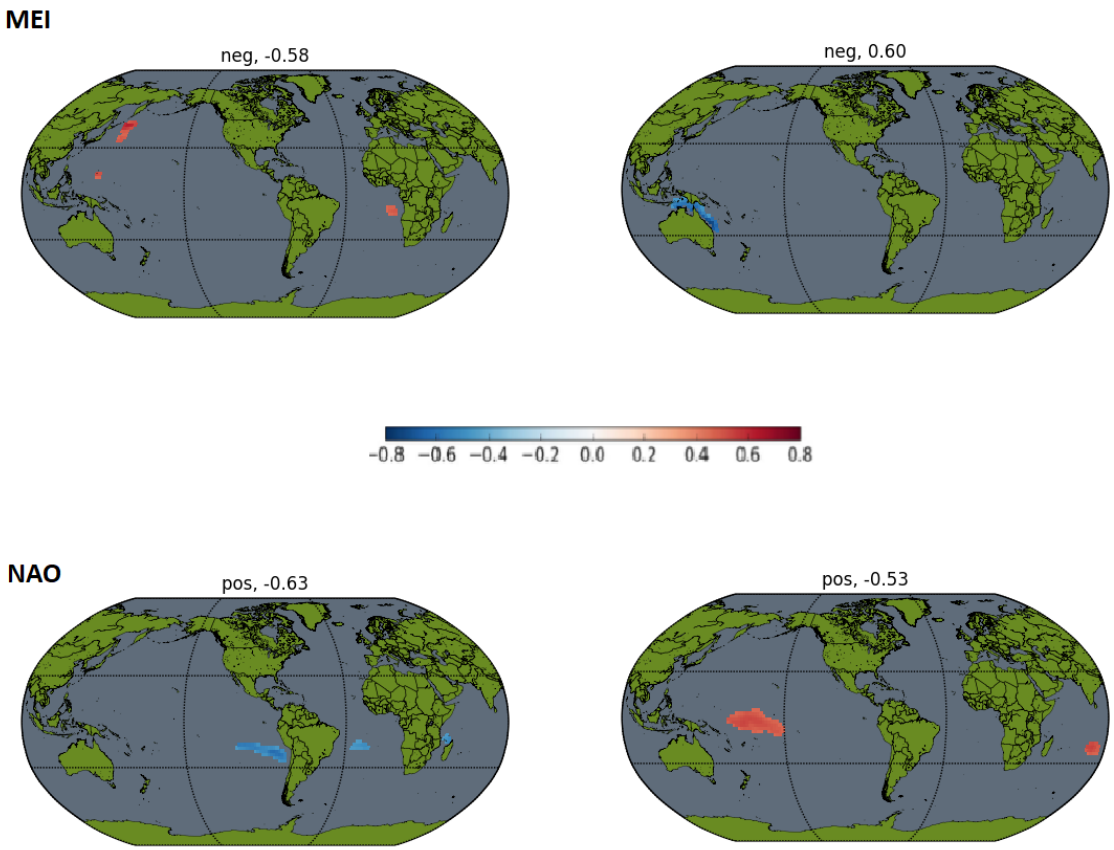


**Figure A.8:** *Correlation maps between pre-season SST anomalies and SON precipitation for the two phases of ENSO (top panel) and NAO (bottom panel).*

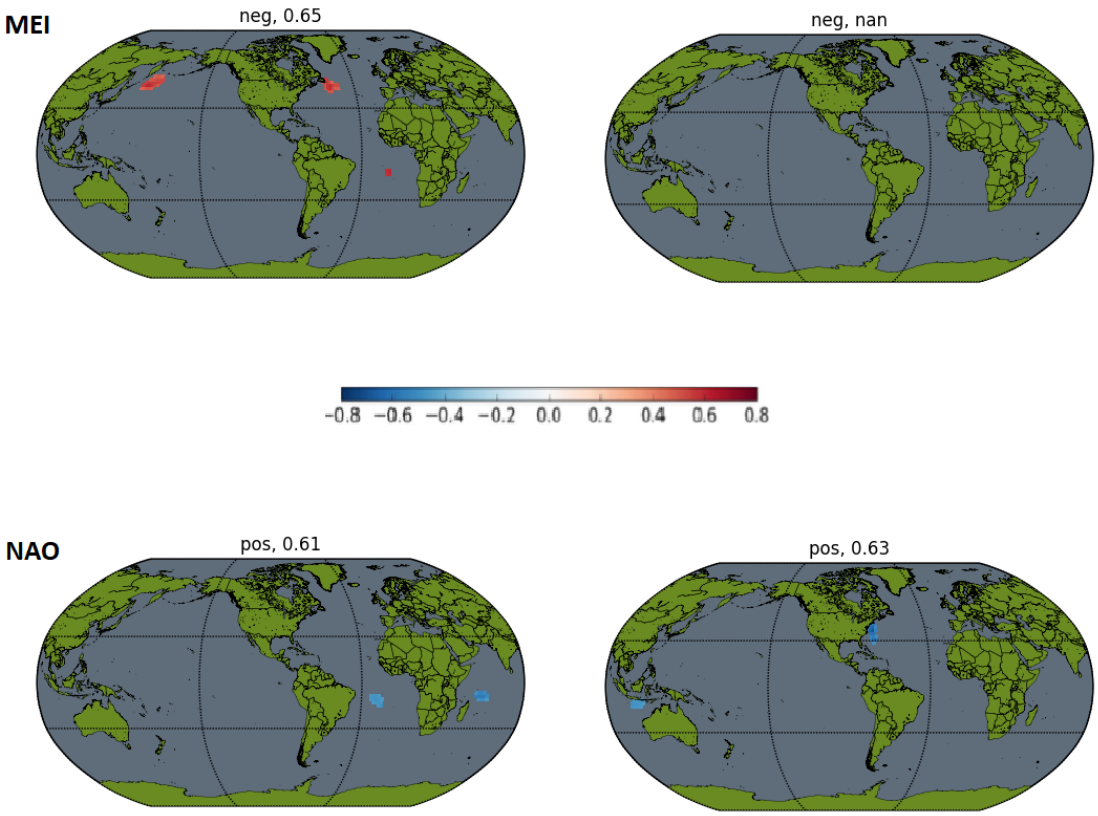


**Figure A.9:** *Correlation maps between pre-season SST anomalies and OND precipitation for the two phases of ENSO (top panel) and NAO (bottom panel).*

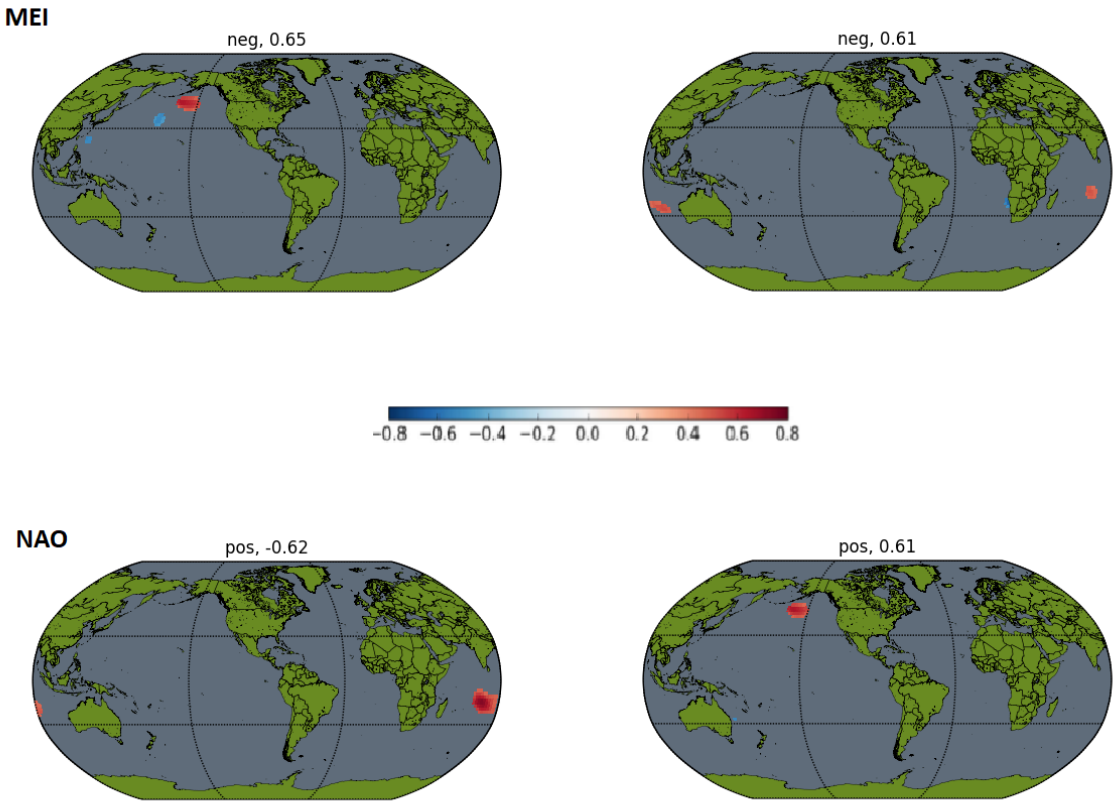


**Figure A.10:** *Correlation maps between pre-season SST anomalies and NDJ precipitation for the two phases of ENSO (top panel) and NAO (bottom panel).*

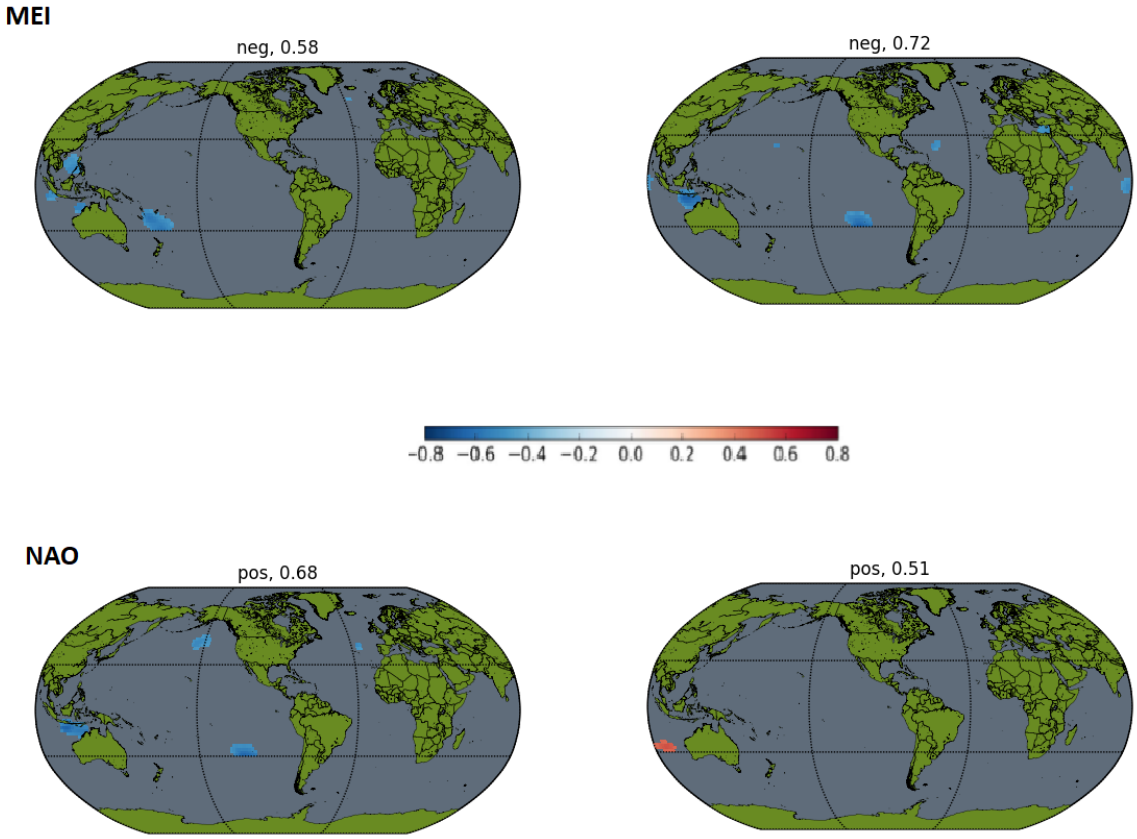


**Figure A.11:** *Correlation maps between pre-season SST anomalies and DJF precipitation for the two phases of ENSO (top panel) and NAO (bottom panel).*

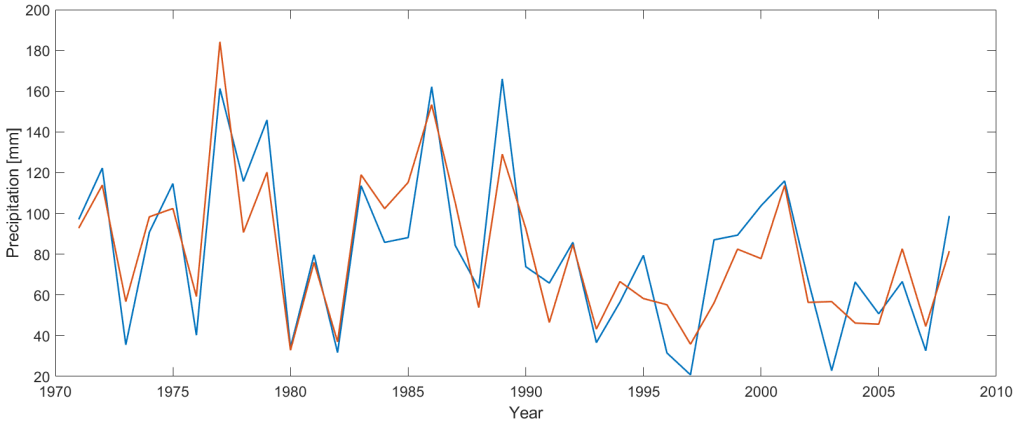


**Figure A.12:** *Observed and predicted (ELM model) precipitation for the FMA period.*

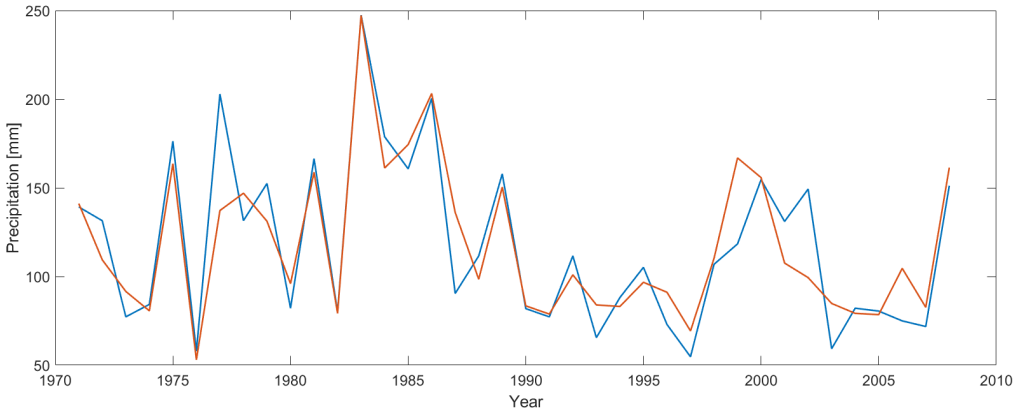


**Figure A.13:** *Observed and predicted (ELM model) precipitation for the MAM period.*

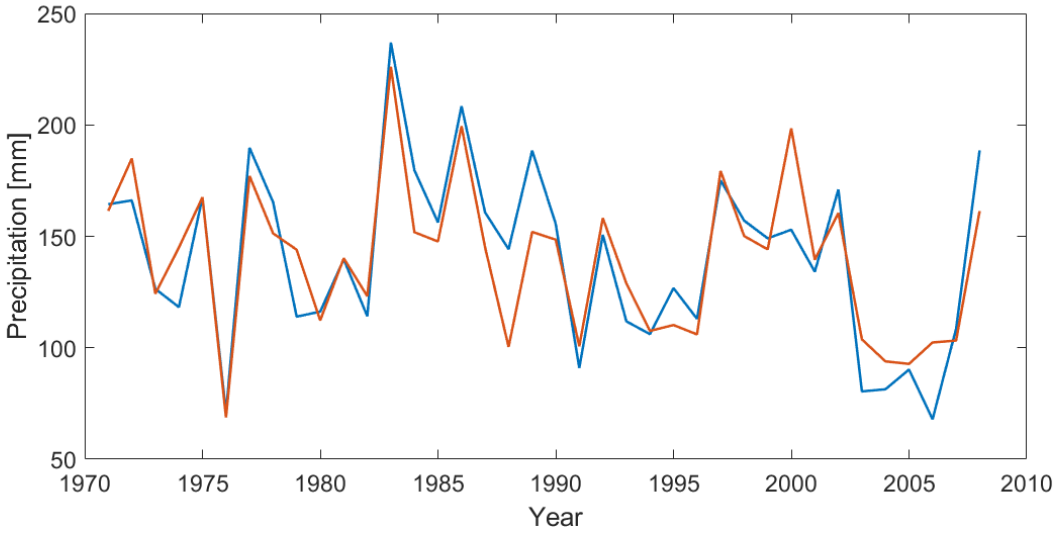


**Figure A.14:** *Observed and predicted (ELM model) precipitation for the AMJ period.*

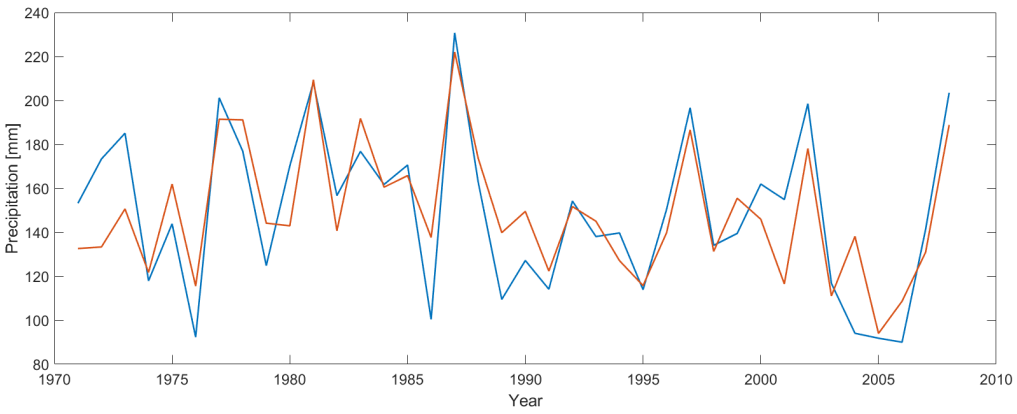


**Figure A.15:** *Observed and predicted (ELM model) precipitation for the MJJ period.*

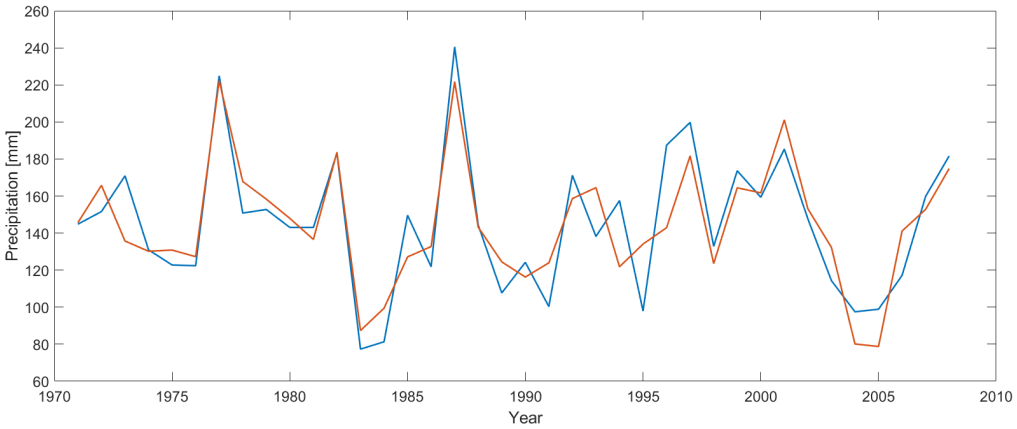


**Figure A.16:** *Observed and predicted (ELM model) precipitation for the JJA period.*

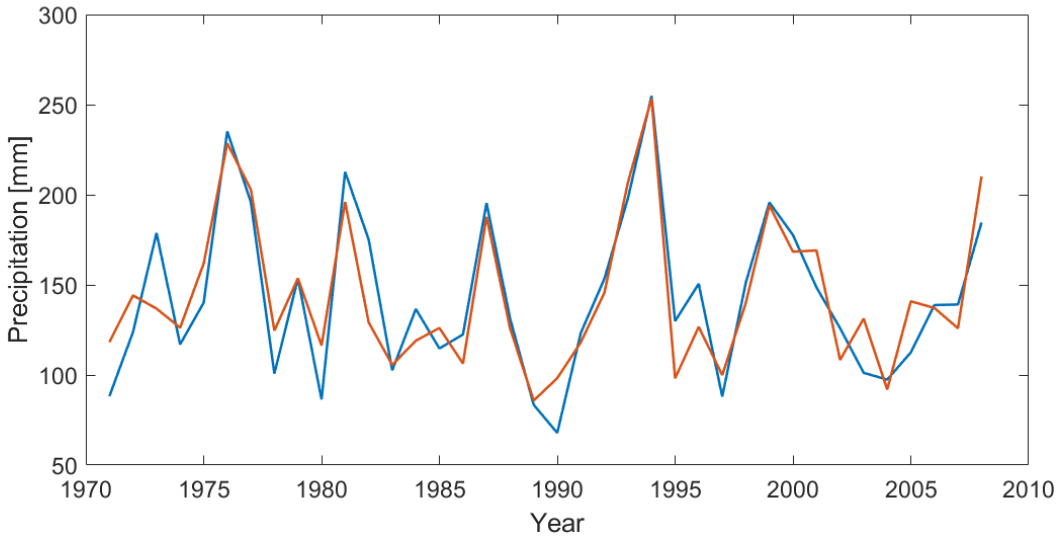


**Figure A.17:** *Observed and predicted (ELM model) precipitation for the JAS period.*

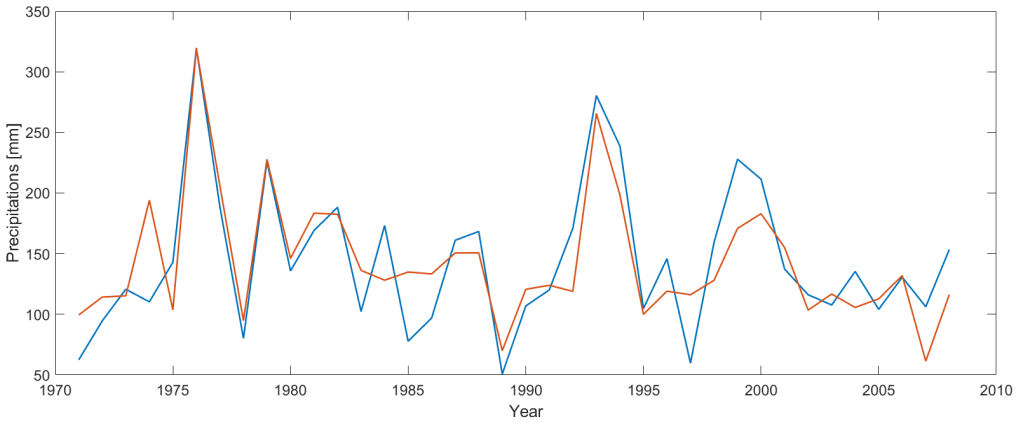


**Figure A.18:** *Observed and predicted (ELM model) precipitation for the ASO period.*

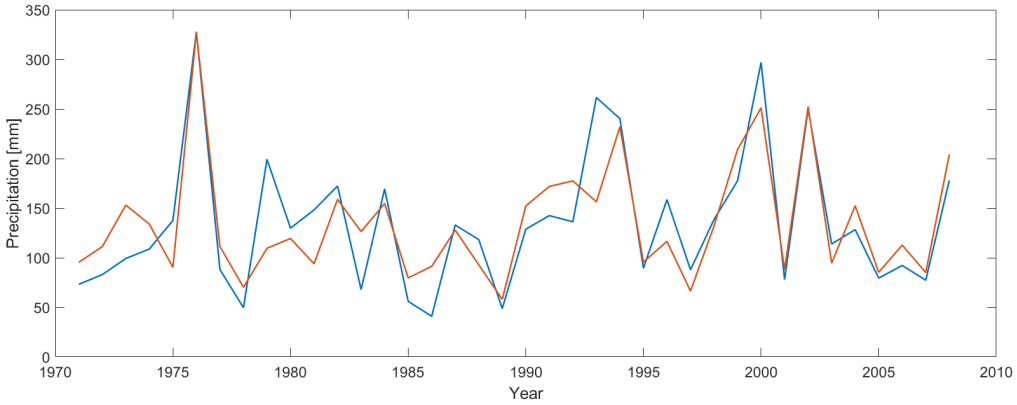


**Figure A.19:** *Observed and predicted (ELM model) precipitation for the SON period.*

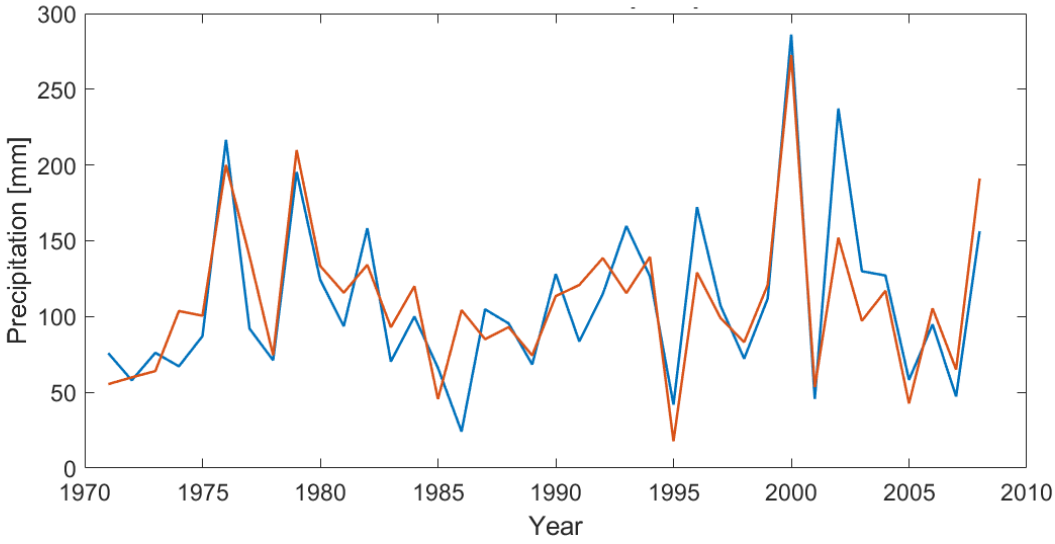


**Figure A.20:** *Observed and predicted (ELM model) precipitation for the OND period.*

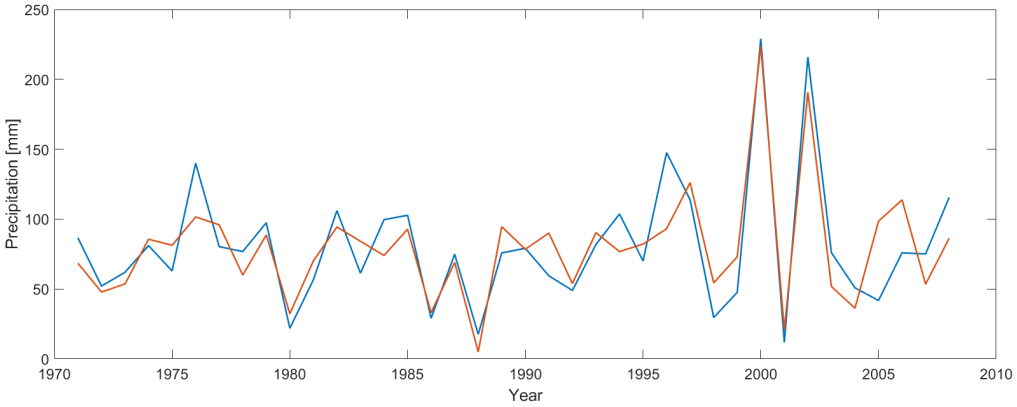


**Figure A.21:** *Observed and predicted (ELM model) precipitation for the NDJ period.*

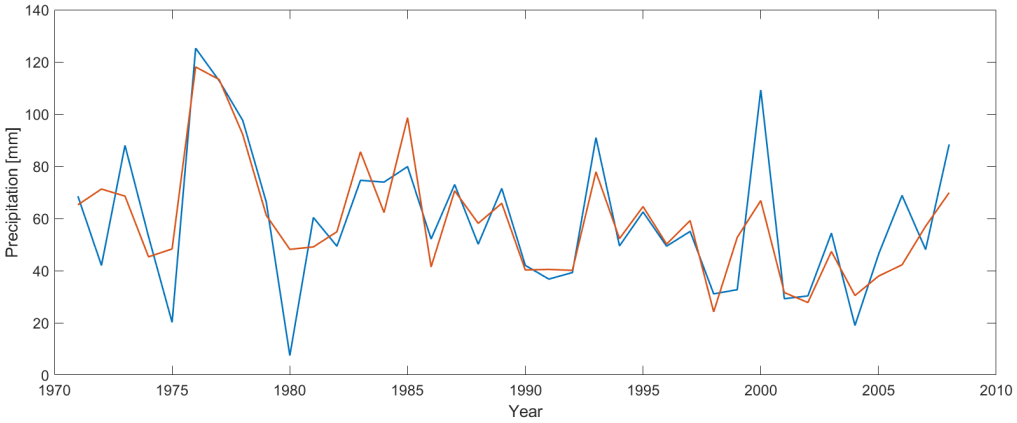


**Figure A.22:** *Observed and predicted (ELM model) precipitation for the DJF period.*

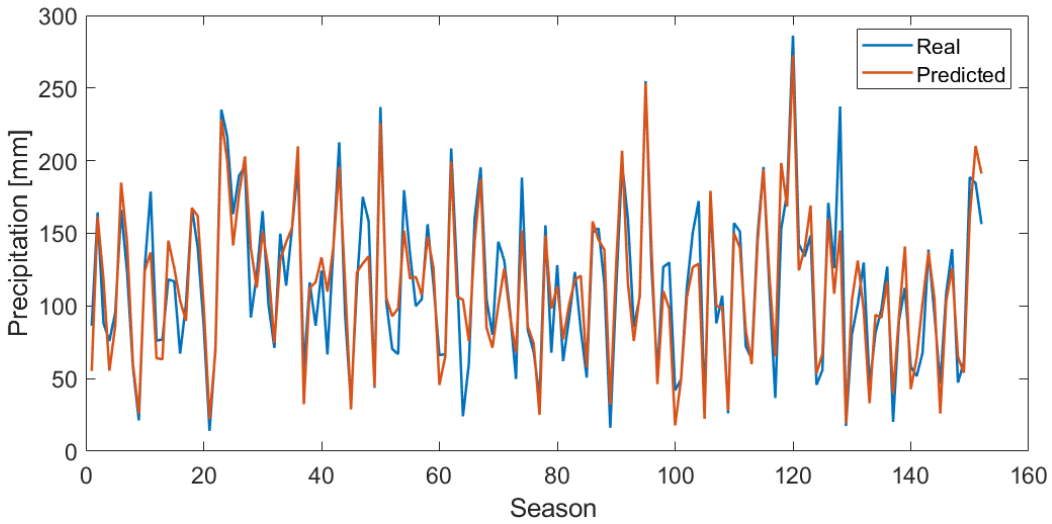


**Figure A.23:** *Observed and predicted (ELM model) seasonal precipitation over the complete period.*